



HUNGARIAN UNIVERSITY OF AGRICULTURE AND LIFE SCIENCES

# Modelling and performance optimization of solar drying chamber used for agricultural products

PhD Dissertation

DOI: 10.54598/006700

by

Halefom Kidane Abrha

Gödöllő  
2025

**Doctoral school**

**Denomination:** Doctoral School of Mechanical Engineering

**Science:** Mechanical Engineering

**Leader:** Prof. Dr. Gábor Kalácska, DSc  
Institute of Technology  
Hungarian University of Agriculture and Life Science, Gödöllő,  
Hungary

**Supervisor:** Prof. Dr. István Farkas, DSc  
Institute of Technology  
Hungarian University of Agriculture and Life Science, Gödöllő,  
Hungary

**Co-Supervisor:** Dr. János Buzás, PhD  
Institute of Technology  
Hungarian University of Agriculture and Life Science, Gödöllő,  
Hungary

.....  
Affirmation of supervisors

.....  
Affirmation of head of school

## CONTENTS

NOMENCLATURE AND ABBREVIATION .....	7
1. INTRODUCTION, OBJECTIVES .....	10
1.1. Introduction .....	10
1.2. Objectives.....	11
2. LITERATURE REVIEW.....	12
2.1. Fundamentals of drying and theories .....	12
2.2. Solar dryers .....	13
2.3. Solar drying chamber .....	17
2.4. Performance evaluation of solar drying systems .....	20
2.5. Characterizing the drying behaviour of agricultural products .....	21
2.5.1. <i>Modelling the drying kinetics of agricultural products</i> .....	21
2.5.2. <i>Thin layer drying models</i> .....	22
2.6. Modelling of the solar drying chamber .....	25
2.7. Optimization of solar drying chambers .....	29
2.8. Economic analysis.....	31
2.9. Summary of literature review .....	31
3. MATERIALS AND METHODS .....	34
3.1. Study area.....	34
3.2. Numerical approaches .....	36
3.2.1. <i>Basic equation solved using CFD analysis in solar drying systems</i> .....	36
3.2.2. <i>Numerical simulation procedures</i> .....	37
3.2.3. <i>Modelling and discretization of the domain</i> .....	38
3.2.3.1. Drying chamber .....	38
3.2.3.2. Trays .....	39
3.2.3.3. Initial and boundary conditions .....	40
3.2.3.4. Quality of the mesh.....	41
3.2.3.5. Solver settings and turbulence choice.....	41
3.3. Computational evaluation .....	42
3.4. Validation of the CFD results.....	44
3.5. Experimental approach.....	44
3.5.1.1. Manufacturing process of the solar air heater.....	45
3.5.1.2. Drying chamber .....	45
3.5.1.3. Trays .....	46

3.6. Instrumentation and data acquisition.....	46
3.7. Sample preparation.....	47
3.8. Uncertainty of the experiment.....	48
3.9. Performance analysis of the solar drying chamber .....	48
3.9.1. <i>Unloading test</i> .....	48
3.9.2. <i>Load test</i> .....	48
3.9.3. <i>Energy analysis of the drying system</i> .....	49
3.9.3.1. Energy analysis of solar air heater .....	49
3.9.3.2. Energy analysis of the drying chamber.....	49
3.9.3.3. Efficiency of the drying system .....	50
3.9.3.4. Specific heat energy consumption and specific moisture extraction rate .....	51
3.9.3.5. Exergy analysis of solar air heater .....	51
3.9.3.6. Exergy analysis of the drying chamber.....	51
3.9.3.7. Exergy analysis of the trays .....	52
3.9.3.8. Exergy efficiency .....	52
3.9.4. <i>Drying rate</i> .....	53
3.9.5. <i>Moisture content</i> .....	53
3.9.6. <i>The effective diffusion coefficient and activation energy</i> .....	53
3.10. Thin-layer drying models .....	54
3.11. Colour analysis .....	55
3.12. Material used to enhance the flow uniformity .....	56
3.13. Procedures in the Taguchi approach .....	58
3.14. Economic analysis and feasibility study .....	58
4. RESULTS.....	61
4.1. CFD results of the trays and validation .....	61
4.1.1. <i>Temperature distribution in the trays</i> .....	61
4.1.2. <i>Validation of the simulation results</i> .....	61
4.2. Experimental results .....	62
4.3. Evaluation of the drying system.....	63
4.3.1. <i>Temperature distribution under the unloading and loading conditions</i> .....	63
4.3.2. <i>Humidity analysis</i> .....	64
4.3.3. <i>Efficiency of the solar air heaters and drying system</i> .....	65
4.3.4. <i>Comparative evaluation of dryer designs</i> .....	66
4.3.5. <i>Specific heat energy consumption and specific moisture extraction rate</i> .....	67
4.3.6. <i>Exergy analysis of solar air heaters</i> .....	68

4.3.6.1. Exergy inflow and outflow of the drying chambers .....	69
4.3.6.2. Exergy inflow of the trays of dryers .....	70
4.3.6.3. Exergy outflow analysis of trays of dryers .....	71
4.3.6.4. Exergy efficiency of the drying system .....	71
4.4. Drying characteristics of golden apple.....	72
4.4.1. <i>Moisture content analysis</i> .....	72
4.4.2. <i>Moisture ratio and drying curve investigation</i> .....	73
4.4.3. <i>Selecting the best-fitting model</i> .....	74
4.4.4. <i>Moisture diffusivity evaluation</i> .....	74
4.5. Colour change analysis .....	75
4.6. Enhancement of the drying uniformity .....	76
4.6.1. <i>Effect of integrating triangular baffles</i> .....	76
4.6.2. <i>Effect of integrating rectangular baffles</i> .....	76
4.6.3. <i>Effect of adding swirler</i> .....	77
4.6.4. <i>Coefficient of variance</i> .....	78
4.7. Temperature distribution of the enhancement methods .....	78
4.7.1. <i>Effect of triangular baffles</i> .....	78
4.7.2. <i>Effect of rectangular baffles</i> .....	79
4.7.3. <i>Effect of swirler</i> .....	80
4.8. Effect of tray spacing .....	80
4.9. Taguchi analysis.....	81
4.9.1. <i>Coefficient of variance as a response parameter</i> .....	81
4.9.2. <i>Pressure as response variable</i> .....	82
4.10. Feasibility study of the drying system.....	83
5. NEW SCIENTIFIC RESULTS .....	85
6. CONCLUSION AND SUGGESTIONS .....	88
7. SUMMARY .....	89
8. ÖSSZEFOGLALÁS (SUMMARY IN HUNGARIAN) .....	90
9. APPENDICES.....	91
A1: Bibliography.....	91
A2: Publications related to the dissertation.....	105
A3: Manufacturing process process of basic drying systems .....	107
A4: Accuracy and technical specifications of measurement devices.....	108
A5: Regression analysis: SHE and SMER of the dryers.....	110
A6: Statistical results of thin layer drying models for apple slice .....	111

A7: Drying rate and standard deviation of the enhancement tools .....	112
A8: Result of different tray spacing configurations .....	113
A9: Results of Taguchi analysis.....	114
A10: Fabrication cost of the drying system .....	115
10. ACKNOWLEDGEMENT .....	116

## NOMENCLATURE AND ABBREVIATION

$A$	Area ( $\text{m}^2$ )
$AH_a$	Absolute humidity of air (-)
$A_{OUT}$	Radiometric analogue voltage output (V)
$C_d$	Discharge coefficient ranges 0.6 to 0.9 for most orifices
$C_p$	Specific heat ( $\text{J kg}^{-1} \text{ } ^\circ\text{C}^{-1}$ )
$d. b.$	Dry basis
$D_h$	Hydraulic diameter (m)
$D_o$	Pre-exponential factor of the Arrhenius equation ( $\text{m}^2 \text{ s}^{-1}$ )
$DP$	Pressure drops (Pa)
$DR$	Drying rate ( $\text{g hr}^{-1}$ )
$E_a$	Activation energy (Joules mole $^{-1}$ )
$E_x$	Exergy ( $\text{kJ kg}^{-1}$ )
$E_{xi}$	Exergy inflow ( $\text{kJ kg}^{-1}$ )
$E_{xl}$	Exergy loss ( $\text{kJ kg}^{-1}$ )
$E_{xo}$	Exergy outflow ( $\text{kJ kg}^{-1}$ )
$F_p$	Fan power (W)
$g$	Gravitational acceleration ( $\text{m s}^{-2}$ ), gram
$g_c$	Dimensional conversion constant (-)
$Gr$	Grashof number (-)
$h$	Specific enthalpy of the system ( $\text{kJ kg}^{-1}$ )
$h_{ce}$	Coefficient of convective heat transfer ( $\text{W m}^{-2} \text{ K}^{-1}$ )
$hr$	Hour
$I_r$	Instantaneous radiation striking the collector's plane ( $\text{W m}^{-2}$ )
$I_R$	Inertia resistance factor ( $\text{kg m}^{-2}$ )
$k$	Thermal conductivity ( $\text{W m}^{-1} \text{ K}^{-1}$ )
$l$	Slice thickness or fixed bed height (m)
$\dot{m}$	Mass flow rate ( $\text{kg s}^{-1}$ )
$m_f$	Final mass of dried product (g)
$m_{fc}$	Final moisture content of the sample (wet basis, %)
$m_i$	Initial mass of the sample (g)
$m_{ic}$	Initial moisture content of the sample (wet basis, %)
$m_w$	Total mass of moisture removed from the product (kg)
$Me$	Equilibrium moisture content on a wet basis (%)
$MR$	Moisture ratio
$P$	Pressure (Pa)
$Pr$	Prandtl number (-)
$Q$	Heat rate (W)
$R$	Universal gas constant ( $\text{J mol}^{-1} \text{ K}^{-1}$ )
$R^2$	Coefficient of determination (%)
$Ra$	Rayleigh number (-)
$Re$	Reynolds number (-)
$RH$	Relative humidity (%)

$RMSE$	Root mean square error (%)
$SSE$	Sum squared error
$t$	Time (s)
$T$	Temperature (°C)
$tr$	Tray
$T_R$	Transpose of tensor stress (N m <sup>-2</sup> )
$v$	Velocity of air (m s <sup>-1</sup> )
$V_{DD}$	Power supply voltage (V)
$x$	Experimental (observed) data
$x^2$	Chi-square
$y$	Predicted (calculated) data
$w. b.$	Wet basis

*Greek symbols*

$\varepsilon$	Turbulence dissipation rate (m <sup>2</sup> s <sup>-3</sup> )
$\mu$	Coefficient of dynamic viscosity (kg m <sup>-1</sup> s <sup>-1</sup> )
$\mu_t$	Turbulent viscosity (kg m <sup>-1</sup> s <sup>-1</sup> )
$\rho$	Density (kg m <sup>-3</sup> )
$\sigma_\varepsilon$	Turbulent model constant for turbulence dissipation rate (m <sup>2</sup> s <sup>-3</sup> )
$\sigma_k$	Turbulent model constant for turbulence kinetic energy (m <sup>2</sup> s <sup>-2</sup> )
$\vec{\tau}$	Stress tensor (N m <sup>-2</sup> )
$\nabla$	Divergence ( $\nabla B = \frac{\partial B_x}{\partial x} + \frac{\partial B_y}{\partial y} + \frac{\partial B_z}{\partial z}$ )

*Subscripts*

$a$	Air
$am$	Ambient
$av$	Average
$dc$	Drying chamber
$eff$	Effective
$f$	Fluid
$i$	In/inlet, cartesian coordinate
$o$	Out/outlet
$p$	Product
$sah$	Solar air heater
$tot$	Total
$we$	External wall
$wi$	Internal wall

*Abbreviations*

$CFD$	Computational fluid dynamics
$FLC$	Full loading capacity (g)
$HLC$	Half loading capacity (g)
$RB$	Rectangular baffles
$SAH$	Solar air heater
$TB$	Triangular baffles



<i>XPS</i>	Extruded polystyrene sheets
<i>WO</i>	Without

## 1. INTRODUCTION, OBJECTIVES

This chapter outlines the significance of the research topic and presents the study's objectives.

### 1.1. Introduction

Drying is a widely used preservation method that humans have practised for centuries for various purposes. It helps to extend shelf life, reduce packaging costs, increase shipping capacity and enhance their appearance. This process also preserves flavour and nutritional value by removing moisture, which inhibits the growth of bacteria, yeast, and mould, thereby preventing food spoilage (Musembi et al., 2016). It is used to improve food stability because it lowers the water activity of the substance, prevents microbial activity, and reduces physical and chemical changes during storage (Meisami and Rafiee, 2009). The fundamental goal of drying is to lower the moisture content to a level that allows the products to be stored for more extended periods without deterioration. Low moisture content in agricultural products impedes the growth of microorganisms such as moulds, bacteria and yeasts as well as chemical processes that degrade product quality (Rabha and Muthukumar, 2017).

Even if drying offers significant advantages, as discussed in the preceding section, it also entails notable drawbacks, particularly regarding its cost and energy consumption. High energy consumption can lead to scarcity, which, in turn, may drive up expenses. As reported by, Li et al. (2023a), in countries like the United States, Canada, France, and the United Kingdom, drying accounts for 10%–15% of total energy consumption, while in Denmark and Germany, it reaches 20%–25%.

Such problems can be mitigated by adopting alternative energy sources, such as solar energy. Obaideen et al. (2021) for decades, renewable energy has been recognized as a significant solution to the energy crisis. Liu (2018) states that solar energy is the fastest-growing and most prominent renewable energy source globally, thanks to its affordability and eco-friendly characteristics. Although the technology is relatively new compared to traditional renewable resources, it has a promising future. A significant decline in costs drives the rapid expansion of solar energy. With these reduced expenses, solar energy is expected to become even more affordable, with installation costs also projected to drop significantly. Fudholi et al. (2018) described that due to present trends toward scarcity and high costs of fossil fuels, as well as uncertainties about future price and availability, the use of solar energy for drying agricultural products is likely to expand and become more economically viable in the near future.

Verma and Goswami (2024) stated that renewable energy sources, particularly solar power, provide considerable environmental and economic advantages. Solar energy is plentiful and sustainable, serving as a viable alternative to conventional fossil fuels. It helps decrease greenhouse gas emissions and combat climate change. Additionally, it promotes reduced dependence on non-renewable energy sources, lowers carbon footprints, and encourages more sustainable agricultural practices. From an economic perspective, solar energy can result in significant savings for farmers, as solar-powered irrigation systems remove the necessity for diesel or electric pumps. Panda et al. (2024) solar energy has the potential to transform agricultural practices by providing a clean, reliable, and cost-effective energy source for a variety of applications, such as irrigation, crop drying, greenhouse heating, and powering farm

equipment. Integrating solar energy into agriculture can reduce reliance on fossil fuels, lower greenhouse gas emissions, enhance energy security, and increase farmers' incomes particularly in rural and remote areas with limited access to the electrical grid. Paneru et al. (2024) solar energy holds significant potential to enhance sustainability as a renewable energy source, mainly when utilized for activities such as cooking and heating.

### 1.2. Objectives

This thesis focuses on the mathematical modelling of drying chambers and apple slices and assess the enhancement of flow uniformity mechanism within drying chambers. The challenge of uneven air distribution is well-documented in both the existing literature and practical applications, including dryers developed by previous students in Hungarian University of Agriculture and Life Sciences, Solar Energy Laboratory. Research shows that such discrepancies in airflow can significantly affect the moisture content of materials, thereby compromising product quality and increasing energy consumption during the drying process.

The overall objective of the study is to model numerically and optimize the performance of the solar drying system used in dry agricultural products. The specific objectives are:

- To conduct a comprehensive thermodynamic performance analysis of the drying system.
- To enhance the airflow distribution within the drying system for better quality and effective drying of agricultural products.
- To investigate the drying kinetics and select a suitable mathematical drying model which describes the drying behaviour of apple slices.
- To study the effect of tray spacing and number of trays on the performance of the solar drying chamber.
- To identify the most influential operational parameters/variables affecting drying system performance.
- To evaluate the economic feasibility and cost-effectiveness of the solar drying system for agricultural products.

By addressing these objectives, this study aims to enhance the flow uniformity of drying chamber and mathematical modelling of the drying kinetics of the golden apple.

## 2. LITERATURE REVIEW

This chapter offers an in-depth review of the fundamental principles of drying and related theories, with a focus on solar dryers and their classifications for agricultural preservation. It covers thin-layer models and delves into energy and exergy analysis to assess the efficiency of drying systems. Additionally, the chapter explores numerical modelling through computational fluid dynamics, highlights, optimization methods and economic analysis of drying systems.

### 2.1. Fundamentals of drying and theories

Drying process is complex and challenged: considered as multiphase, multiphysics, and multiscale dimensions. It is multiphase because it involves multiple phases within the materials: a solid phase (dry material matrix), a liquid phase (both free and adsorbed water), and a gas phase (water vapour and dry air). It is considered multiphysics due to the coupled heat, mass, and momentum transport occurring within the material and the exchange processes at the air-material (or material-material) interfaces. Additionally, it is multiscale because these transport and exchange processes take place at different spatial scales (Barbosa et al., 2023). Physically, drying involves heat and mass, leading to a decrease in a material's liquid content (Kolesnikov and Gavrilov, 2020). Fig. 2.1 provides a conceptual explanation of the heat and mass transfer in the drying process.

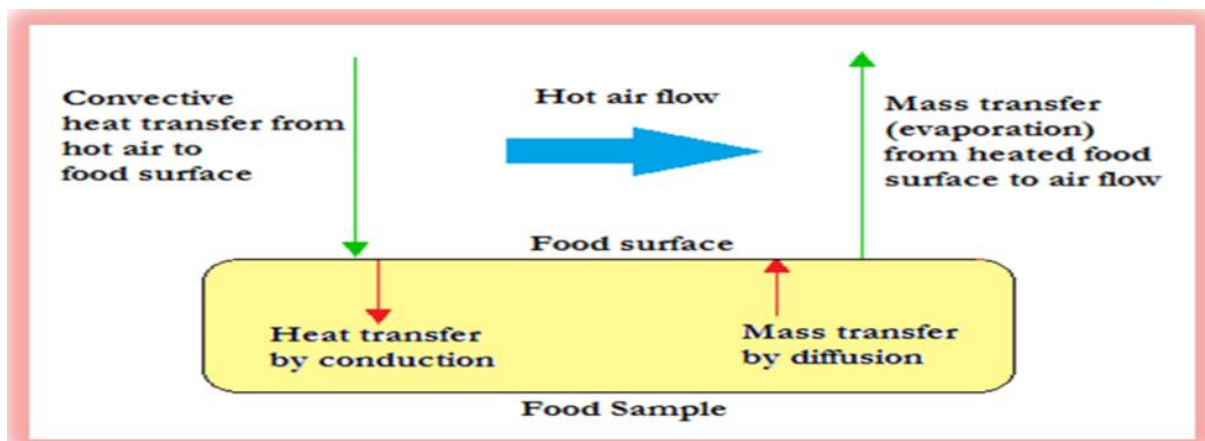


Fig. 2.1. Schematic representation of mass and heat transfer in drying processes (Singh, 2015)

After a short period of initial phase, the drying process of material involves two primary phases: the constant rate period and the falling rate period. In the constant rate period, the moisture content declines steadily as surface moisture evaporates, driven by external conditions such as temperature and air velocity. This phase transitions into the falling rate period, which is divided into two stages. The first stage, known as the initial falling rate period, sees a reduction in the rate of moisture removal compared to the constant rate phase. The second stage, referred to as the curvilinear falling rate period, is marked by a further slowdown in moisture reduction following a curvilinear trend (Erbay and Icier, 2010). An example of a drying curve for an agricultural product, illustrating the different drying stages, is shown in Fig. 2.2.

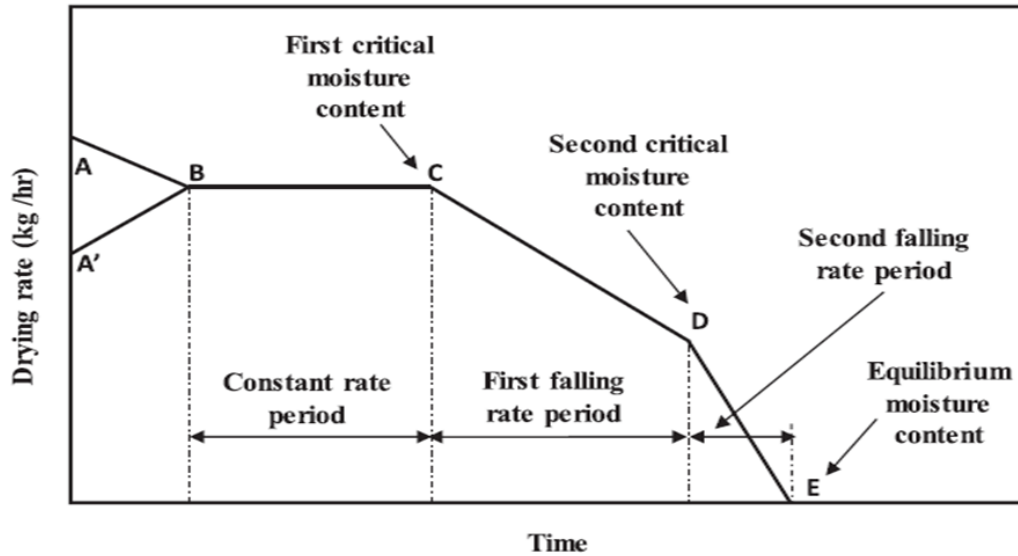


Fig. 2.2. Different phases of the drying process (Srinivasan and Muthukumar, 2021)

## 2.2. Solar dryers

Open sun drying is one of the oldest and simplest methods for preserving agricultural products. It is still practised in rural and remote areas where access to electricity is limited. In this method, the crops or fruits that need to be dried are placed on a flat surface or the ground and exposed to direct sunlight, as shown in Fig. 2.3. So, such type a mechanism has many drawbacks and is labour intensive. Enormous amounts of these goods decomposed as a result of a variety of factors, including weather, insect attacks, and other contaminants. A large area is needed to spread the fruit out to dry, and a drying control mechanism is required, etc. Hence, to overcome the negative side of open sun dryers, as noted by Sharma et al. (2009), artificial or controlled drying methods called solar dryers have been used in recent times to improve quality control, eliminate spoilage, and minimize losses.

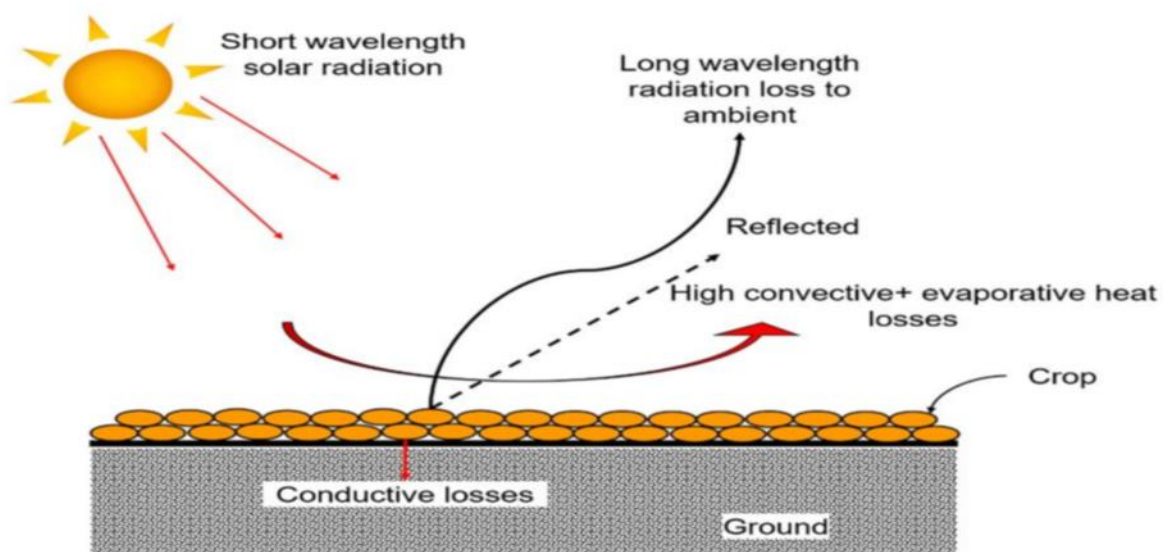


Fig. 2.3. Open-sun-drying method (Gorjian et al., 2021)

Controlled solar drying is a more advanced technology that combines a solar thermal energy gathering system with a drying chamber. Solar energy can be collected separately and delivered to the drying chamber using a solar thermal collector unit or solar thermal energy collection device integrated with the drying chamber in a single unit. Solar drying under controlled conditions is more efficient, healthier, hygienic, faster, and less expensive than open sun dryers. An example of the controlled type of solar drying is shown in Fig. 2.4.

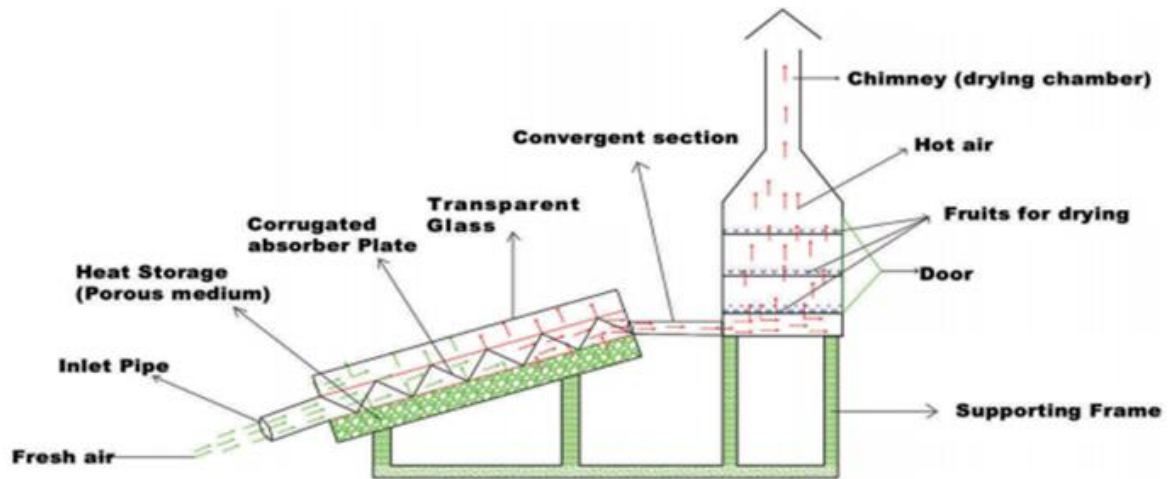


Fig. 2.4. Schematic diagram of flat plate solar collector with drying chamber (Ullah et al., 2018)

Solar dryers, in general, have the following main parts. Trays, where the material to be dried is placed and where the drying takes place, solar collector to convert solar radiation into heat, auxiliary energy source (optional), heat transfer equipment for transferring heat to the drying air or the material, means for keeping the drying air in flow, heat storage unit (optional), measuring and control equipment (optional) and ducts, pipes, and other appliances.

#### *Types of solar dryer technologies*

Different researchers have designed, manufactured, studied, and optimized numerous types of solar dryers. These dryers were classified based on various criteria by researchers. Richter et al. (2013) classified solar dryers as direct and indirect solar dryers. Direct solar dryers are simple to build. However, they have several drawbacks, such as direct sunshine exposure, which can be damaging to food quality (natural colour loss, destruction of vitamins, and nutritional value). As a result, it is not a good idea to use it to dry light-sensitive products. Another classification was given by Srinivasan et al. (2021) as natural convection and forced convection, as shown in Fig. 2.5. In natural convection, the air movement occurs due to density differences across the drying chamber. In forced convection the air movement across the drying cabinet is achieved by using an exhaust fan or blower unit powered electrically via grid or solar photovoltaic panels.

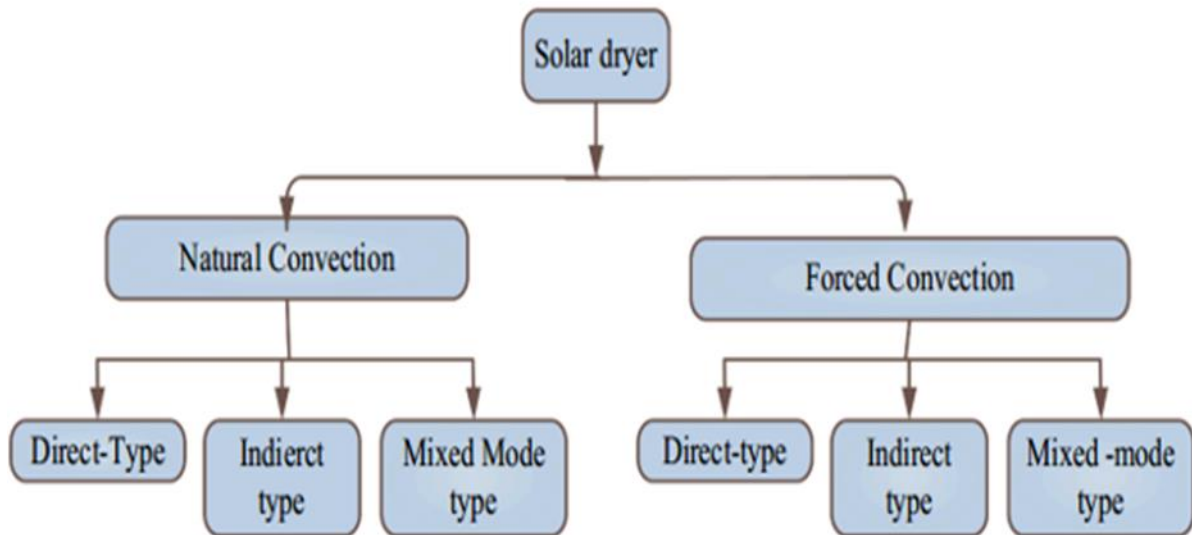


Fig. 2.5. Broad classification of solar dryers (Srinivasan et al., 2021)

El Hage et al. (2018) also classify solar dryers based on three parameters. According to the methods of air movement, solar dryers are classified as active and passive, based on heat transfer modes as direct, indirect, hybrid and mixed solar dryers and based on types of drying chambers such as cabinet, greenhouse and tent. Classification of solar dryers based on different methods is depicted in Fig. 2.6.

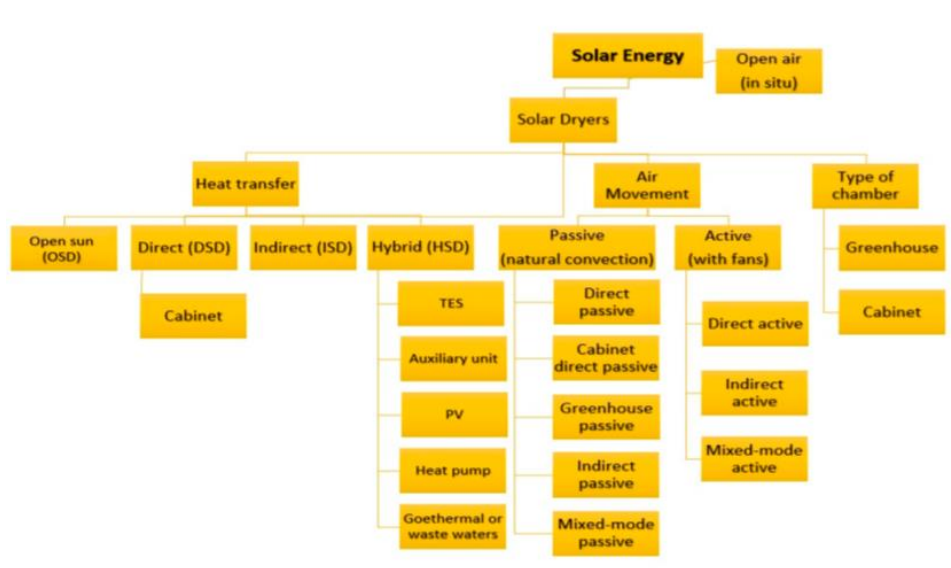


Fig. 2.6. Schematic summary of the classification of solar dryers (Fernandes and Tavares, 2024)

In direct solar drying, the product is placed on the drying cabinet; hence, it is immediately exposed to sunlight, as shown in Fig. 2.7(a), which can cause dehydration. A black-painted heat-absorbent surface is given with this sort of drying system, which can collect sunlight and convert it into heat; the crop to be dried is placed directly on this surface (Singh Chauhan et al., 2015). In the indirect solar dryer, the product is dried in an opaque drying chamber without being exposed to direct sunlight, as illustrated in Fig. 2.7(b). Solar air collectors or heaters provide the hot and dry air needed to dry items. The mixed-mode model combines the benefits



of both direct and indirect solar dryers (Srinivasan et al., 2021). Indirect solar dryers have main components and different auxiliaries' parts. The main parts include a solar air heater (solar collector), drying system (drying chamber), chimney, ducts for air supply, fans etc parts. Fans and blowers are mainly used if the dryer is a forced type of solar dryer (Devan et al., 2020).

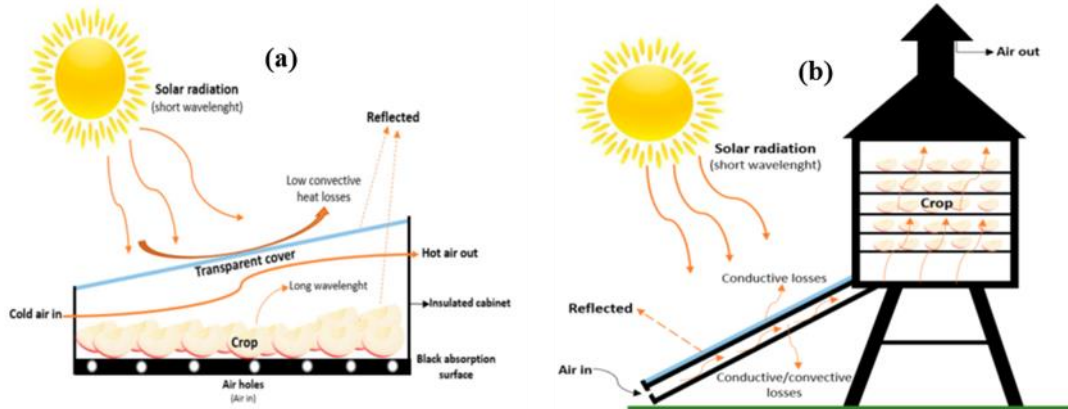


Fig. 2.7. Direct solar drying: (a) Indirect solar dryer, (b) (Fernandes and Tavares, 2024)

The modular solar dryers illustrated in Fig. 2.8, was designed and manufactured by Farkas (2013), are another type of solar dryer. These dryers are operated either by using natural ventilation of ambient air or artificial ventilation of ambient air when the photovoltaic module is applied or a combination of both. The dryers have three main parts. A drying cabin, air solar collector, and photovoltaic module with an electric fan are the three components. A drying cabinet with different trays is used to dry different products. The tray holders were designed to be used for both surface and bulk drying. An air solar collector that may be attached to the dryer and used to pre-heat the input air. It has a clear top, a plastic absorber inside, thermal insulation at the bottom, and a PV module with an electrical fan for artificial air circulation. The PV panel is mounted on the dryer's front side and has a variable inclination angle.

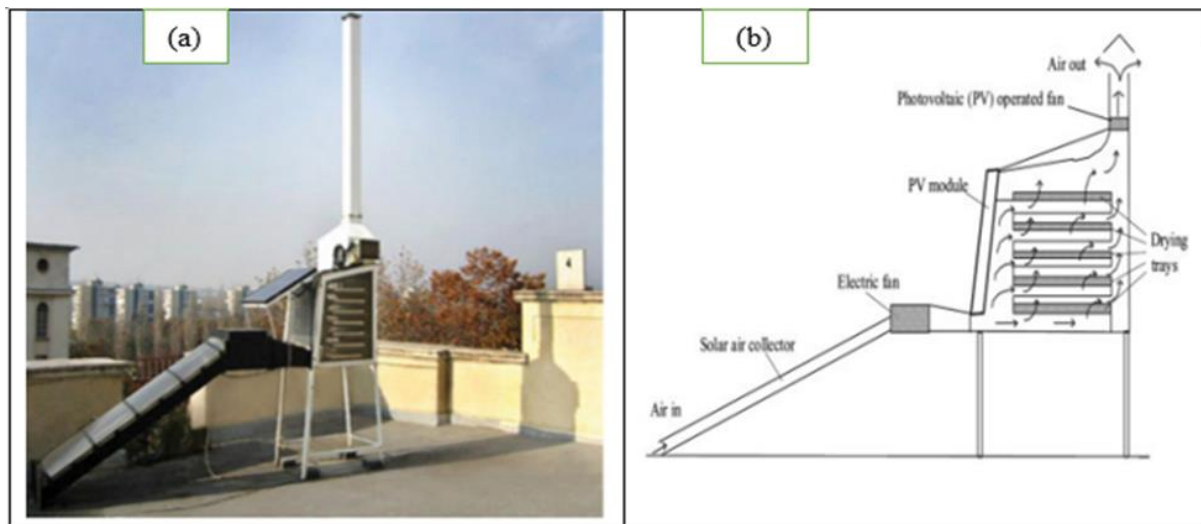


Fig. 2.8. Modular solar dryer: (a) picture, (b) scheme

The drying chamber, which is the core component of indirect solar drying systems and the primary focus of this thesis, is discussed in detail in the following sections.



### 2.3. Solar drying chamber

The drying chamber is an equipment where the product that needs to be dried is placed. Drying chambers can be used for a wide range of purposes. Curing, tempering, heating, burning in, and even long-term heating are all examples of drying or sterilization tasks where they can be found. The main drawback of a drying chamber is an uneven distribution of temperature to the products being dried. It is critical to have a temperature distribution that is entirely homogenous in order to achieve the most incredible drying results.

Numerous authors and researchers were actively engaged in designing, developing prototypes, manufacturing, and conducting experiments to evaluate the performance of solar drying chambers. Their goal is to optimize various methods to enhance the efficiency of these systems. However, as noted by Husham et al. (2018), the design of drying chambers is still an area of ongoing research aimed at achieving uniform drying and improving drying performance.

Sabareesh et al. (2021) identified several key parameters used in the design of solar drying chambers, including the mass flow rate of air in kg/s, the total mass of moisture removed from the product ( $m_w$ ) in kg, the enthalpy of vaporization of water within the product ( $h_{fg}$ ) in kJ/kg, the velocity of air at the collector exit, the length of the diverging branches at the chamber inlet, the angle of the air grills at the inlet, and the number of exit vents. Ndukwu et al. (2020) designed and developed a low-cost, wind-powered active solar dryer integrated with glycerol as thermal storage and evaluated its performance. The dryer was tested at temperatures ranging from 24 °C to 50 °C and relative humidity between 10% and 52%. The results indicated that drying with the active mixed-mode wind-powered fan solar dryer (AWPFS), combined with glycerol, required less time than drying with AWPFS alone or with a non-wind-powered solar dryer (PNWPS). Furthermore, pre-treating potatoes by dipping them in a salt solution and blanching for 30 seconds before drying enhanced the drying rate. Exergy efficiency ranged from 14.5% to 80.9% while drying efficiencies ranged from 25.03% to 31.5%.

Al-Neama and Farkas (2018) constructed and tested a solar drying chamber with five trays for drying apple products. The dryer chamber has dimensions of 0.50 m in length, 0.50 m in width, and 1 m in height. The result revealed that the temperature values in the five trays of the drying chamber increased over time, reaching peak values of 29.4 °C, 28.4 °C, 27.8 °C, 26.8 °C, and 25.5 °C, from the first to fifth, respectively, at 13:20. The corresponding maximum relative humidity in each tray at 10:00 was 38%, 39%, 44%, 48%, and 50%, from the first to the fifth tray. Al-Juamili et al. (2007) designed and conducted experiments using a solar drying system to dry apricots, grapes and beans. Based on the experimental results, it was concluded that the moisture content of apricots decreased from 80% to 13% in one and a half days, the moisture content of grapes decreased from 80% to 18% in two and a half days, and the moisture content of beans was reduced from 65% to 18% in just one day. The results indicated that the temperature of the air inside the cabinet had the most significant impact on the drying rate. In contrast, the effect of varying the air speed inside the cabinet was minimal and could be considered negligible.

Hao et al. (2021) proposed a dual-working medium drying system to address the limitations of traditional solar drying processes. The study used a flat-plate solar collector with a dual-

function hybrid dryer as a case study to determine the optimal air temperature management strategy for the drying chambers and assess the system's projected operating conditions. Traditional thermodynamics methods were employed to examine the impact of environmental factors on the performance of solar heating units. The study identified the effects of ambient temperature, solar radiation intensity, and the supply airflow of solar heating units on the outlet air temperature and collection efficiency. The most significant factor influencing the outlet temperature of the solar heating units was found to be ambient relative humidity. Additionally, five machine-learning techniques using Python software were applied to forecast the thermal performance of the solar heating units. The model achieved  $R^2$  values of 0.98 for training data and 0.94 for testing data.

Aissa et al. (2014) designed and operated a solar drying chamber to dry sponge cotton over five days in July 2008. The experiments were conducted under varying conditions, with ambient air temperatures ranging from 35.0 °C to 49.5 °C, drying air temperatures between 35.2 °C and 69.8 °C, solar radiation intensities from 30 to 1258 W/m<sup>2</sup>, and drying air flow rates from 0.016 to 0.08 kg/s. In each experiment, the mass flow rate of air remained constant throughout the day. The study investigated the variation of moisture ratio, drying rate, overall dryer efficiency, and temperature distribution along the drying chamber for different drying air temperatures and airflow rates. The results indicated that drying air temperature was the primary factor controlling the drying process. The air mass flow rate significantly influences overall drying performance, with overall efficiencies ranging from 1.85% to 18.6%.

Yassen et al. (2021) designed and investigated two novel solar dryers: the novel indirect solar dryer (NISD) and the novel mixed indirect solar dryer (NIMD), as shown in Fig. 2.9. The primary objective of the study was to evaluate the thermal performance of these dryers in comparison to a traditional indirect solar dryer (TISD). The three dryers were constructed and thermally tested as part of the experimental procedure. The NISD was a unique drying chamber featuring three absorbent surfaces, while the NIMD consists of a flat plate solar collector and the NISD. The results indicated that the air temperature at the entry of the drying chamber increased by 60% for the TISD and 68% for the NIMD. In the lower section of the drying chamber, the air temperature decreased by 35% for the NISD and increased by 39% for the NIMD relative to the TISD. In the upper section, the air temperature increased by 14% for the NISD and 49% for the NIMD compared to the TISD. The thermal efficiency of the NISD was 9% higher, and the thermal efficiency of the NIMD was 55% higher than that of the TISD. The improved thermal efficiency of the NIMD was attributed to the combined presence of the solar collector and drying chamber absorbers, which also contributed to better thermal uniformity throughout the drying chamber.

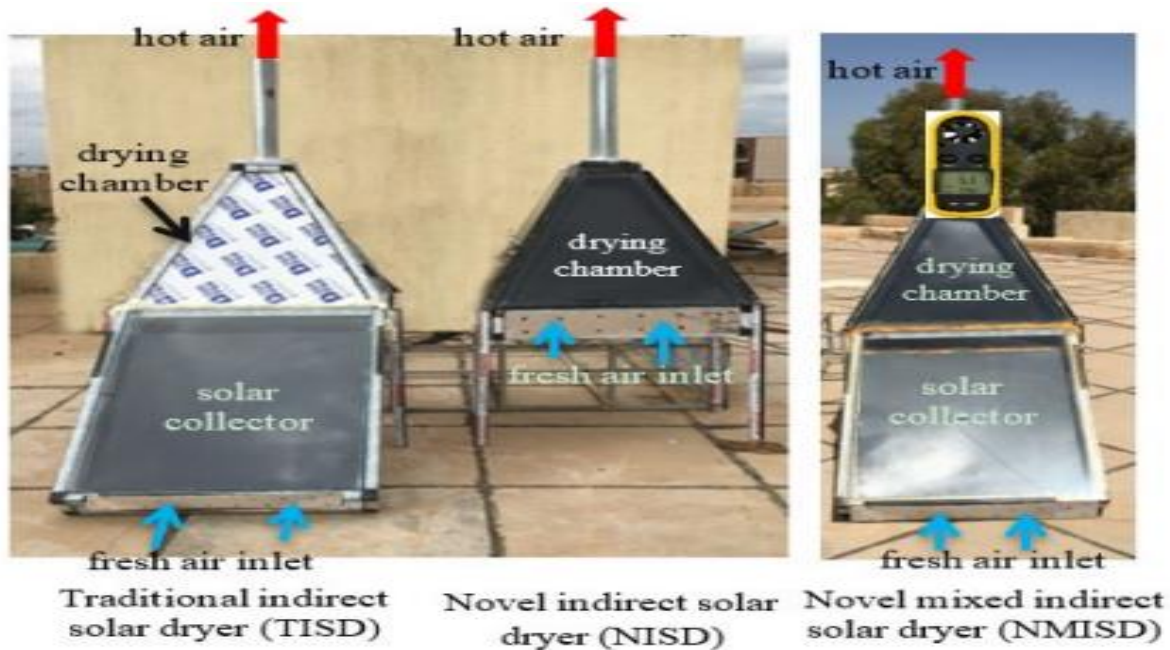


Fig. 2.9. The experimental set-up of innovative indirect solar dryers (Yassen et al., 2021)

Eltief et al. (2007) evaluated the performance of the drying chamber in a forced convective solar-assisted drying system, which consists of a v-groove collector, an auxiliary heater, and two variable-speed centrifugal fans. Temperature measurements were taken using K-type thermocouples, and solar radiation was recorded using an Eppley pyranometer. The drying temperature was identified as the most critical factor in the drying process. The temperature changes in the drying chamber were analysed using heat transfer principles, with formulas based on thermal effectiveness and the number of transfer units. These general equations describe the operation of the drying chamber in the solar drying system. The study concluded that the system's efficiency improves when the drying chamber is well-designed and suitably insulated.

Sabareesh et al. (2021) explored a novel approach for indirect forced convection solar drying of ginger, combining the use of liquid desiccant, supplied as droplets via an ultrasonic atomizer, for dehumidifying the air stream, and paraffin wax as thermal energy storage. The solar dryer had a drying chamber with a 1 kg loading capacity, used to dry fresh ginger with an initial moisture content of over 80%, which was reduced to nearly 10%. The study compared the performance of forced convection solar drying of ginger at airflow rates of 0.153 kg/s and 0.077 kg/s to open sun drying, both with and without air dehumidification, using liquid calcium chloride as a desiccant. At a flow rate of 0.153 kg/s, the drying process with liquid desiccant took 13 hours less than open sun drying and 9 hours less than drying without desiccant. At a flow rate of 0.077 kg/s, the moisture content was reduced to approximately 20%, saving 11 hours compared to open sun drying and 6 hours compared to drying without desiccant.

Jain and Tewari (2015) developed a solar crop dryer with thermal energy storage designed to maintain continuous drying of herbs, preserving their colour and flavour sensitivity, in Jodhpur, India. The dryer has a 12 kg capacity. Analysis conducted during June in Jodhpur revealed that the temperature in the drying chamber remained 6 °C higher than the ambient temperature even after sunlight hours, lasting until midnight. The economic performance of the dryer was

evaluated based on the optimum cost of raw materials and the product sale price, resulting in a return on capital of 0.65 and a simple payback period of 1.57 years.

Mishra et al. (2021) used solar drying with a 10 kg loading capacity. However, the developed dryer with a 10 kg capacity was tested at 30% loading (3 kg), i.e., the minimum expected loading, to avoid exaggerated results. The designed dryer was subjected to energy, exergy, economic, and environmental (4E) evaluations to determine its thermodynamic performance, financial feasibility, and environmental impact under natural convection and mixed-mode forced convection.

### **2.4. Performance evaluation of solar drying systems**

Numerous researchers have extensively evaluated the efficiency and performance of solar dryers based on a wide range of criteria. These criteria typically include drying rate, energy efficiency, moisture removal rate, product quality, energy consumption, environmental impact, and cost-effectiveness, among others. These evaluation methods are primarily grounded in the principles of the first law of thermodynamics, which focuses on the conservation and flow of energy. However, while the first law offers a foundational understanding of energy dynamics, it does not account for the quality of energy or the irreversibilities and losses within the system, highlighting the need for a more comprehensive analysis.

To overcome this limitation, the second law of thermodynamics, specifically through exergy analysis, offers a more comprehensive evaluation. Exergy analysis considers both the quantity and quality of energy used and lost during the drying process, providing deeper insights into thermodynamic efficiency and identifying opportunities for improvement. Together, these principles enable a more thorough understanding and optimization of solar drying systems for sustainable agricultural practices.

Fudholi et al. (2014), energy and exergy analyses are crucial for understanding and improving the efficiency of drying processes in thermal systems. Exergy analysis, in particular, plays a key role in identifying energy losses and optimizing system design, making it a powerful tool for enhancing overall performance and achieving optimal drying conditions. Panwar et al. (2012) exergy is an accurate measure of the grade or quality of energy and offers distinctive perspectives on the varieties, positions, and reasons behind inefficiencies, thus aiding in the identification of potential enhancements.

Exergy analyses are commonly conducted to identify the position, nature, and extent of thermodynamic inefficiencies in drying processes, employing principles from the second law of thermodynamics (Folayan et al., 2018). It provided an examination of the advanced exergy analysis, highlighting both its strengths and limitations (Morosuk and Tsatsaronis, 2013). The total exergy of a system ( $E_{sys}$ ) consists of a summation of physical exergy ( $E_p$ ), which is a deviation from the system's temperature and pressure; chemical exergy ( $E_c$ ), the system's chemical composition; kinetic exergy ( $E_{ke}$ ); the system velocity measured and potential exergy ( $E_{pe}$ ) is the system height measured about the environment (Tsatsaronis, 2007):

$$E_{sys} = E_p + E_{ke} + E_{pe} + E_c \quad (2.1)$$

There are two primary categories of losses in solar air heaters. The first category, external exergy losses, involves optical losses associated with capturing solar energy and losses resulting from heat transfer between the heater components and the surrounding environment. The second category, internal exergy losses or exergy destruction, includes losses due to fluid friction, the absorption of solar radiation by the absorber plate, and heat transfer to the working fluid (Matheswaran et al., 2018).

Exergy analysis of the solar drying system is conducted by assessing the exergy input, output, and losses of different components, including trays and the drying chamber (Dincer, 2011). The fundamental approach to conducting an exergy analysis of a drying chamber involves establishing the exergy values at steady-state conditions and assessing the exergy changes throughout the process (Chowdhury et al., 2011). The variance in flow exergy from the inlet to the outlet of the drying chamber equates to the combined total of thermal exergy loss and exergy destruction resulting from irreversibilities (Rabha et al., 2017). Exergy analysis is valuable for assessing the thermodynamic performance of a system, designing more efficient solar thermal systems, and optimizing drying processes. It provides insights into the quality of energy, the extent of energy losses, and the influence of surrounding factors (Mugi and Chandramohan, 2021b).

### **2.5. Characterizing the drying behaviour of agricultural products**

Drying is a highly complex process involving simultaneous heat, mass, and momentum transfer, as well as material transformations. This makes theoretical models inadequate for accurately predicting drying times due to a lack of understanding of the microscopic mechanisms involved (Panagiotis et al., 2015). In addition to this, as stated by Bains and Langrish, 2007, interruptions or changes in drying conditions, such as temperature variations, can affect the moisture loss from food materials, leading to different drying profiles. Therefore, it is essential to choose a suitable drying model that can accurately predict drying kinetics and account for the impact of these varying conditions on moisture loss. Kaleta and Górnicki (2010) mathematical modelling is a key aspect of drying technology that helps design engineers choose optimal operating conditions and appropriately size drying equipment to achieve desired performance.

Therefore, it's essential to interpolate or predict the events during the interruption using simulation or mathematical modelling techniques.

#### *2.5.1. Modelling the drying kinetics of agricultural products*

Mathematical modelling of drying kinetics is essential for accurately predicting the moisture content of food materials at any stage of the drying process, which in turn supports the optimization, quality assurance, and effective control of the drying operation (Gamli, 2014). The mathematical modelling of the drying process of agricultural products is a crucial tool that allows for the anticipation of drying efficiency, drying rate, drying behaviour, the reduction of time and costs in practical drying methods, and the development of suitable drying equipment and processes. This approach ultimately supports the optimization and advancement of drying technologies for agricultural products (Siqueira et al., 2013; Kaleta et al., 2013). Thus, accurate

predictions contribute to ensuring optimal product quality and minimizing process time (Kaleta et al., 2013).

### 2.5.2. Thin layer drying models

Thin-layer drying is the drying of a single thin layer of particles or slices, as shown in Fig. 2.10, in which the temperature distribution can be considered to be uniform, and lumped parameter models can be used (Panagiotis et al., 2015). The thin layer drying equation is crucial in the drying simulation. The equation depicts moisture exchange between a thin layer of drying product and the ambient air. A thin layer indicates the spatial area that is chosen infinitesimally small, within which fluctuations in humidity and temperature of the air can be assumed linear from a mathematical standpoint (Wang et al., 2004). Thin layer drying equations are used to estimate drying times and to generalize drying curves for a variety of items (Menges and Ertekin, 2006). Thin layer equations offer a comprehensive framework for understanding the drying process, regardless of the controlling mechanism involved. They are utilized to estimate drying durations for different products and to create generalized drying curves (Toğrul and Pehlivan, 2004).

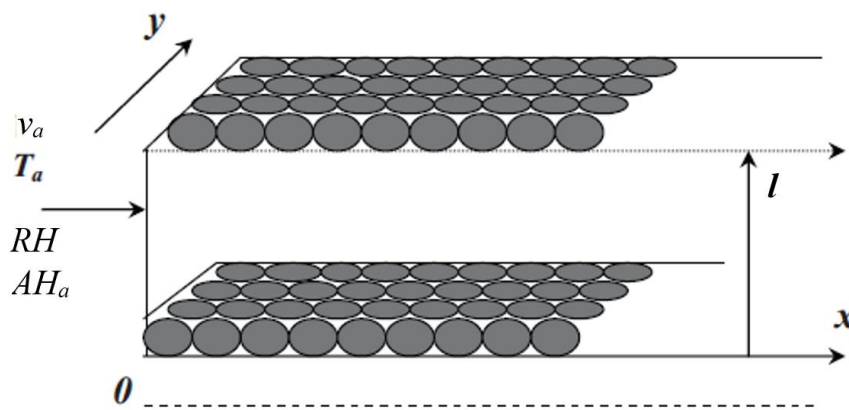


Fig. 2.10. Illustrative representation of deep bed, thin layer drying, and thin layer stacked (Ben Mabrouk et al., 2012)

Mathematical models that illustrate the drying behaviour of agricultural products are generally categorized into three main groups: namely: empirical, semi-theoretical and theoretical models (Kaleta et al., 2013). Theoretical drying equations are focused on the internal resistance to moisture transfer within the material. At the same time, empirical and semi-theoretical models also account for the external resistance to moisture transfer between the drying air and the product surface (Inyang et al., 2018). The theoretical approach employs either diffusion equations or simultaneous heat and mass transfer equations. In contrast, the semi-theoretical approach relies on approximations of these theoretical equations and empirical equations, validated by their effectiveness in fitting experimental data (Akpınar and Bicer, 2005).

Various researchers have developed numerous theoretical, semi-theoretical, and empirical thin-layer equations to model the drying process. Many of them used different types of thin layer models to describe and predict the drying behaviours of agricultural products, and the corresponding statical methods were used to select the thin layer models. For instance, Bagheri et al. (2013) modelled the drying behaviour of tomato slices dried in a laboratory solar drier.

Nine thin-layer drying models were fitted to the experimental moisture ratios of the samples. Tomato slices with thicknesses of 3, 5, and 7 mm were dried at air velocities of 0.5 and 1 m s<sup>-1</sup>. To select the best acceptable moisture ratio model, statistical parameters such as  $R^2$ ,  $RMSE$ , and  $\chi^2$  were used, and the Page model was determined to be the best. Toğrul and Pehlivan (2004) evaluated mathematical models used to describe thin layer drying kinetics of some fruits (i.e., grapes, peaches, figs and plums) under an open-air sun drying process. The diffusion model approximation for apricots (non-pre-treated or SO<sub>2</sub>-sulphured) and figs, the modified Henderson and Pabis model for apricots (NaHSO<sub>3</sub>-sulphured), grape, and plum, and the Verma model for peach were found to best models to describe drying behaviours of the fruits. Borah et al. (2015) studied the drying kinetics of whole and sliced turmeric rhizomes (*Curcuma longa* L.) carried out in a solar conduction dryer. Lewis, Page, Modified Page and Henderson and Pabis mathematical models were applied to simulate the drying behaviour of turmeric rhizome. Hence, the Page model was found as the best-fitted thin layer drying model when simulation was done for all the drying data.

Hussein et al. (2016) used a hybrid drying method, solar and open sun drying, to study the thin layer of the tomato slices. The goodness of fit to the experimental data was optimized using six thin layer drying models (Page, Logarithmic, Henderson and Pabis, Newton (Lewis), Wang and Singh, and Parabolic).  $R^2$ ,  $\chi^2$  and  $RMSE$  were used to compare the models. When compared to conventional drying processes, the hybrid drying approach dried the tomato slice faster. In a hybrid drying process, tomato slices of 4, 6 and 8 mm thickness were dried from 94.22 to 10% (wet basis) for 300, 360, and 420 minutes, respectively. However, solar and open sun drying took 420, 510, 600, 510, 630, and 840 minutes, respectively. Only a falling rate drying period was used for the drying. In comparison to other models, the Page model was shown to suit the experimental data better. The practical moisture diffusivity values in hybrid dried slices were found to be between  $2.00 \cdot 10^{-10}$  and  $5.84 \cdot 10^{-10}$  m<sup>2</sup>/s,  $1.37 \cdot 10^{-10}$  and  $4.40 \cdot 10^{-10}$  m<sup>2</sup>/s in solar-dried slices, and  $1.33 \cdot 10^{-10}$  and  $4.01 \cdot 10^{-10}$  m<sup>2</sup>/s in open sun-dried tomato slices of 4 to 8 mm thickness.

Sobukola et al. (2007) investigated thin layers of crain-crain (CC), fever (FV), and bitter (BT) leaves cultivated in Abeokuta, Nigeria, were dried in the open sun. The drying process occurred during the falling rate period, and the drying curves revealed no constant rate period. Eight thin-layer mathematical drying models were compared using  $R^2$  and  $RMSE$ . As a result, the drying curves of the three leaves were satisfactorily described by Midilli et al. (2002) model, with  $R^2=0.9980$ ,  $\chi^2 = 2.0 \cdot 10^{-4}$  and  $RMSE = 1.09 \cdot 10^{-2}$  for CC leaves,  $R^2$  of 0.9999,  $\chi^2 = 2 \cdot 10^{-6}$  and  $RMSE = 1.11 \cdot 10^{-3}$  for FV leaves, and  $R^2 = 0.9998$ ,  $\chi^2 = 1.9 \cdot 10^{-5}$  and  $RMSE = 3.3 \cdot 10^{-3}$  for BT leaves. The effective diffusivity of CC, BT, and FV leaves was determined as  $52.91 \cdot 10^{-10}$ ,  $48.72 \cdot 10^{-10}$ , and  $43.42 \cdot 10^{-10}$  m<sup>2</sup>/s, respectively.

Dissa et al. (2009) compared the thin-layer drying kinetics of hot-air technologies such as convection oven drying (OVD), uncontrolled sun drying (UAD), and modified ventilation greenhouse solar drying (MVD). The impact of these drying procedures on the colour, rehydration properties, and microstructure of Tommy Atkins mango slices was also studied. Mango slices of three various thicknesses were used in the experiments: 3 mm, 6 mm and 9 mm. Midilli et al. (2002) model's parameters succeed the best model with  $R^2 = 0.9810 - 0.9981$ ,

$\chi^2 = 1.465 \cdot 10^{-6} - 3.081 \cdot 10^{-5}$ , and  $RMSE = 0.0003 - 0.0004$ ). Furthermore, raising the slice thickness to 6 mm and 9 mm lengthened the drying durations, resulting in substantial changes in sample quality, such as total colour (E), rehydration, and microstructure. *UAD*-dried samples experienced the most colour change and the highest rehydration ratio values when compared to *OVD*- and *MVD*-dried samples. The *UAD*-dried samples' surfaces also developed a more porous structure with noticeable fissures. *MVD* was found to be a suitable alternative method for drying 3 mm mango slices on a wide scale based on the findings.

Yildiz et al. (2001) experimented to study the thin-layer behaviour of sultana grapes grown in Antalya, Turkey. An indirect forced convection solar dryer was used during the experiment. An electric fan drove air heated by the solar air heater through the device. Twenty-two experiments were conducted to investigate the influence of drying air temperature and velocity on the thin-layer drying of Sultana grapes. Eight distinct thin-layer mathematical drying models were tested to estimate solar drying curves. According to the findings, a two-term drying model with an  $R^2$  of 0.979 was selected.

Akbulut and Durmuş (2009) examined both experimentally and theoretically by the drying parameters of mulberry grown in Elazığ using a solar dryer system. The drying tests were carried out at seven different drying mass flow rates ranging from 0.0015 to 0.036 kg/s. The drying time decreased when the drying mass flow rate was increased, according to the results of the drying experiments done at various drying mass flow rates. A new mathematical model of thin-layer solar drying of mulberry samples is also presented in this work. To determine the most appropriate form of drying curves, ten different mathematical models from the literature and a new model were applied to the experimental data and compared based on  $R^2$  and  $\chi^2$ . Thus, the Midilli et al., (2002) and newly designed models were found to be superior to the other models in terms of representing drying characteristics. The effective moisture diffusivity values were  $3.47 \cdot 10^{-12} - 1.46 \cdot 10^{-9} \text{ m}^2/\text{s}$ .

Vijayan et al. (2016) designed solar dryer with indirect forced convection and a porous sensible heat storage medium. They modelled and analyse the performance analysis of thin layer drying of bitter melon. Different air mass flow rates were used in the experiments, and other drying models were used to explain the drying behaviour of sliced bitter melon. The results indicate that the system effectively reduces the moisture content of bitter melon from 92% to 9% (wet basis) within 7 hours, which is significantly faster than the 10 hours required by open sun drying. The system demonstrated a maximum specific moisture extraction rate of 0.215 kg/kWh at a mass flow rate of 0.0636 kg/s, with a particular energy consumption of 4.44 kWh/kg. Additionally, the system's efficiency metrics were notable, with a collector efficiency of 22% and a drying efficiency of 19%, showcasing its potential for energy-efficient and time-effective drying processes. The Two-term model and the Midilli–Kucuk (2003) model have been identified as the most effective mathematical models for describing the drying behaviour of specific samples under the indirect solar dryer and open sun drying, respectively.

### *Modelling the drying behaviour of apple*

Several studies had analysed the drying of apple slices using various solar drying methods and thin-layer models. For instance, Stegou-Sagia and Fragkou (2018) investigated slices with a



thickness of 10 mm using a solar-assisted drying technique, with the logarithmic model selected to describe the drying behaviour. Demirpolat (2019) studied the drying of apples with 15 mm thickness, with the Midilli and Kucuk (2003) identified as the most suitable fit for the drying process. The research highlighted that various factor, including the inlet and outlet temperatures, the temperature and humidity within the drying room, and the air velocity, influenced the efficiency of the collector. The study utilized statistical tools such as *RMSE*,  $R^2$ , and  $\chi^2$  to evaluate the model's performance.

Atalay et al. (2017) utilized a solar dryer equipped with thermal energy storage and used apple slices with a thickness averaging  $5 \pm 2$  mm. The models were compared using the Nelder-mead least squares method in Java language. The diffusion approximation model was chosen to analyse the drying kinetics. Blanco-Cano et al. (2016) examined 2.4 mm thick slices in an indirect solar dryer, and Wang and Singh's model was selected. The study demonstrated that the predicted outcomes of the drying models closely matched the experimental measurements of apple drying under variable conditions in a lab-scale solar dryer. The results showed a strong agreement, with deviations of less than 10%, attributed to the thermal inertia of the apple samples.

Noori et al. (2021) studied apple slices of approximately  $5 \pm 0.1$  mm using both open sun and cabinet solar dryers. The Approximation Diffusion, Verma et al. (1985) model and Midilli and Kucuk (2003) models demonstrated a better fit collected experimental data. The performance of these mathematical models was assessed by comparing key statistical indicators:  $R^2$ ,  $\chi^2$ , and *RMSE*. Das and Akpınar (2020) explored the drying of 14 mm thick slices using a solar dryer with and without a solar tracking system.  $R^2$ ,  $\chi^2$  and *RMSE* were used to evaluate the quality of the fit. Thus, the Midilli et al., (2002) model was selected to represent the thin-layer drying behaviour of apple slices based on the listed statistical tools. Aktaş et al. (2009) used a heat pump dryer in combination with a solar dryer to dry 4 mm thick apple slices. They employed *SEE* and  $R^2$ , selecting the Henderson and Pabis model to describe the drying behaviour *MR* of the given sample.

### 2.6. Modelling of the solar drying chamber

Modelling and simulation techniques are vital in executing an ideal strategy for dryer process control, building a good design for a new dryer construction, or evaluating the performance of an existing set-up. The method of modelling is obviously determined by the goal for which the model will be employed. A physics-based approach is recommended for dryer design and performance analysis, whereas black-box models identified on the basis of data can be successfully implemented for process control purposes (Farkas et al., 2000).

The application of computational fluid dynamic tools in the drying process of agricultural products is of great importance; it helps to develop and analyse the drying parameters of a particular product. The *CFD* tool acts as a virtual sensor for examining flux concentration and flow distributions within a computational domain. Through *CFD* application, parametric studies and geometric changes of drying equipment can be done during the design stage, hence building confidence in achieving better design solutions and quality of food products (Norton et al., 2010). The *CFD* tool makes possible prediction of temperature distributions and airflow

simulation within a dryer. ANSYS, MATLAB, and COMSOL are some of the well-known advanced *CFD* tools currently used to describe the drying process.

Computational fluid dynamics has become one of the most powerful tools in modern research. It is widely adopted across various fields due to its efficiency and cost-effectiveness in solving engineering problems related to fluid flow and heat transfer. As described by Getahun et al. (2021), *CFD* modelling and simulation techniques are critical for developing efficient solar dryers and analysing and predicting the performance of various types of sun-drying systems that protect food quality.

Many authors used *CFD* for different purposes. The major problem with using solar dryers is the drying chamber's inability to produce uniform drying, resulting in a nonhomogeneous product. One of the main advantages of *CFD* is that it investigates the distribution of drying parameters inside the drying chamber. For instance, Al-Kayiem and Gitan (2021) designed a prototype of a hybrid solar-thermal dryer and manufactured the prototype with three separate chambers, and each has one angular-movable tray for experimental measurements to test the drying uniformity of the dryer. The computational model, which was developed in ANSYS fluent software, was used to investigate the drying uniformity of the dryer. The simulation results were validated by comparing the experimental results and inspected using statistical analysis. The influence of air velocity and turbulence intensity distribution inside the drying cabinet at different tray inclination angles of ( $0^\circ$ ,  $10^\circ$ ,  $20^\circ$ ,  $30^\circ$  and  $35^\circ$ ) was studied. Based on experimental and computational results, the tray with a  $30^\circ$  inclination achieves the best uniformity. According to statistical analysis, roughly 93% of velocity frequency is at  $0.7 - 0.8$  m/s air velocity level for  $30^\circ$  tray inclination (see Fig. 2.11). Hence, maximum drying uniformity level can be performed by a novel multi-chamber drying cabinet (MCDC) with a  $30^\circ$  tray inclination.

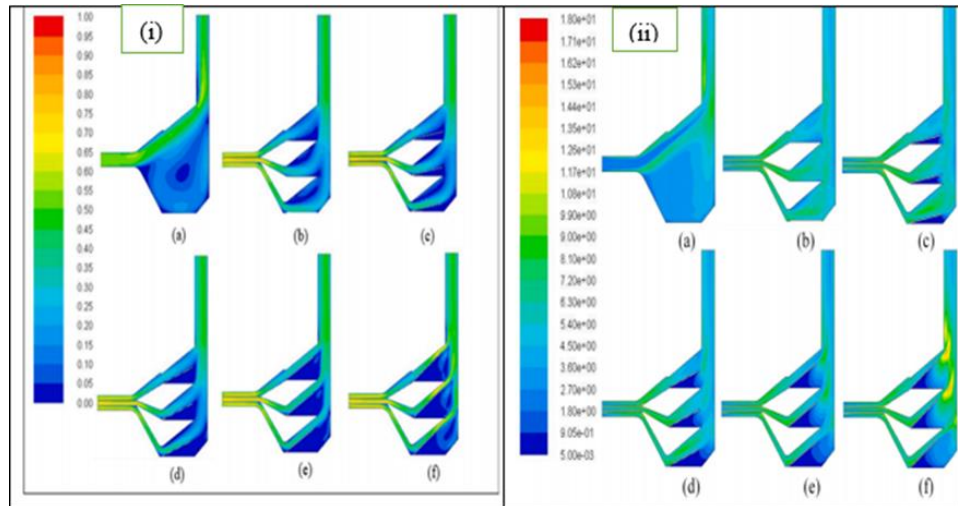


Fig. 2.11. (i) Velocity contours for all considered cases: (a) base case, (b) at  $0^\circ$ , (c) at  $10^\circ$ , (d) at  $20^\circ$ , (e) at  $30^\circ$  and (f) at  $35^\circ$  tray angles; (ii) Turbulence intensity contours for all considered cases: (a) base case, (b) at  $0^\circ$ , (c) at  $10^\circ$ , (d) at  $20^\circ$ , (e) at  $30^\circ$  and (f) at  $35^\circ$  tray angles

Benhamza et al. (2021) applied computational fluid dynamics and image processing to explore and optimize the drying uniformity analysis of an indirect solar dryer. A two-dimensional quasi-steady numerical model was created and experimentally validated. Ansys fluent software was used to test the effect of adding a passive chimney and three mass flow rates on the drying air distribution. The result showed that the air temperature uniformity was improved significantly by 21.7 and 20.3% for the mass flow rate of  $\dot{m} = 0.0141$  and  $0.06$  kg/s, respectively, while it was slightly increased for  $\dot{m} = 0.08$  kg/s. The average temperature increased by 16, 11 and 8 K for the mass flow rate of  $\dot{m} = 0.0141$ ,  $0.0636$ , and  $0.0872$  kg/s, respectively. Using a solar chimney improved the drying air temperature by  $7$  °C.

Husham et al. (2018) reviewed factors affecting uniformity and its enhancement methods of solar thermal drying, the performance of solar-assisted desiccant systems for dehumidification of drying air, the effect of geometrical parameters on drying performance, and the drying performance of different products. So, from the reviewed results, temperature, humidity and velocity influence drying uniformity, and it can be increased by integrating a dehumidification system and/or optimizing the drier design. In the case of drying, the performance of desiccant systems was influenced by the desiccant material, dehumidifier design, and regeneration mechanism used. On the other hand, solar dryer performance or design is highly related to drying chamber geometrical parameters, numerous drying chambers, and dryer design modelling and optimization.

Babu et al. (2019) used *CFD* to evaluate several airflows drying chamber arrangements in the tray dryer. Four different optimum designs of drying chambers for drying leaves were built and theoretically assessed using Ansys fluent software. The research tests evaluate and present the limiting air-side pressure drops as well as the realized dried output from the four setups. The optimal arrangement and construction were also discussed. The trays increased the dryer's performance in the series. The pressure drop and moisture dehydration were also evaluated using *CFD*. Tarigan (2018) assessed the mathematical modelling and simulation of a solar agricultural dryer with a backup biomass burner and thermal storage. The solar collector and drying chamber are simulated using thermodynamic and numerical models, while the backup heater (biomass burner) is simulated using *CFD* simulation. The presence of a glass cover on a solar collector significantly increases the collection's temperature; however, increasing the number of glasses covers from one to two has no significant effect on the temperature. The average drying air temperature in the drying chamber was  $56$  °C, which is adequate for the drying of agricultural products, according to the *CFD* simulation.

Sonthikun et al. (2016) designed and constructed a solar-biomass hybrid dryer for natural rubber sheet drying. A solar collector, a drying chamber, a heat exchanger, and a biomass furnace make up the dryer. In a novel drying chamber design, a computational fluid dynamics technique was employed to predict temperature and airflow distributions. In terms of statistical characteristics, the simulated findings for temperature were highly close to experimental values. To confirm the utility of air-circulating fans, a *CFD* simulation of airflow distribution inside a solar biomass hybrid dryer is performed. The solar-biomass hybrid dryer was put to the test by drying 100 sheets of natural rubber. In 48 hours, the moisture content of the rubber sheet is reduced from  $34.26\% - 0.34\%$ , resulting in a significant reduction in drying time and

biomass usage. The natural rubber sheet's colour and texture were observed more than the usual smoke rubber drying.

Ashfaq et al. (2017) designed and developed a new dryer to overcome uneven air distribution issues of heated air within the drying chamber. ANSYS-Fluent *CFD* model was used to simulate a newly built dryer with the unique feature of a central airflow channel for uniform air distribution in the drying chamber. The newly developed solar-assisted paddy dryer was shown to be capable of producing uniform air dispersion along the length of the drying chamber based on numerical simulations and experimental results. As a result, because air dispersion has a substantial impact on product quality for uniform drying, this design would ultimately result in good-quality drying. Finally, this method increased the paddy dryer's overall performance.

Rosli et al. (2021) made a simulation to select the best configuration of drying chamber tray arrangement for better distribution of velocity and temperature to dry marine products. As a result, the layouts of five trays were investigated to see which one provided the best homogeneity of airflow distribution within the drying chamber. The homogenous air flow in the drying chamber was analysed using *CFD* simulation in a steady state condition. To confirm that the process is correct, a validation is performed by comparing the data produced from the literature research *CFD* simulation. Then, using *CFD* simulations, the drying chamber with various tray layouts is simulated to provide velocity and temperature distributions at nine displayed places on trays. Based on the findings, it was determined that design (a) and (d) were the best for uniformity since there was less air flow difference for each point supplied, resulting in more distribution uniformity as shown in Fig. 2.12.

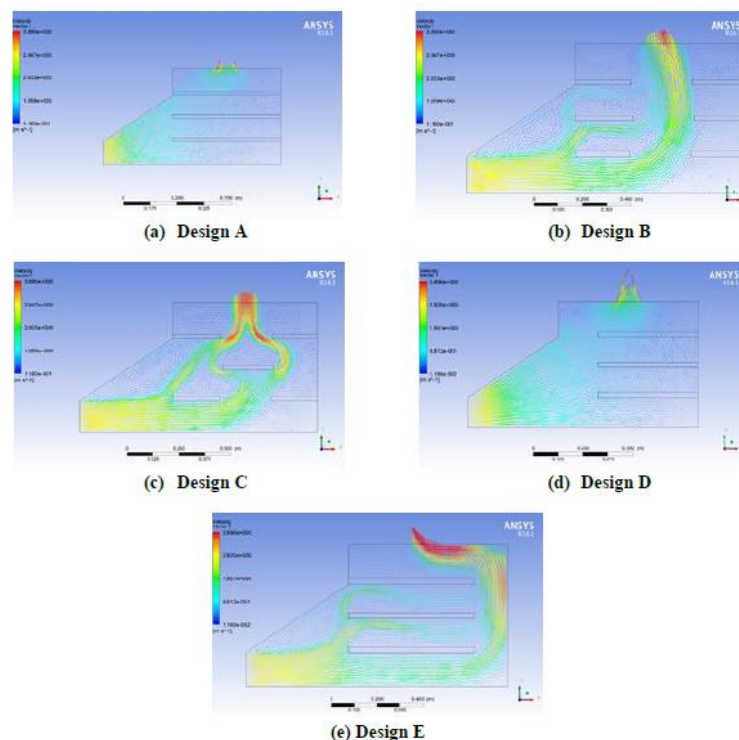


Fig. 2.12. Design of drying chamber for five variation configurations of trays and vector profiles of air flow velocity distribution using *CFD* simulation (Rosli et al. (2021))

Zoukit et al. (2019) simulated, designed and experimental performance evaluation of an innovative hybrid solar-gas dryer and a new configuration of a hybrid solar-gas dryer was proposed and designed. In the proposed arrangement, instead of direct heating, which is commonly used in gas dryers, an original indirect air heater was contemplated, where the flue gases exhaust outside the drying chamber, avoiding their diffusion in the product. A numerical simulation of a hybrid solar-gas dryer operating under forced convection with an air mass flow rate of 0.025 kg/s is presented in this research. The temperature and humidity thresholds in the chamber, as well as the heat dispersion, were all simulated. The thermal efficiency of the dryer was calculated in three modes: solar mode (SM), gas mode (GM), and hybrid mode (HM). *CFD* models found appropriate results for drying a variety of local items efficiently. The temperature and relative humidity were in the proper ranges for drying a variety of agricultural products, according to experimental and simulation data. Indeed, the average drying temperature and relative humidity were 25 °C and 80 °C, respectively, and 31.3 - 6.2%. For *SM*, *GM*, and *HM*, the maximum dryer efficiencies were found to be around 42%, 37%, and 40%, respectively.

Madadi Avargani et al. (2023) examined the effectiveness of an indirect solar dryer for drying diverse materials under varied operational settings as illustrated in Fig. 2.13. The system comprises a solar air collector with a v-corrugated absorber plate and a drying chamber featuring four perforated plates. The investigation involves complex multiphysics processes, including fluid dynamics, simultaneous heat and moisture transfer, and optical analysis of the SAH under typical daytime conditions. A practical computational fluid dynamic model was proposed to analyse the system's performance.

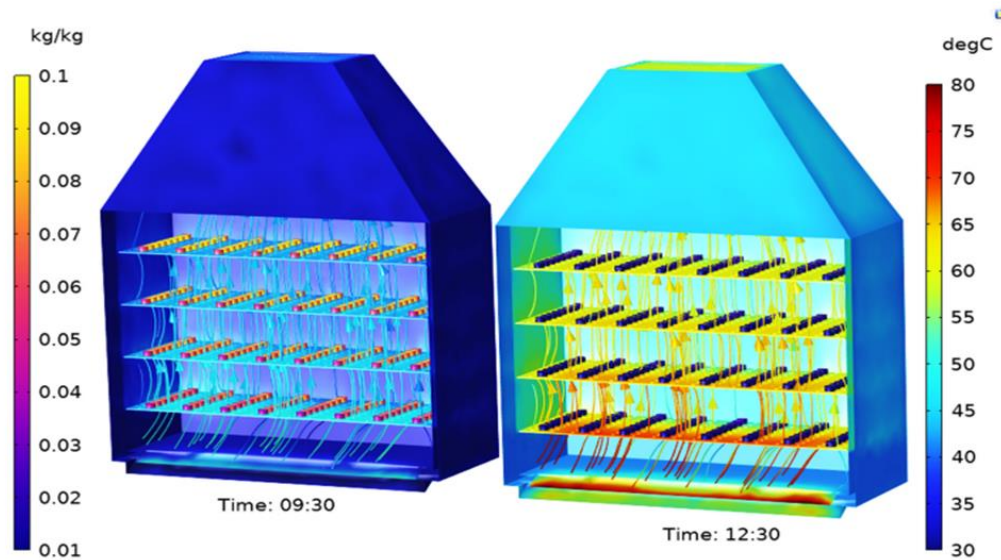


Fig. 2.13. Temperature contours, airflow patterns within the drying chamber, and moisture distribution across the trays observed during okra drying (Madadi Avargani et al., 2023)

## 2.7. Optimization of solar drying chambers

Solar dryers are an essential technology for efficient and sustainable drying of agricultural and industrial products. However, a common challenge in their operation is the issue of uneven

airflow within the drying chamber, which leads to non-uniform drying, reduced product quality, and increased energy consumption. To address this, optimization techniques can be applied to improve airflow uniformity, enhance heat distribution, and ensure consistent drying.

The optimization of solar dryers focuses on determining the ideal combination of operational parameters to achieve peak performance. Advanced techniques, such as Artificial Neural Networks (ANN), Genetic Algorithms (GA), Response Surface Methodology (RSM), Particle Swarm Optimization (PSO), and the Taguchi method, have been utilized to model solar drying processes and equipment, enabling precise prediction of optimal configurations. Technological advancements have further driven the development of innovative solar dryer designs, ensuring superior efficiency and performance (Joshi et al., 2019). This study concentrates on the implementation of the Taguchi method.

#### *Optimization using the Taguchi approach*

Sahu et al. (2023) the Taguchi method is a highly regarded approach for experimental design (DOE) and optimization, extensively applied across diverse industries and engineering disciplines. It systematically analyses various design factors and parameters, identifying the optimal combination to achieve desired performance targets. By selecting the most effective control factors, the method minimizes the number of experimental trials while maximizing efficiency. Davis and John (2018), the Taguchi method stands out over other methods due to its ability to optimize multiple factors simultaneously with fewer experiments, offering simplicity and versatility for engineering applications. It involves setting objectives, selecting control parameters, designing experiments using orthogonal arrays and analysing results through the signal-to-noise (S/N) ratio, making it a powerful optimization tool.

Taguchi method is a practical approach to experimental design that reduces the number of experiments required based on the given control factors. Each experiment consists of a specific level for each control factor, and the combinations of these levels are determined using predefined orthogonal arrays. Afterwards, each experiment is repeated several times, with the result from each replication referred to as the process response. The responses from all experiments are then converted into a signal-to-noise (S/N) ratio for comparison. The experiment with the highest  $S/N$  ratio identifies the optimal levels of the control factors (Nowzari et al., 2020). Taguchi method employs orthogonal arrays (OAs) from experimental design theory to efficiently analyse a large number of variables with fewer experiments (Abbasi et al., 2014). The orthogonal arrays (OA) determined using Eq. (2.2) (Sahu et al., 2023):

$$OA = L_n \cdot A \cdot F \quad (2.2)$$

where  $L_n$  represents the total number of experimental or test runs,  $A$  indicates the levels of the factors or variables, and  $F$  refers to the number of factors.

Taguchi method involves creating orthogonal arrays to systematically evaluate a set of parameters, including certain input variables. The experimental results are then converted into  $S/N$  ratios to assess performance. The  $S/N$  ratio is categorized into three types: larger-the-better, smaller-the-better, and nominal best (Rashid, 2023). Chauhan et al. (2017), the higher-the-better approach is used when the objective is to maximize a parameter, while the lower-the-

better approach is applied when minimizing a parameter is desired. In contrast, the nominal-the-best approach is suitable for scenarios where the objective must be maintained at a specific target value to achieve optimal performance.

### **2.8. Economic analysis**

The economic viability of a drying system is a critical factor that plays a decisive role in convincing producers to adopt the system, irrespective of the specific drying method it employs. Financial considerations often outweigh other aspects, as they directly impact the feasibility and profitability of the technology for the end user (Jahromi et al., 2022). Economic analysis serves as a crucial factor that must be considered, as it helps determine the overall costs linked to a drying system. It also enables the calculation of the system's payback period, offering insight into the time required to recover all incurred expenses (Sethi et al., 2021). The economic viability of a solar drying system is determined by both the capital (investment) cost and production costs. The capital investment of the dryer encompasses expenses such as the solar collector, drying chamber, fan, various sensors, construction, installation, and other related costs. Production costs, on the other hand, include expenditures for fresh materials, electricity, biomass fuel, labour, maintenance, and depreciation (Yahya et al., 2018).

Many authors assess the economic viability of solar drying systems using various parameters. Simo-Tagne and Ndi-Azese (2021) stated that to conduct a thorough analysis of a solar dryer project, three key financial concepts should be considered: annualized cost, life cycle savings, and payback period. Mohammed et al. (2020) used economic performance parameters, such as the annualized cost of drying, payback period, and net present value, to assess the commercial sustainability of solar dryers. Philip et al. (2022) analysed the economics of greenhouse solar dryers using three methods. Namely, annualized cost technique, life cycle change and payback period analysis; annualized cost technique compares solar and electrical drying costs but struggles with fluctuating fuel prices. Life cycle savings provide a more accurate long-term assessment by calculating present-value savings over the dryer's lifespan. Payback period analysis measures how quickly the initial investment is recovered, appealing to users seeking quick returns. While each method has advantages, life cycle savings is the most comprehensive for evaluating economic viability. Aniesrani et al. (2024) used net present value and cost-benefit ratio to analyse the financial aspect of solar dryers, solar-hybrid and infrared dryers.

### **2.9. Summary of literature review**

Drying play's great role in post harvesting stage of agricultural products in many ways. Drying using open sun was exercised by human's long time ago. Nevertheless, such type of mechanisms has several drawbacks. So, the problems of open sun drying are solved by sing solar dryers. Solar dryers are economically feasible and environmentally friendly drying methods in recent times. Solar drying can be done either directly or indirectly. Indirect solar dryers have three main components in common. These components are solar collector, drying chamber and chimney.

Accurate modelling is crucial for predicting drying kinetics, optimizing conditions, and ensuring product quality. Thin-layer drying models, which assume uniform temperature



distribution, are widely used to estimate drying times and generalize drying curves for various agricultural products. These models are categorized into empirical, semi-theoretical, and theoretical types, each addressing different aspects of moisture transfer.

The evaluation of solar drying systems is a fundamental step in the drying process and can be conducted using analysis methods such as energy and exergy analysis. Energy analysis primarily examines energy conservation by assessing energy and mass balances. However, it does not account for energy quality or system losses. To overcome this limitation, exergy analysis is employed. Based on the second law of thermodynamics, exergy analysis evaluates both the quantity and quality of energy, offering a deeper understanding of the thermodynamic efficiency of drying systems. This approach helps identify energy losses and optimize system performance more effectively.

Modelling and simulation techniques play a crucial role in optimizing dryer process control, designing new dryers, and evaluating existing setups. Physics-based models are preferred for design and performance analysis, while black-box models are effective for process control. *CFD* tools, such as Ansys and COMSOL, helps to analyse drying parameters, airflow distribution, and temperature uniformity, leading to improved dryer designs and food quality.

Taguchi method systematically analyses design factors to identify optimal combinations, minimizing the number of experiments while maximizing efficiency. It uses orthogonal arrays and signal-to-noise ( $S/N$ ) ratios to evaluate performance, with three  $S/N$  ratio types: larger-the-better, smaller-the-better, and nominal-is-best. The economic analysis is crucial for assessing the economic viability and profitability of drying systems, particularly solar dryers. Various authors have employed different financial metrics to evaluate the commercial sustainability of such systems.

The reviewed literature on solar drying systems reveals several critical limitations. Many studies lack clear discussions of their own limitations and fail to suggest directions for future research, which impedes progress in the field. Evaluations of thin-layer drying models tend to rely heavily on basic statistical metrics such as  $R^2$ ,  $RMSE$ , and  $\chi^2$ , while neglecting more advanced and robust validation methods. Additionally, research has been disproportionately focused on drying fruits, particularly apples and apricots, with insufficient attention given to leafy vegetables, high-moisture crops, and animal products like fish and other meats. Some studies validate their simulations only by comparing them with previous results rather than conducting independent experimental validation, which may reduce the reliability of their findings. Furthermore, computational fluid dynamics (*CFD*) simulations are mostly confined to laboratory settings and rarely consider real-world challenges such as operational variability and economic feasibility. These limitations underscore the need for more rigorous, comprehensive, and application-oriented research to advance the development and practical implementation of solar drying technologies.

Based on the literature reviewed conducted an, it can be concluded that this study effectively addresses the identified gap in existing knowledge. The primary gap identified in the literature is the lack of comprehensive uniformity analysis and systematic optimization of solar drying chamber designs still needs more research. While some studies have explored uniformity enhancement (e.g., through *CFD* or tray adjustments), these efforts remain fragmented and



insufficiently validated. In many literatures baffles have been widely used in various applications, such as solar air systems, heat exchangers, ducts, industrial ovens, boilers, furnaces, etc., to improve performance and flow uniformity. However, to the best authors' knowledge, no previous research has explored their use of baffles and swirlers in solar drying chambers to address drying uniformity. The study was conducted through, numerical and experimental approaches. The computational evaluation of solar drying chambers, including airflow distribution (via CFD modelling), and the experimental approaches includes thermal analysis (energy and exergy analysis), the effect of tray configuration and trays spacing etc, and the drying kinetics of apple slices. Key parameters affecting system efficiency, such as loading capacity and operational variables, were thoroughly investigated. Taguchi analysis was employed to determine the optimal operating conditions. The primary objectives were to enhance airflow uniformity within the drying chambers and to study the drying behaviour of apple slices. Furthermore, a feasibility study was carried out to evaluate the practical viability of the proposed design.

### 3. MATERIALS AND METHODS

This chapter presents the methodologies and procedures employed to achieve the study's final output on solar drying systems. It provides an in-depth description of the materials, methods, and equipment used in the experimental procedures, along with the scientific approaches applied to achieve the thesis objectives. It also offers a comprehensive overview of the experimental design, data collection processes, and the graphical analyses performed.

### 3.1. Study area

The experiment was conducted in the Solar Energy Laboratory of the Hungarian University of Agriculture and Life Sciences (MATE), formerly Szent István University, located in Gödöllő, Hungary (47°35'39"N, 19°34'58"E). The testing period spanned from July to September 2024. The experiment was conducted between 10:00 AM and 4:00 PM. The data reported in this thesis are exclusively from experiments carried out under clear sky conditions, with the absence of any cloud cover. The study area is displayed in Fig. 3.1.

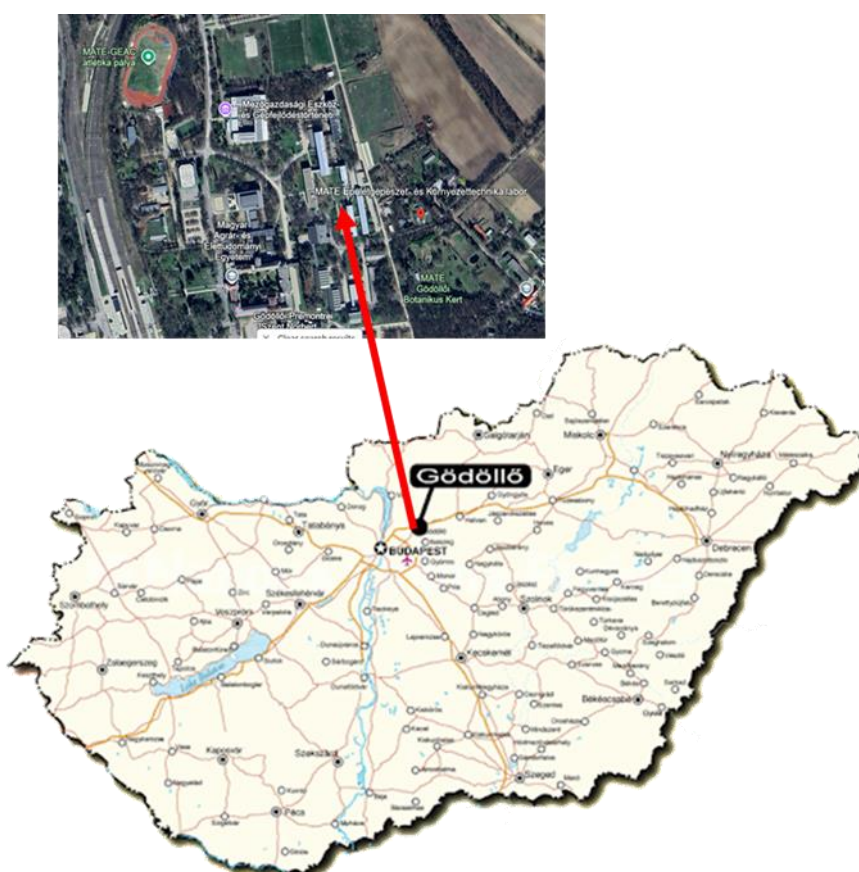


Fig. 3.1. Geographical representation of the study site

The study employed a dual-method approach, combining computational analysis and experimental analysis. The methodology and general overview used to achieve the objectives are illustrated in Fig. 3.2.

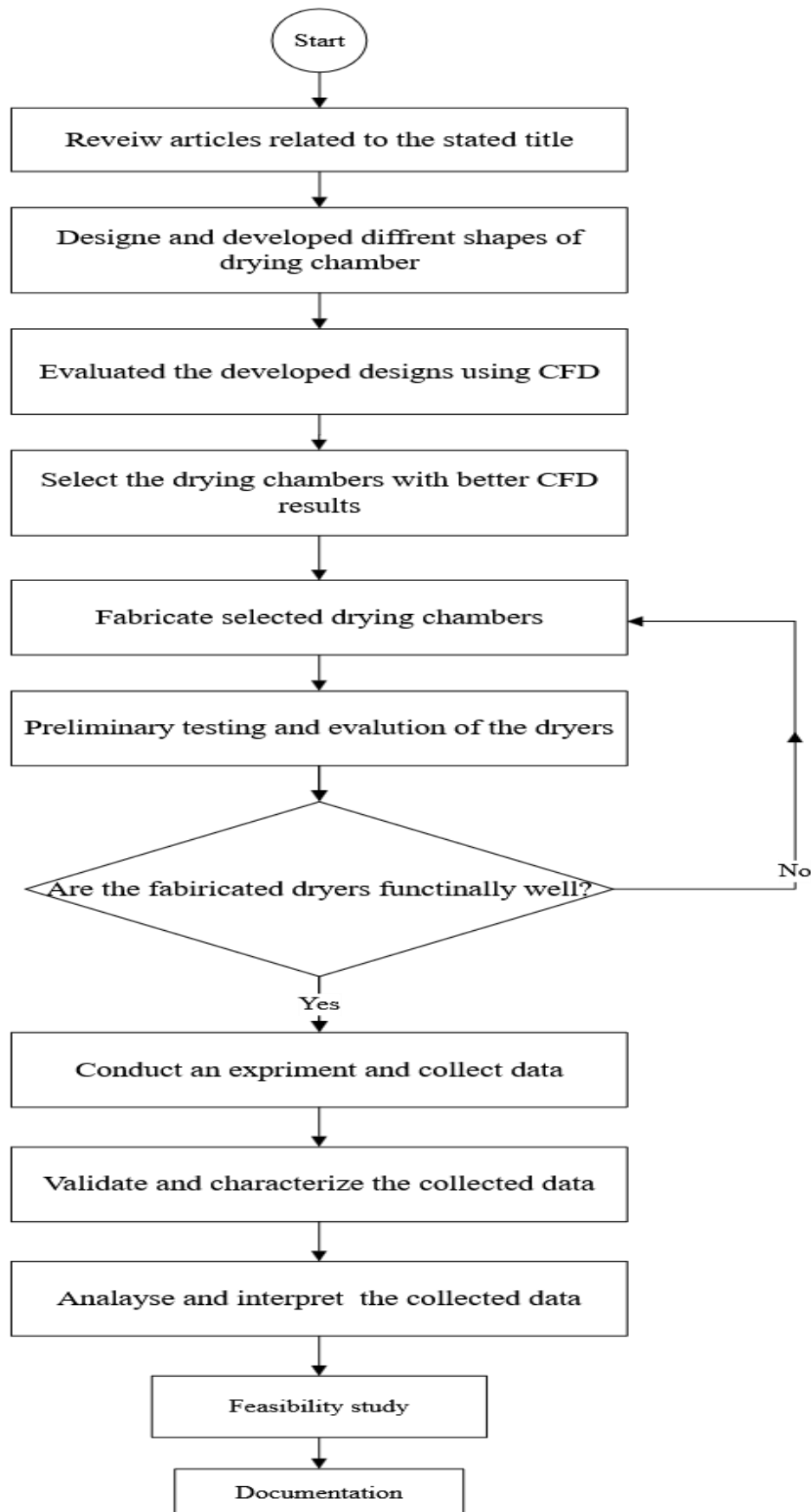


Fig. 3.2. Conceptual framework of the research work

### 3.2. Numerical approaches

The numerical approach begins with computational modelling of the existing drying chamber in the laboratory, designed and fabricated by Al-Neama and Farkas (2018) (see Fig. 3.3). Their design serves as the foundational reference for this research, guiding subsequent improvements to enhance efficiency and performance. CFD was applied to analyse the airflow dynamics of the drying chamber vital tool for designing solar drying systems, enabling an in-depth examination of airflow patterns, heat distribution, and moisture removal efficiency. Based on the simulation results, two optimized dryer designs were selected, fabricated, and experimentally tested. The experiments focused on examining the drying behaviour of apple slices, assessing the airflow distribution within the chamber, and identifying the most effective design for improving drying efficiency.

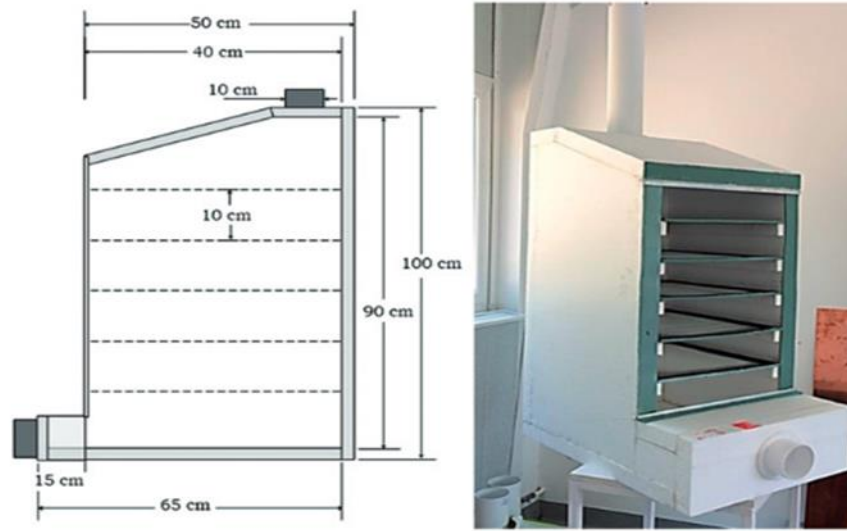


Fig. 3.3. Existing drying chamber (Al-Neama and Farkas, 2018)

#### 3.2.1. Basic equation solved using CFD analysis in solar drying systems

The mathematical equation of the three primary conservation laws which the *CFD* solves are expressed as follows: Eq. (3.1) – Eq. (3.4) (Aukah et al., 2018):

I. Continuity conservation equation:

$$\frac{\partial \rho}{\partial t} + \nabla(\rho \cdot \vec{v}) = 0 \quad (3.1)$$

II. Momentum conservation equations:

$$\frac{\partial}{\partial t}(\rho \vec{v}) + \nabla \cdot (\rho \vec{v} \times \vec{v}) = -\nabla P + \nabla \cdot \vec{\tau} + S_M \quad (3.2)$$

$$\vec{\tau} = \mu \left[ \nabla \vec{v} + (\nabla \vec{v})^T - \frac{2}{3} \delta \nabla \cdot \vec{v} \right] \quad (3.3)$$

where  $\vec{v}$  is velocity with magnitude and direction.

III. Energy conservation equations:

$$\frac{\partial(\rho h_{tot})}{\partial t} - \frac{\partial P}{\partial t} + \nabla \cdot (\rho \vec{v} h_{tot}) = \nabla \cdot (k_d \nabla T) + \nabla \cdot (\vec{v} \cdot \vec{\tau}) + \vec{v} \cdot S_E + S_M \quad (3.4)$$

The turbulence kinetic energy ( $k$ ) and its corresponding dissipation rate ( $\varepsilon$ ) in the form of conservation can be expressed using Eq. (3.5) (Aukah et al., 2018):

IV. Turbulent kinetic energy:

$$\frac{\partial(\rho k)}{\partial t} + \nabla \cdot (\rho \vec{v} k) = \nabla \cdot \left[ \left( \mu + \frac{\mu_t}{\sigma_k} \right) \nabla k \right] + P_k - \rho \varepsilon \quad (3.5)$$

V. Turbulent dissipation rate:

$$\frac{\partial(\rho \varepsilon)}{\partial t} + \nabla \cdot (\rho \vec{v} \varepsilon) = \nabla \cdot \left[ \left( \mu + \frac{\mu_t}{\sigma_\varepsilon} \right) \nabla \varepsilon \right] + \frac{\varepsilon}{k} (C_{\varepsilon 1} P_k - C_{\varepsilon 2} \rho \varepsilon) \quad (3.6)$$

where  $C_{\varepsilon 1}$ ,  $C_{\varepsilon 2}$ ,  $\sigma_k$ , and  $\sigma_\varepsilon$  are given constants, and their values are 1.44, 1.92, 1.0 and 1.3, respectively, for most analyses.

#### 3.2.2. Numerical simulation procedures

To simplify the simulation process, the following assumptions were implemented:

- the fluid is incompressible,
- the drying chamber was assumed well insulated,
- the apple slice was assumed as circular,
- the trays were assumed as porous jump media with constant porosity, and source terms were assumed,
- the resistance to airflow or pressure loss is isotropic.

The key stages in *CFD* involve geometry creation, meshing, running simulations, analysing results, and validating against experimental or theoretical data. The overall methodology for conducting the simulation process using *CFD* is illustrated in Fig. 3.4.

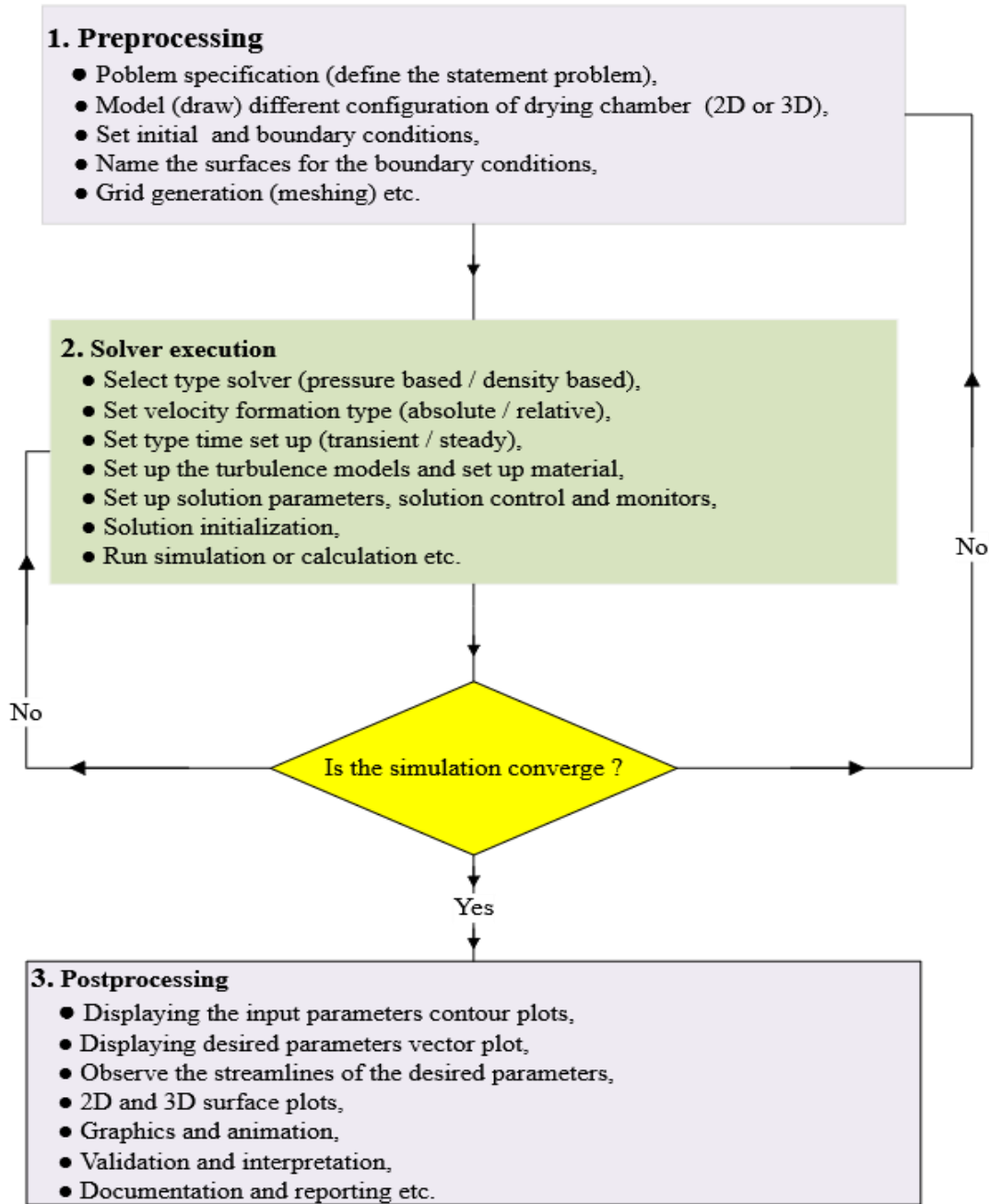


Fig. 3.4. Flowchart of the simulation process

### 3.2.3. Modelling and discretization of the domain

The *CFD* process comprises three fundamental stages. The first step, pre-processing, involves defining the geometry of the domain under study, dividing it into discrete segments through mesh generation, and setting up boundary conditions to define the problem. Solid work 2023 was used to draw the 3D geometry of the components.

#### 3.2.3.1. Drying chamber

The design in SolidWorks was saved in IGS file format and imported into ANSYS fluent 2024R1, as shown in Fig. 3.5. As noted by Nakasone et al. (2006), Ansys is a versatile tool for finite element analysis, allowing the modelling and evaluation of mechanical systems across

diverse scenarios such as heat transfer, fluid dynamics, and structural analysis. It reduces reliance on physical prototypes by enabling detailed simulations of design parameters and operating conditions.

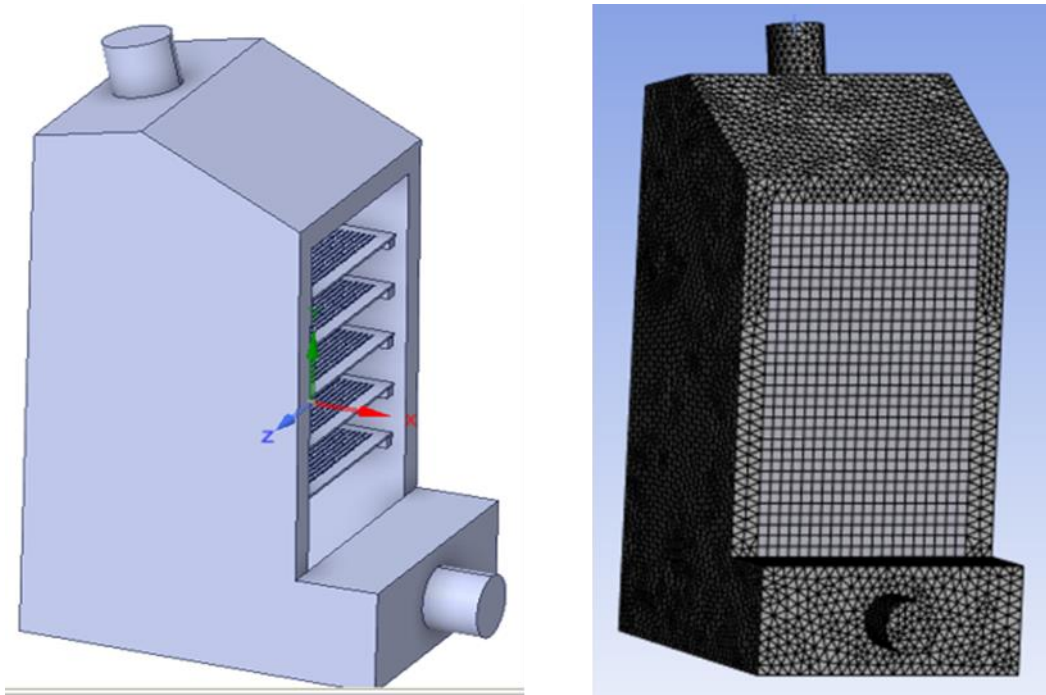


Fig. 3.5. Three-dimensional illustration of the solar existing drying chamber with its generated mesh

#### 3.2.3.2. Trays

The tray was designed as perforated plate with square openings, each measuring 0.02 m by 0.02 m. There is a 10 mm clearance between the tray and the drying chamber wall. The trays were considered thin perforated plates (0.001 m) with square holes, as shown in Fig. 3.6.

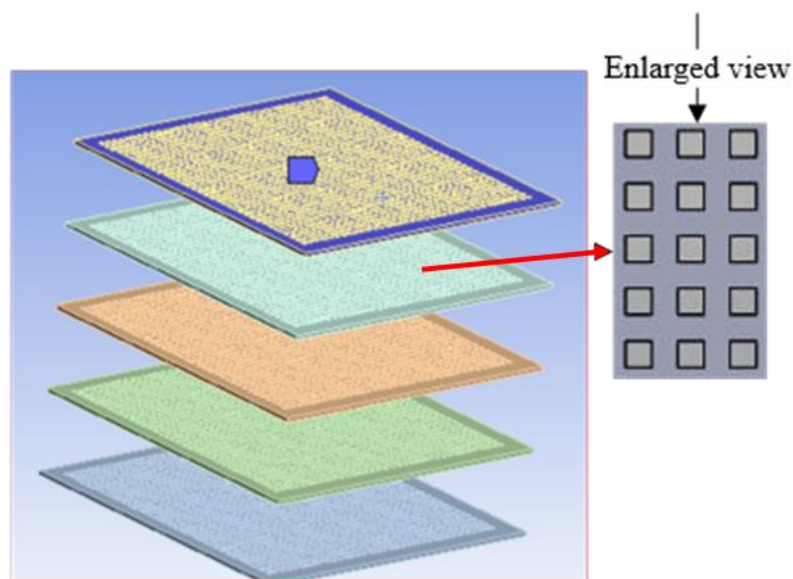


Fig. 3.6. Trays for product holding

### 3.2.3.3. Initial and boundary conditions

The physical and thermal boundary conditions used during *CFD* analysis were velocity inlet as an inlet and pressure outlet as an outlet. Wall boundary conditions with "no slip" for all walls were applied. A default gauge pressure value of zero pascal was applied at the exit of the solar drying chamber. The tray was considered a perforated plate.

The convective heat transfer coefficient between the product and the airflow ( $h_{ce,p}$ ) within the drying chamber depends on the Nusselt number, as given by Eq. (3.7) (Reza Rouzegar et al., 2023):

$$h_{ce,p} = \frac{Nu_{a,dc,p} k_{a,dc}}{D_{h,dc}}, \quad (3.7)$$

where:  $Nu_a$  the Nusselt number of the fluid (a)  $k_a$  is thermal conductivity of fluid (a) and  $D_{h,dc}$  is the hydraulic diameters of the drying chamber.

For  $17 < Re < 70000$ : Nusselt number is calculated using Eq. (3.8) (Sami et al., 2011):

$$Nu = 0.37 Re^{0.6} \quad (3.8)$$

however, if  $Re > 70000$  Eq. (3.9a) was recommended:

$$Nu = 0.023 Re^{0.8} Pr^{0.4} \quad (3.9a)$$

The values of  $Pr$ ,  $Re$  were determined by the following equations (Akpınar and Bicer, 2005):

$$Re = \frac{v \rho l}{\mu} \quad (3.9b)$$

$$Pr = \frac{\mu C_p}{k} \quad (3.9c)$$

The hydraulic diameters ( $D_{h,dc}$ ) within the drying chamber can be calculated using Eq. 3.10 (Simo-Tagne et al., 2021):

$$D_{h,dc} = \frac{4 V_{dc}}{A_{dc}} \quad (3.10)$$

The convective heat transfer coefficient between the wall and the air within the drying chamber ( $h_{ce,wi}$ ) is expressed in Eq. (3.11) (Simo-Tagne et al., 2019):

$$h_{ce,wi} = \frac{k_a Nu_{wa}}{D_{h,wa}} \quad (3.11)$$

where the  $Nu_{wa}$  is used to determine the convective heat transfer coefficient between the wall and the air within the drying chamber is determined as:

$$Nu_{wa} = \left[ 0.825 + \frac{0.387 Ra_{we}^{\frac{1}{6}}}{\left[ 1 + \left( \frac{0.492}{Pr} \right)^{\frac{9}{16}} \right]^{\frac{8}{27}}} \right]^2 \quad (3.12a)$$

The value of  $Ra$  and  $Gr$  are calculated using the following expressions (Simo-Tagne et al., 2019):

$$Ra = Pr Gr \quad (3.12b)$$



$$Gr = \frac{\Gamma g D_h^3 \rho^2 \Theta T}{\mu^2} \quad (3.12c)$$

in which:

$$\Gamma = \frac{1}{T_{am}} \quad (3.12d)$$

and:

$$\Theta T = T_{dc,o} - T_{am} \quad (3.12e)$$

The convective heat transfer for the drying chamber between the external wall and the surrounding ambient air ( $h_{ce,am}$ ) can be computed utilizing Eq. (3.13). The stated formula in Eq. (3.13) is specifically for wind speeds less than 4 m/s (Tarigan, 2018):

$$h_{ce,am} = 5.7 + 3.8 v_a \quad (3.13)$$

Thus, the following calculated values of the working fluid were utilized in the analysis: the  $C_{pa} = 1.0084$  kJ/kg.K,  $k_a = 0.0265$  W/m.K,  $\mu_a = 1.864 \cdot 10^{-5}$  kg/m s,  $\rho_a = 1.159$  kg/m<sup>3</sup>.  $D_{h,dc}$  was set to 0.4 m with turbulence intensity (I) of 4.24%, and the  $Re$  was calculated to be 40,415.77. Additionally, the  $Nu$  was found to be 302.554. Finally, the  $h_{ce}$  set as 54.17353 W/(m<sup>2</sup>.°C). These parameters were crucial for accurately modelling the thermal and fluid dynamics of the system under study, particularly during the numerical investigation.

#### 3.2.3.4. Quality of the mesh

A combination of unstructured and structured grid types featuring quadrilateral and hexahedral elements was used to generate the mesh for domain discretization. The resulting mesh consists of 254,070 elements and 1,023,157 nodes. Mesh quality measurements, such as aspect ratio, skewness, and orthogonal quality, were used to determine whether the mesh is adequate or not. Based on the results of the mesh quality criteria indicators, the mesh is within the recommended ranges (see Table 3), and the model is ready for the next step or simulation.

Table 3.1 Average value of mesh quality determinates

Parameter	Acceptable range (Ansys-10,2013)	Result	Remarks
Skewness	Excellent: 0 – 0.25 Good: 0.25 – 0.5	0.21	Average skewness values fall within the acceptable range
Aspect ration	$\leq 5$	1.8	Values for both domains are within acceptable ranges for simulation.
Orthogonal quality	Ideal: 0.15 – 1.0 (Closer to 1 indicates better quality)	0.85	The orthogonal quality values meet the criteria for adequacy in both domains.

#### 3.2.3.5. Solver settings and turbulence choice

The following solver settings were employed: a double precision, segregated steady solver was used to ensure high numerical accuracy and stability during simulations. The standard method

for pressure was applied to calculate pressure fields within the domain. At the same time, second-order upwind discretization was utilized for momentum, turbulence, and energy equations to enhance accuracy in the numerical solution. A SIMPLE algorithm was employed for pressure-velocity coupling. Regarding turbulence modelling, the Reynolds Averaged Navier-Stokes method was employed, utilizing the  $k-\varepsilon$  model to simulate turbulence behaviour within the airflow effectively. This configuration is essential for capturing the complexities of turbulent flow dynamics in large air spaces.

Finally, iterative convergence, residuals, and under-relaxation factors were carefully adjusted to ensure solution convergence. For the level of accuracy, the limited residual values for the solution convergence (minimum values reached), when the residuals equation for each parameter was set to  $10^{-4}$  for continuity,  $z$ -velocity,  $y$ -velocity,  $x$ -velocity and  $k-\varepsilon$  and  $10^{-8}$  for energy.

#### **3.3. Computational evaluation**

More than ten new designs were created and analysed using *CFD* analysis. Four designs demonstrating high uniformity and velocity are illustrated in Fig. 3.7 (in 2D) and Fig. 3.8 (in 3D, along with their respective simulation results). Based on the simulation results, designs II and IV featuring high-velocity and more uniform streamlines were fabricated and experimentally analysed. These designs were selected for their superior airflow dynamics, which are expected to enhance drying efficiency. Fig. 3.10 displays the two optimal fabricated designs (II and IV) along with one benchmark design, which is identical to dryer II (see Fig. 3.9). However, in the following sections dryer IV is designated as 'dryer 1'.

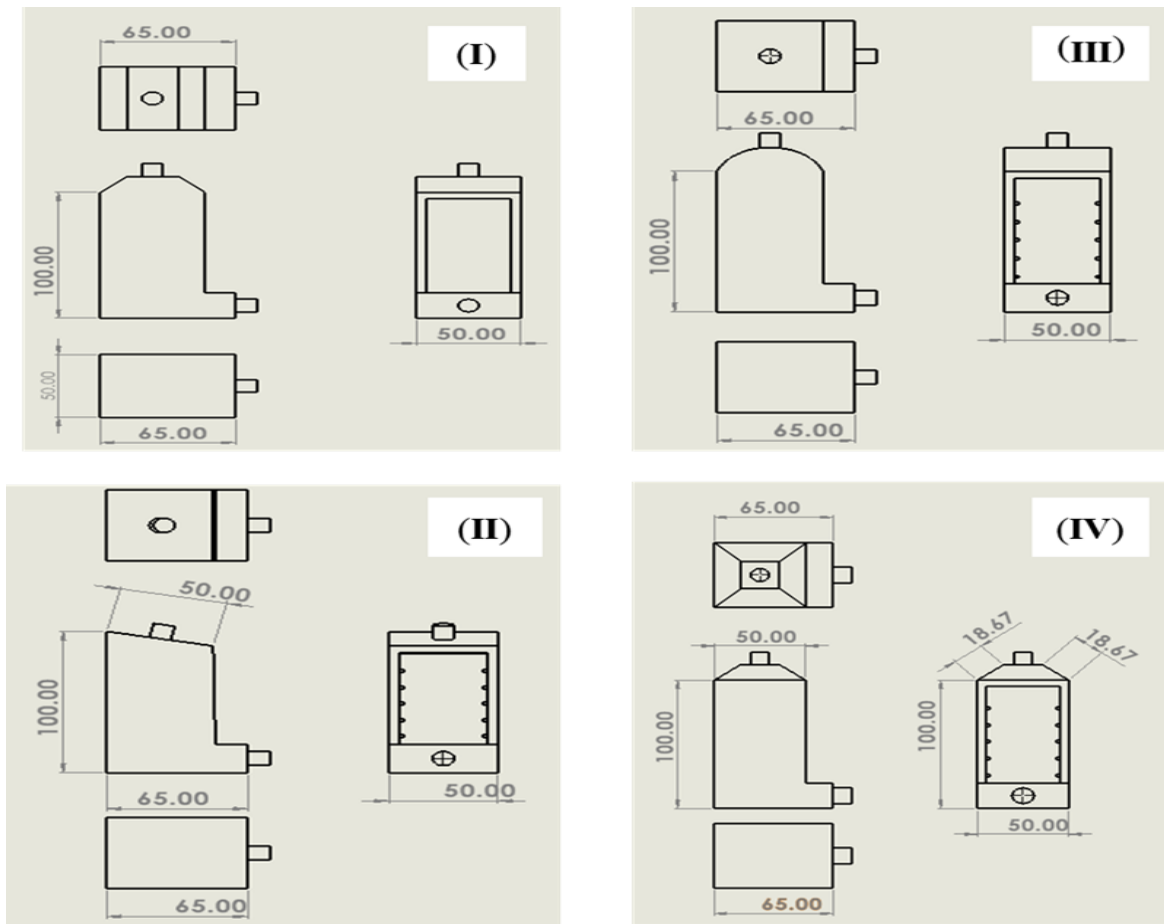


Fig. 3.7. 2D drawing of the selected designs

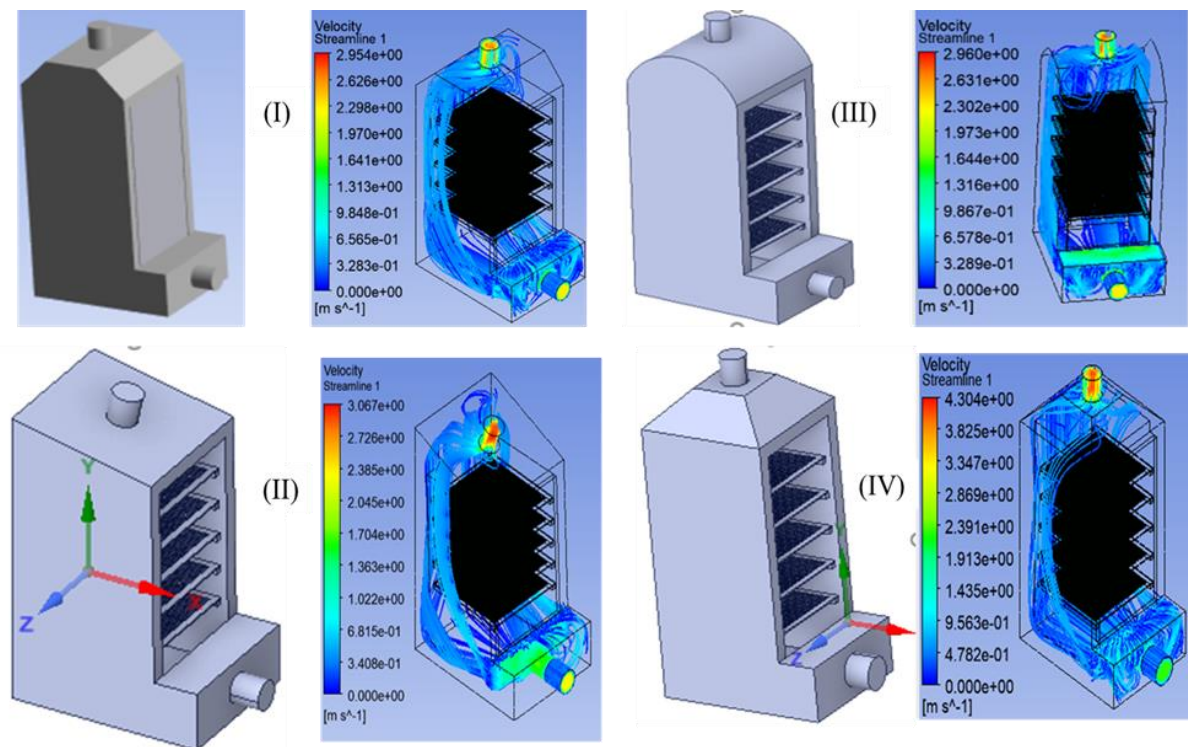


Fig. 3.8. Selected models with CFD streamline results

### 3.4. Validation of the CFD results

The results of *CFD* simulations can be validated through experimental data or by referencing established literature. Additionally, some researchers perform grid independence tests to ensure accuracy. The *RMSE*, per cent bias (*PBIAS*), and relative error (*ER*) were used to validate the simulation results. *RMSE* and *PBIAS* are widely used statistical metrics to assess model accuracy by quantifying deviations between observed and predicted values outcomes (Sanghi et al., 2017). *RMSE* is given by the following:

$$RMSE = \sqrt{\sum_{i=0}^n \frac{(x_i - y_i)^2}{n}} \quad (3.14)$$

*PBIAS* indicates the model's tendency to underestimate (positive *PBIAS*) or overestimate (negative *PBIAS*) values, with 0 representing the ideal, unbiased:

$$PBIAS = \left[ \frac{\sum_{i=1}^n (x_i - y_i) 100}{\sum_{i=0}^n y_i} \right] \quad (3.15)$$

The relative error method (*ER*) is also used as a validation metric to demonstrate the variance between experimental and predicted data (Iranmanesh et al., 2020):

$$ER (\%) = \frac{|y_i - x_i|}{y_i} 100 \quad (3.16)$$

### 3.5. Experimental approach

#### *Fabrication of drying system components*

An indirect type, forced convection solar dryer consisting of a flat plate solar air heaters were coupled to a drying chamber was constructed and investigated experimentally for drying of golden apple slices. The general specification of the drying component used during the experiment are listed out in Table 3.2.

Table 3.2 Specifications of the solar drying system components

Component	Description
Solar air heater (SAH)	<ul style="list-style-type: none"> <li>• Dimensions: 1.25 m x 0.5 m</li> <li>• Single-glazed with diffuser inlet</li> <li>• Circular outlet (0.1 m diameter)</li> <li>• Plexiglass cover with 0.004 m thickness and 0.16 W/m.K thermal conductivity</li> <li>• Copper absorber plate with 125 cm length, 50 cm width, and 1.2 mm thickness and thermal conductivity 385 W/m.K coated with black matt paint</li> <li>• 0.05 m gap between copper absorber and the glass cover</li> <li>• Installed at a 45° inclination</li> </ul>
Connector pipe	<ul style="list-style-type: none"> <li>• Length: 1.45 m with diameter of 0.1 m</li> <li>• Integrated with a venturi meter (measures flow rate and pressure drop)</li> </ul>
Drying chamber	<ul style="list-style-type: none"> <li>• Dimensions: 1 m (height) x 0.5 m (width) x 0.65 m (length)</li> <li>• Material: 5 cm thick extruded polystyrene (XPS) with thermal conductivity of 0.033 W/(m K)</li> </ul>

Trays	<ul style="list-style-type: none"> <li>• Material: fiberglass mesh trays (48 cm x 50 cm)</li> <li>• Trays spaced 0.1 m apart for air circulation</li> <li>• Number of trays: 4</li> </ul>
Auxiliary equipment	<ul style="list-style-type: none"> <li>• Fans: 21 W – 33 W and airflow rate 145 m<sup>3</sup>/h – 187 m<sup>3</sup>/h</li> <li>• Metal dryer supporters</li> <li>• Junction box: used to housing the electrical system and the dimmers</li> </ul>

#### 3.5.1.1. Manufacturing process of the solar air heater

In this setup, two identically shaped and dimensioned solar air heaters were employed, as illustrated in Appendix A3.

#### 3.5.1.2. Drying chamber

The drying chamber was constructed from high-performance extruded polystyrene (XPS) insulation board which low thermal conductivity. The plenum chamber which is used to stabilize the pressure and velocity of the air coming from the collector. It is 0.25 m in high from the base of the drying chamber and made based on the recommendations of (Forson et al. 2007). The second component is the door, which is made from transparent material to provide clear visibility of the products undergoing the drying process. It is designed for easy loading and unloading of items. Heated air enters the drying cabinet from below the trays and flows upward through the samples. The construction procedure of the drying chamber is shown in Appendix A3.

Some of the sensors used during the experiment, viewed from the back of the drying and inside the drying chamber. Every sensor was laid on the centre of each tray. In addition, some of the auxiliary equipment's used are also shown in Fig. 3.9.

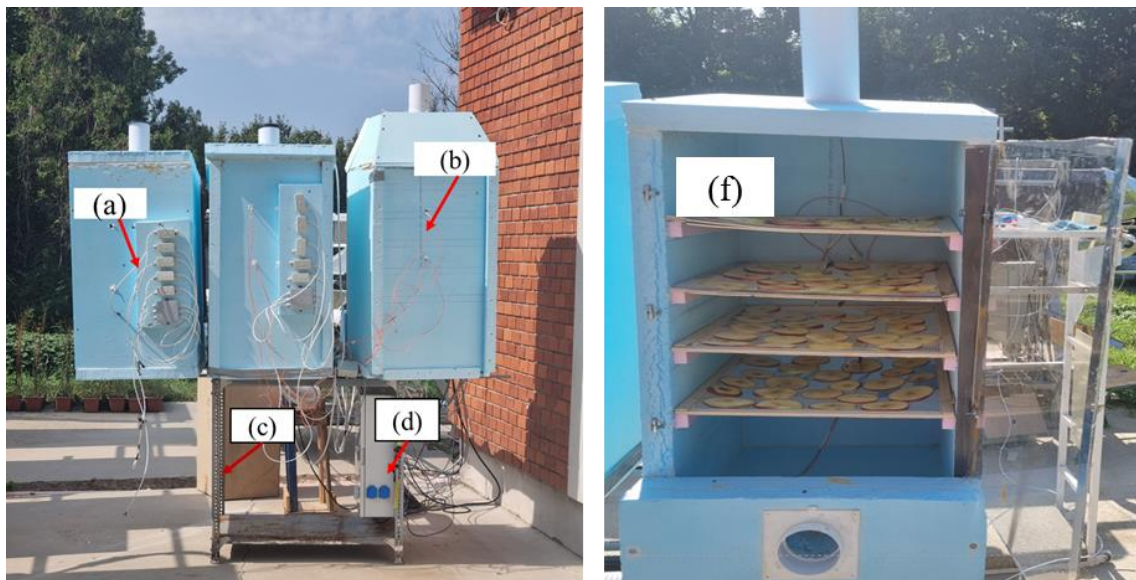


Fig. 3.9. The fabricated drying chamber with one bench mark: *RH* sensor (a), *RTD* sensors (b), drying chamber stand (c), junction box (d) and the sensors inside the drying chamber (f)

#### 3.5.1.3. Trays

The trays were constructed from fiberglass mesh (see Appendix A3) these trays promote efficient air circulation while providing stable support for the drying material and each tray was spaced 0.1 m. The complete experimental setup, including the supportive aluminium bar, connections, junction box, and materials used to construct the drying chambers, is illustrated Fig. 3.10.

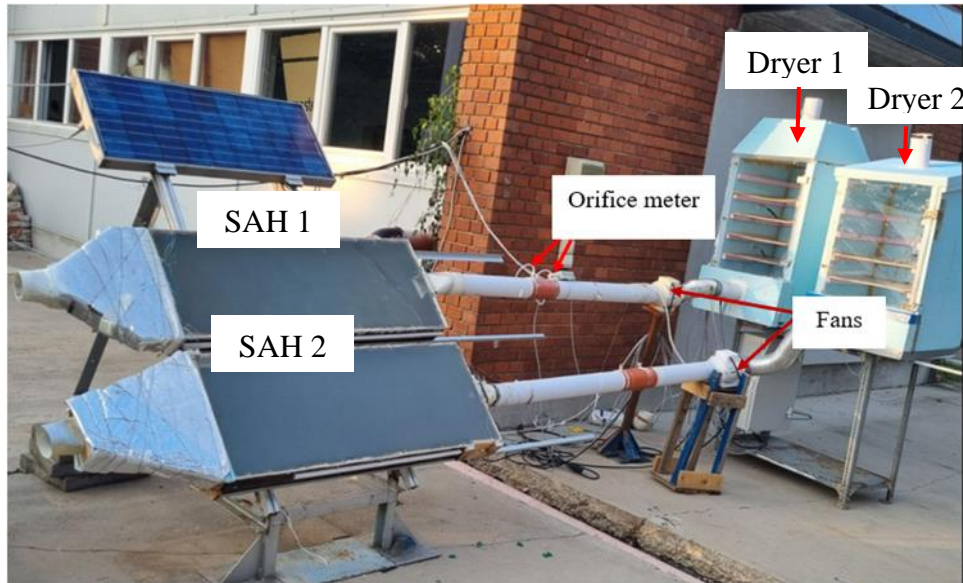


Fig. 3.10. The setup of the drying system

#### 3.6. Instrumentation and data acquisition

The measurement instruments used in this study, including their technical specifications, certified accuracies, and 2D schematics, are summarized in Appendix A4. Additionally, Fig. 3.11 illustrates the sensor configuration within the drying system. RTD sensors were positioned at the centre of each tray.



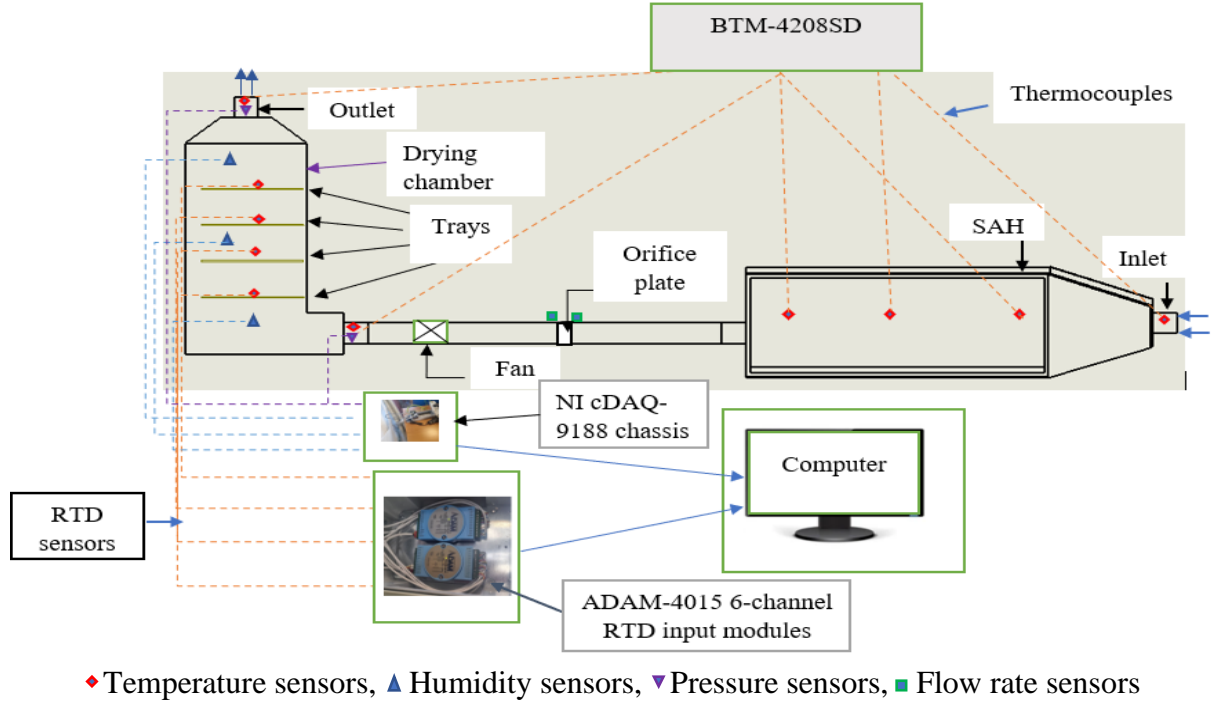


Fig. 3.11. Arrangement of the sensors (side view)

During the experiment, multiple software tools were employed for data acquisition, analysis, and optimization. Key software applications and their functions are summarized in Table 3.3.

Table 3.3 Software used in data acquisition and analysis

Software	Function	Purpose/Application
LabVIEW	Data logger	Read and record humidity and pressure drop data.
CieLab	Data analysis	Analyse colour changes before and after drying.
Minitab	Statistical analysis	Conduct Taguchi DOE (design of experiments) analysis.

For the humidity sensors, the following formulas were employed based on the manufacturer's guidelines:

$$\text{Voltage output} = V_{\text{supply}} (0.0062 (\text{sensor RH}) + 0.16), \text{ typical at } 25^\circ\text{C} \quad (3.17)$$

Thus:

$$\text{Sensor RH} = \frac{V_{\text{OUT}} - 0.16}{0.006 \cdot V_{\text{supply}}} \quad (3.18)$$

Temperature compensation:

$$\text{True RH} = \frac{\text{Sensor RH}}{1.0546 - 0.00216 T} \quad (3.19)$$

where  $T$  in  $^\circ\text{C}$  represents the temperature at the sensor's location.

### 3.7. Sample preparation

Three kilograms of apples were purchased from a local grocery store (Coop, Gödöllő, Egyetem tér 17, 2100, Hungary). From this randomly selected batch, 2 kg of apples were chosen for their suitable size and lack of external defects before being sliced. The apples had diameters ranging from  $0.075 (\pm 0.01)$  to  $0.083 (\pm 0.01)$  meters. Using a manual knife cutter, the apples were

sliced horizontally along their axes, producing cylindrical pieces with thicknesses between 0.004 and 0.0065 ( $\pm 0.001$ ) meters. As noted by Doymaz and Özdemir (2014), this circular thin-layer design significantly shortens drying times and improves drying efficiency. Each slice was weighed to determine the appropriate drying time and then arranged on a prepared tray in the drying chamber to initiate the drying process.

### 3.8. Uncertainty of the experiment

A comprehensive understanding of the method's performance and the measurement range must be rooted in a detailed analysis of experimental uncertainty. It is crucial to account for all key factors that contribute to this uncertainty (Badaoui et al., 2022). The errors and uncertainties in the experiments originated from factors such as instrument selection, conditions, calibration, environmental influences, observations, readings and test planning (El Khadraoui et al., 2017). Uncertainty represents the degree of doubt regarding the result of any measurement and is calculated using Eq. 3.20 (Heydari and Mesgarpour, 2018):

For variable  $y$ , which is a function of variable  $x_1, x_2, \dots x_n$ , associated uncertainty is defined as follows:

$$U(y) = \sqrt{\left(\frac{\partial y}{\partial x_1}\right)^2 u^2(x_1) + \left(\frac{\partial y}{\partial x_2}\right)^2 u^2(x_2) + \dots \left(\frac{\partial y}{\partial x_n}\right)^2 u^2(x_n)} \quad (3.20)$$

To determine the uncertainty associated with the experimental measurement of each parameter  $x_1, x_2, \dots x_n$ , can apply the following relationship (Heydari and Mesgarpour, 2018):

$$U = \frac{\gamma}{\sqrt{3}} \quad (3.21)$$

where:  $\gamma$  is the accuracy of the equipment.

The combined total uncertainty of all instruments is approximately 3.59%, which is acceptable to conduct experiment.

### 3.9. Performance analysis of the solar drying chamber

Three different tests were carried out during the dryer's evaluation. The first is unloading (without loading the material that is ready to dry), followed by half-loading and full-loading. The purpose of this test was to determine the temperature generated by the collector and to determine collector efficiency.

#### 3.9.1. Unloading test

The No load test was done to determine the maximum possible rise in temperature of the collector compared to that of the ambient. Also, this test helped to determine the maximum possible rise in temperature of the drying chamber compared to the ambient temperature.

#### 3.9.2. Load test

The weight of the sliced golden apple was measured at hourly intervals using an electronic balance from 10:00 AM to 4:00 PM. The reduction in the weight of the apple slices was recorded and used to calculate moisture loss, moisture ratio, drying kinetics, and to select the appropriate thin-layer drying models. Moisture content during the drying period was calculated



on a wet basis. The loading test was conducted in stages: initially at half capacity (HLC), followed by semi-full capacity (SFC), and finally full capacity (FLC).

### 3.9.3. Energy analysis of the drying system

The air used solar drying of agricultural products includes heating, cooling, and humidification. These processes are modelled as steady-flow systems, with analysis based on mass and energy conservation principles for both air and moisture (Midilli and Kucuk, 2003).

General equation of mass conservation of drying air:

$$\sum(\dot{m}_{hui} + \dot{m}_{pi}) = \sum(\dot{m}_{huo}) \quad (3.22)$$

General equation of energy conservation:

$$\dot{Q} - \dot{W} = \sum \dot{m}_o \left( h_o + \frac{v_o^2}{2} + Z_o g \right) - \sum \dot{m}_i \left( h_i + \frac{v_i^2}{2} + Z_i g \right) \quad (3.23)$$

#### 3.9.3.1. Energy analysis of solar air heater

Air collectors, or flat-plate solar air heaters, serve as adiabatic radiative heat exchangers that convert solar energy into heat. This heat is then transferred from the absorber to the working fluid, usually air, through convection (Kurtbas and Durmuş, 2004). The energy of the solar collector, which includes the energy gained by the collector ( $Q_{sah,i}$ ) and the energy supplied to the solar dryer ( $Q_{sah,o}$ ), is calculated as follows (Gilago et al., 2023a):

$$Q_{sah,i} = I_r A_{sah} \alpha \tau \quad (3.24)$$

where  $\alpha$  and  $\tau$  denote the absorptance and transmittance coefficients, respectively, with values of 0.95 and 0.85 respectively (Prakash and Kamatchi, 2024):

$$Q_{sah,o} = \dot{m}_a C_{p,a} (T_{sah,o} - T_{am}) \quad (3.25)$$

The specific heat (J/kg.°C) of air was calculated using the Eq. (3.26) provided by (Ekka and Palanisamy, 2020):

$$C_{p,a} = 999.2 + 0.1434 T_{av} + 1.101 \cdot 10^{-4} T_{av}^2 - 6.758 \cdot 10^{-8} T_{av}^3 \quad (3.26)$$

where:  $T_{av} = \frac{T_{am} + T_{\infty}}{2}$  and  $T_{\infty}$  is the temperature of the surface or boundary of the intended material.

The mass flow rate was determined by the following Eq. (3.27), as outlined (Ghorbani et al., 2020):

$$\dot{m} = C_d v A \sqrt{2 g_c \rho_a D_p} \quad (3.27)$$

where  $D_p$  is the pressure drops of the SDP806/SDP816-500 Pa pressure sensor with square root configuration based on the company's manual instruction, can be calculated as follows:

$$D_p = \text{sign} \left( \frac{A_{OUT}}{V_{DD}} - 0.5 \right) \left( \frac{A_{OUT}}{V_{DD} \cdot 0.4} - 1.25 \right)^2 525 \quad (3.28)$$

where  $\text{sign} ()$  = indication flow direction (+ or -).

#### 3.9.3.2. Energy analysis of the drying chamber

Energy and mass transfer within the drying system are illustrated in Fig. 3.12, while the corresponding governing equations, based on conservation principles, are formulated in Eq. (3.29).

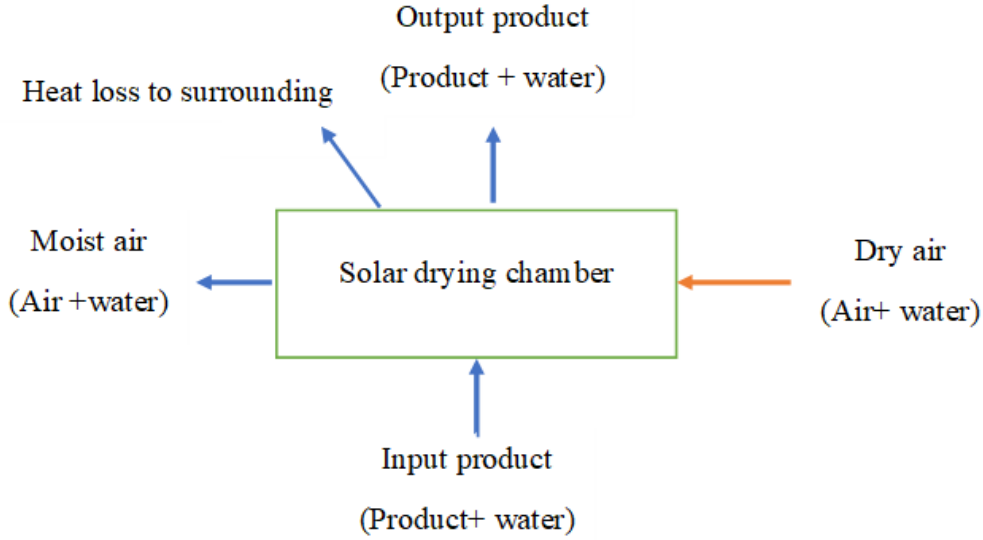


Fig. 3.12. Visual representation of the energy balance in the drying chamber

$$Q_{air,i} + Q_{product,i} = Q_{air,o} + Q_{product,o} + \text{heat losses} \quad (3.29)$$

where  $Q$  is heat gain or heat loss by the system.

The energy within the drying cabinet ( $E_{dc,i}$ ) was evaluated using Eq. (3.30) (Mugi and Chandramohan, 2021a):

$$E_{dc,i} = I_{av} A_{dc} t_d \quad (3.30)$$

### 3.9.3.3. Efficiency of the drying system

The efficiency of the solar air heater ( $\eta_{sah}$ ) was computed by employing Eq. (3.31):

$$\eta_{sah} = \frac{Q_{sah,o}}{Q_{sah,i}} = \frac{\dot{m}_a c_{p,a} (T_{sah,o} - T_{am})}{A_{sah} I_r \alpha \tau} \quad (3.31)$$

The system efficiency of a solar dryer quantifies the effectiveness of utilizing input energy (solar radiation) for product drying. The efficiency of the forced convection solar dryer ( $\eta_{dc,f}$ ) was determined using Eq. 3.32 (Rezaei et al., 2022):

$$\eta_{dc,f} = \frac{M_{rw} h_{fg}}{I_{av} A_{dc} t_d + F_p} \quad (3.32)$$

where  $\alpha$  represents the absorptivity of the copper plate, which is 0.95, and  $\tau$  denotes the transmissivity of the window glass, which is 0.88 (Balijepalli et al., 2017). The value of latent heat of vaporization ( $h_{fg}$ ) of water can be estimated using the following Eq. (3.33) (Prakash and Kamatchi, 2024):

$$h_{fg} = 2501.8 - 0.002378 (T_{dc,o} - 273.15) \quad (3.33)$$

where  $M_{rw}$  is the total amount of moisture extracted from the product to achieve the desired moisture level from its initial content and is determined using the following Eq. (3.34) (Hossain et al., 2025):

$$M_{rw} = \frac{m_i (m_{ic} - m_{fc})}{100 - m_{cf}} \quad (3.34)$$

#### 3.9.3.4. Specific heat energy consumption and specific moisture extraction rate

These two parameters, specific heat energy consumption (SHE) and specific moisture extraction rate (SMER), are inversely proportional and play a critical role in evaluating the performance of solar dryers to ensure optimal efficiency. An increase in drying duration leads to a rise in *SHE* and a reduction in particular *SMER* and given by the following expressions (Prakash and Kamatchi, 2024):

$$SHE = \frac{Q_{sah,i}}{m_i - m_f} = \frac{(I_r A_{sah} \alpha \tau) t_d}{m_i - m_f} \quad (3.35)$$

$$SMER = \frac{m_i - m_f}{Q_{sah,i} t_d} \quad (3.36)$$

#### 3.9.3.5. Exergy analysis of solar air heater

The exergy terms, including input ( $E_{x,i,sah}$ ), output ( $E_{x,o,sah}$ ), and losses ( $E_{x,l,sah}$ ) associated with the solar air heater, are defined by the following formulas (Mugi and Chandramohan, 2021b):

$$E_{x,i,sah} = \left[ 1 - \frac{T_{sah,o}}{T_s} \right] Q_{sah,i} \quad (3.37)$$

where  $T_s$  represents the apparent temperature of the sun, which is approximately 6000 K (Abuşka, 2018).

The exergy outflow of the solar air heater is given as follows:

$$E_{x,o,sah} = \dot{m}_a C_{p,a} \left[ (T_{sah,o} - T_{sah,i}) - T_{sah,i} \ln \left( \frac{T_{sah,o}}{T_{sah,i}} \right) \right] \quad (3.38)$$

$$E_{x,l,sah} = E_{x,i,sah} + E_{x,o,sah} \quad (3.39)$$

#### 3.9.3.6. Exergy analysis of the drying chamber

The exergy flow diagram of the drying chamber is illustrated in Fig. 3.13, providing a comprehensive representation of exergy inflow, exergy outflow, and associated losses within the system.

If the pressure between the inlet and out of the drying chamber is negligible, the inflow exergy and outflow exergies at a steady-state by Eq. (3.40) and Eq. (3.41) respectively (Celma and Cuadros, 2009):

$$E_{x,i} = \dot{m}_a C_{p,a} \left[ (T_{dc,i} - T_{am}) - T_{am} \ln \left( \frac{T_{dc,i}}{T_{am}} \right) \right] \quad (3.40)$$

$$E_{x,o} = \dot{m}_a C_{p,a} \left[ (T_{dc,o} - T_{am}) - T_{am} \ln \left( \frac{T_{dc,o}}{T_{am}} \right) \right] \quad (3.41)$$

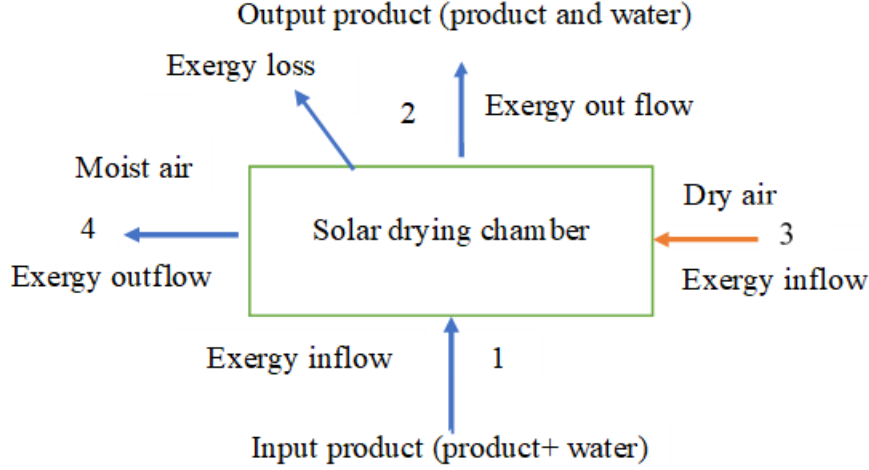


Fig. 3.13. Exergy flow diagram of the drying chamber

### 3.9.3.7. Exergy analysis of the trays

If the pressure between the inlet and out, energies like kinetic, potential energies, etc., are neglected inflow exergy of the trays inside the drying chamber can be determined using Eqs. (3.42 – 45):

$$\text{Exergy inflow of bottom tray: } E_{x,tr1,i} = \dot{m}_a C_{p,a} \left[ (T_{tr1} - T_{am}) - T_{am} \ln \left( \frac{T_{tr1}}{T_{am}} \right) \right] \quad (3.42)$$

$$\text{Exergy inflow of second tray: } E_{x,tr2,i} = \dot{m}_a C_{p,a} \left[ (T_{tr2} - T_{am}) - T_{am} \ln \left( \frac{T_{tr2}}{T_{am}} \right) \right] \quad (3.43)$$

$$\text{Exergy inflow of third tray: } E_{x,tr3,i} = \dot{m}_a C_{p,a} \left[ (T_{tr3} - T_{am}) - T_{am} \ln \left( \frac{T_{tr3}}{T_{am}} \right) \right] \quad (3.44)$$

$$\text{Exergy inflow of fourth tray: } E_{x,tr4,i} = \dot{m}_a C_{p,a} \left[ (T_{tr4} - T_{am}) - T_{am} \ln \left( \frac{T_{tr4}}{T_{am}} \right) \right] \quad (3.45)$$

The outflow exergies of the trays in the drying chamber trays can be calculated using Eqs. (3.46 – 49):

$$\text{Exergy outflow of bottom tray: } E_{x,tr1,o} = \dot{m}_a C_{p,a} \left[ (T_{tr2} - T_{am}) - T_{am} \ln \left( \frac{T_{tr2}}{T_{am}} \right) \right] \quad (3.46)$$

$$\text{Exergy outflow of second tray: } E_{x,tr2,o} = \dot{m}_a C_{p,a} \left[ (T_{tr3} - T_{am}) - T_{am} \ln \left( \frac{T_{tr3}}{T_{am}} \right) \right] \quad (3.47)$$

$$\text{Exergy outflow of third tray: } E_{x,tr3,o} = \dot{m}_a C_{p,a} \left[ (T_{tr4} - T_{am}) - T_{am} \ln \left( \frac{T_{tr4}}{T_{am}} \right) \right] \quad (3.48)$$

$$\text{Exergy outflow of fourth tray: } E_{x,tr4,o} = \dot{m}_a C_{p,a} \left[ (T_{dc,o} - T_{am}) - T_{am} \ln \left( \frac{T_{dc,o}}{T_{am}} \right) \right] \quad (3.49)$$

where:  $i = 1, 2, 3$  etc., in which the arrangement of the trays from bottom to top.

### 3.9.3.8. Exergy efficiency

Exergy efficiency offers a more detailed measure for evaluating the thermal performance of ISDs by accounting for energy losses and inefficiencies during conversion and use. In contrast to basic energy efficiency, exergy efficiency considers both the quality and quantity of energy, delivering a thorough assessment of system performance (Kumar et al., 2024). It serves as a

gauge for the thermal system's converted energy quality. It is the ratio of exergy outflow to exergy inflow, as shown in Eq. (3.50) (Maia et al., 2017):

$$\text{Exergy efficiency } (\eta_{Ex}) = \frac{E_{x,o}}{E_{x,i}} = \frac{E_{x,i} - E_{x,l}}{E_{x,i}} \quad (3.50)$$

#### 3.9.4. Drying rate

The drying rate is a critical parameter that is determined by the product's temperature and moisture content, as well as the temperature, relative humidity, and velocity of the drying air (Belessiotis and Delyannis, 2011). It is a key parameter for assessing the efficiency of the drying process. It quantitatively indicates how swiftly the drying progresses and how effectively it reaches the target moisture level for preservation. This metric is vital for evaluating and comparing the performance of various drying methods, providing valuable insights into the overall effectiveness of the drying system (Yadav et al., 2018). The drying rate is the total duration recorded throughout the entire drying process of the products undergoing drying and expressed using Eq. (3.51) (Ullah et al., 2022):

$$DR = \frac{dM}{dt} = \frac{M_t - M_{t+\Delta t}}{\Delta t} \quad (3.51)$$

#### 3.9.5. Moisture content

To assess the moisture content ( $m_c$ ) of the samples on a wet basis throughout the day as they undergo the drying process (Rajesh et al., 2024):

$$m_c = \frac{m_i - m_d}{m_i} \quad (3.52)$$

#### Moisture ratio

The moisture ratio ( $MR$ ) of the product is calculated using Eq. (3.53) (Doymaz and İsmail, 2011):

$$MR = \frac{m_t - m_e}{m_0 - m_e} \quad (3.53)$$

where:  $m_t$ ,  $m_0$ , and  $m_e$  represent the moisture content of the product at any given time during drying (kg of water per kg of dry matter), the initial moisture content (kg of water per kg of dry matter), and the equilibrium moisture content (kg of water per kg of dry matter), respectively.

Since the products were not continuously subjected to consistent relative humidity and temperature, the values of  $m_e$  were significantly smaller than  $m_t$  or  $m_0$ . As a result, the error caused by the simplification is insignificant. Thus, Eq. (3.53) will be simplified to Eq. (3.54) (El-Beltagy et., 2007):

$$MR = \frac{m_t}{m_0} \quad (3.54)$$

#### 3.9.6. The effective diffusion coefficient and activation energy

The term effective moisture diffusivity ( $D_{eff}$ ) describes the overall transport coefficient that includes all moisture transport processes, such as molecular diffusion, liquid diffusion, vapour diffusion and hydrodynamic flow (Rani and Tripathy, 2021). Fick's law of diffusion is commonly applied in drying processes to calculate the diffusion coefficient (Doymaz, 2013):

$$MR = \frac{8}{\pi^2} \sum_{n=0}^{\infty} \frac{1}{(2n+1)^2} \exp\left(-\frac{(2n+1)^2 D_{eff} \pi^2 t}{4 l^2}\right) \quad (3.55)$$

where  $n$  is a positive integer.

For prolonged drying durations, Eq. (3.55) simplifies to a limiting version of the diffusion equation, as described in Eq. (3.56):

$$MR = \frac{8}{\pi^2} \exp\left(-\frac{D_{eff} \pi^2 t}{4 l^2}\right) \quad (3.56)$$

hence,  $D_{eff}$  is determined by graphing experimental drying data, and  $\ln MR$  is plotted against drying time using Eq. (3.57). This plot resulted in a linear relationship with a slope indicating:

$$Slope (m) = \frac{D_{eff} \pi^2 t}{4 l^2}. \quad (3.57)$$

The relationship between effective moisture diffusivity and temperature can be expressed through a straightforward Arrhenius-type correlation, as illustrated in Eq. (3.58) (Falade and Solademi, 2010):

$$D_{eff} = D_o \exp\left(-\frac{E_a}{R T}\right) \quad (3.58)$$

The activation energy ( $E_a$ ) can be computed by applying the natural logarithm to both sides of the equation demonstrated below:

$$\ln D_{eff} = \ln\left(D_o \exp\left(-\frac{E_a}{R T}\right)\right) \quad (3.59)$$

The graph of the natural logarithm of  $D_{eff}$  against the reciprocal of  $T$  results in a linear slope of  $m_1$ :

$$m_1 = \frac{E_a}{R} \quad (3.60)$$

where  $R$  is the universal gas constant ( $8.314 \cdot 10^{-3} \text{ kJ (mol K)}^{-1}$ ).

### 3.10. Thin-layer drying models

The thin-layer drying models used to evaluate the drying kinetics of the apple products in the study are listed in Table 3.4.

Table 3.4 Selected thin layer equation applied to drying curves (Rafiee et al., 2009)

S/N	Model name	Formula
1	Newton	$MR = \exp(-k t)$
2	Wang and Singh's models	$MR = 1 + a t + b t^2$
3	Midilli and Kucuk	$MR = a \exp(-k t^n) + b t$
4	Page model	$MR = \exp(-k t^n)$
5	Modified page model	$MR = \exp(-(k t)^n)$
6	Logarithmic	$MR = a \exp(-k t) + c$
7	Two-term	$MR = a \exp(-k t) + b \exp(k_1)$
8	Two-term exponential model	$MR = a \exp(-k t) + (1 - a) \exp(k a t)$
9	Weibull distribution	$MR = a - b \exp(-(k t^n))$
10	Handerson and Pabis	$MR = a \exp(k t)$

In the table the  $t$  is time,  $k$ ,  $k_1$ ,  $k_2$  are drying constants (1/hr), and  $a$ ,  $b$ ,  $c$  and  $n$  are empirical constants or model coefficients (-).

#### Evaluation methods of the thin layer models

The modelling of drying behaviour in agricultural products involved statistical regression and correlation analysis, using both linear and nonlinear regression models to identify relationships between variables, especially when there are no existing empirical relationships (Akpınar and Bicer, 2005). To select the best thin-layer drying model for a specific application the following steps are employed. First, compute values for selected statistical parameters. Next, prioritize models with the highest or lowest values depending on the statistical tool, then finally select the model (Kucuk et al., 2014; Inyang et al., 2018). Four statistical metrics were used in this study to determine the best-fitting model for the drying behaviour of the product, as presented in Table 3.5.

Table 3.5 Selected statical parameters

Name of statistical tool	Formula	Source
Coefficient of determination	$R^2 = \frac{n \sum_{i=1}^n x_i y_i - (\sum_{i=1}^n x_i)(\sum_{i=1}^n y_i)}{\sqrt{[n \sum_{i=1}^n x_i^2 - (\sum_{i=1}^n x_i)^2][n \sum_{i=1}^n y_i^2 - (\sum_{i=1}^n y_i)^2]}}$	(Kumar et al., 2023)
Chi-square	$\chi^2 = \frac{\sum_{i=1}^n (x_i - y_i)^2}{n - C}$	
Root mean square error	$RMSE = \sqrt{\sum_{i=0}^n \frac{(x_i - y_i)^2}{n}}$	(Jamil and Akhtar, 2017)
Sum squared error	$SSE = \sum_{i=1}^n (x_i - y_i)^2$	(Nainggolan et al., 2019)

In the table the  $n$  is the number of data and  $C$  is the number of constants.

#### 3.11. Colour analysis

Colour is a crucial factor in agricultural products. Because the chromophores in fruits and vegetables typically alter during ripening, colour is frequently utilized as a key indicator of

quality (Nguyen et al., 2021). The total colour difference ( $\Delta E$ ) was also determined as follows: Eq. (3.61) (Srivastava et al., 2025):

$$\Delta E = \sqrt{(L^* - L_0^*)^2 + (a^* - a_0^*)^2 + (b^* - b_0^*)^2} \quad (3.61)$$

where:  $L^*$ ,  $a^*$ ,  $b^*$  values are the measured values of dried sample under different drying methods;  $L_0^*$ ,  $a_0^*$ ,  $b_0^*$  values are the measured values of fresh samples.

The  $L^*$  value in the colour meter indicates the brightness of the surface colour; the larger the  $L^*$  value, the whiter the colour. The  $a^*$  value indicates the range from red to green; the larger the positive value, the redder the colour, the smaller the negative value, the greener the colour. The  $b^*$  value indicates the range from yellow to blue; the larger the positive value, the more yellow the colour, the smaller the negative value, the bluer the colour. The larger the  $\Delta E$  value is, the greater the colour difference between the dried and the fresh samples (Srivastava et al., 2025).

The colour saturation ( $C$ ) and chroma angle (HUE) are calculated as Eqs. (3.62) and (3.63) respectively (Li et al., 2023b):

$$C = \sqrt{(a^*)^2 + (b^*)^2} \quad (3.62)$$

$$\text{HUE} = \tan^{-1} \left( \frac{b^*}{a^*} \right) \quad (3.63)$$

### 3.12. Material used to enhance the flow uniformity

One of the main challenges with solar dryers is the non-uniform airflow within the drying chamber. This inconsistency often leads to uneven drying times, causing some areas to become over-dried while others remain moist. Such variations can negatively impact the quality, texture, and nutritional value of the dried products. To mitigate such issues, I employed rectangular baffles, triangular baffles, and a swirler (see Fig. 3.14) to improve the airflow distribution. Additionally, Taguchi analysis was used to identify the optimal configuration, ensuring the best performance in terms of uniform drying efficiency. The triangular baffles measuring 0.18 m by 0.18 m with a base of 0.06 m, rectangular baffles measuring 0.12 m in height by 0.23 m in length and a swirler were integrated into the plenum of the drying chamber.



Fig. 3.14. Different types of flow enhancement materials are used



The enhancement materials integrated within the drying chamber are illustrated in Fig. 3.15.

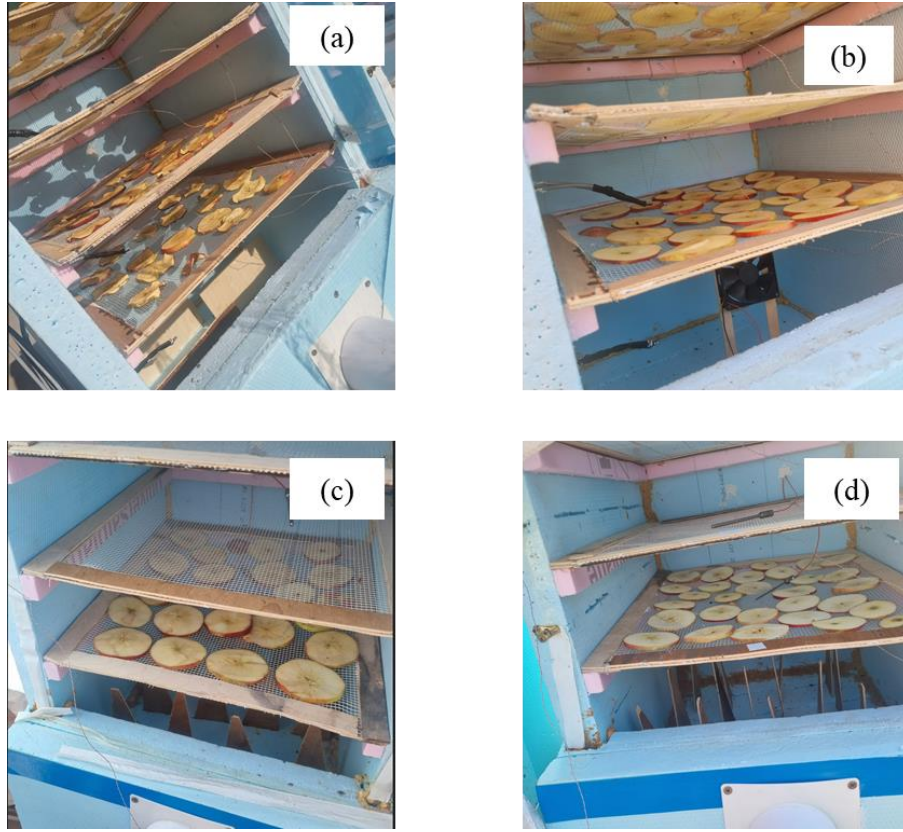


Fig. 3.15. Flow enhancement materials integrated within the drying chamber: rectangular baffles (a), swirler (b) and triangular baffles (c, d)

#### *Evaluation uniformity*

To assess uniformity, statistical methods such as mean, variance, standard deviation ( $\sigma$ ) and coefficient of variance ( $C_v$ ) were applied. The expressions for mean, variance and standard deviation can be formulated as follows, as indicated by (Lee et al. 2015):

$$\text{Mean } (\bar{x}) = \frac{1}{n} \sum_{i=0}^n x_i \quad (3.64)$$

$$\text{Variance } (V_{ar}) = \frac{1}{n} \sum_{i=0}^n (x_i - \bar{x})^2 \quad (3.65)$$

$$\sigma = \sqrt{V_{ar}} \quad (3.66)$$

where  $n$  is the number of data points.

To measure the extent of variation the coefficient of variation is a widely accepted metric to measure the extent of variation, defined as the ratio of the  $\sigma$  to the  $\bar{x}$  (Cook et al., 2014). The smaller the  $C_v$ , the greater the stability (Zheng and Pan, 2014):

$$C_v = \frac{\sigma}{\bar{x}} \quad (3.67)$$

### 3.13. Procedures in the Taguchi approach

The Taguchi method follows a systematic series of steps to optimize performance. First, a target value is defined, focusing on maximizing, minimizing, or achieving a specific performance measure. Next, the key design parameters influencing the performance are identified, and the levels at which these parameters will vary are determined. An experimental design is then created using orthogonal arrays, which systematically organize the experiments to ensure efficiency and balanced testing. The experiments are conducted based on this design to collect data on the effects of each parameter. The collected data is then analysed to determine the impact of the parameters and identify the optimal settings. Finally, confirmation experiments are performed to verify the results unless the optimal parameter combination matches one of the original experimental setups in the array (Kamaruddin et al., 2010).

The following equations were applied during the Taguchi analysis (Chauhan et al., 2017):

$$\text{Larger-the-better: (S/N) ratio} = -10 \log_{10} \frac{1}{n} \left( \sum_{i=1}^n y_{ij}^2 \right) \quad (3.68)$$

$$\text{Smaller-the-better: (S/N) ratio} = -10 \log_{10} \frac{1}{n} \left( \sum_{i=1}^n \frac{1}{y_{ij}^2} \right) \quad (3.69)$$

$$\text{Nominal is best: (S/N) ratio} = -10 \log_{10} \frac{1}{n} \left( \sum_{i=1}^n \frac{\bar{y}^2}{s^2} \right) \quad (3.70)$$

where  $n$  is number of replications,  $s$  is variance,  $y$  is observed response value, and  $\bar{y}$  represents the mean response.

In the study, I was selected four key control parameters: solar radiation (SR), ambient temperature ( $T_{am}$ ), inlet temperature of the dryer ( $T_{in}$ ), and the enhancement configuration (Type-C) of the drying chamber. The configurations examined included triangular baffles, rectangular baffles, and swirls. To evaluate the performance of the drying chamber and its flow uniformity, were focused on critical responses such as pressure drop and uniformity. I analysed three distinct configurations of equipment to ascertain their effectiveness in achieving optimal drying conditions and efficiency. The approach followed the principle that smaller values are better (SB) for all the specified response variables. The analysis of the Taguchi method was conducted using Minitab-22.2.2 software. The input parameters utilized in the study are presented in Table 3.6.

Table 3.6 Input parameters and their respective levels

S/N	Parameter	Units	Level 1	Level 2	Level 3
1	Average solar radiation (SR)	W/m <sup>2</sup>	810	830	850
2	Average ambient temperature ( $T_{am}$ )	°C	27	30	33
3	Average inlet Temperature ( $T_{in}$ )	°C	40	41	42
4	Type of configuration (Type-C)	-	RB	TB	SW

### 3.14. Economic analysis and feasibility study

This study presumed that the dryer operates annually for apple drying between June and September. Consequently, the expenses associated with the solar dryer excluded out of those months. Economic performance indicators were assessed considering Hungary's fiscal

conditions for the 2024/2025 period. The annual investment cost ( $C_a$ ) for the dryers was determined using the parameters outlined in Eq. (3.71) (Mohammed et al., 2020; Philip et al., 2022):

$$C_a = C_{ac} + C_{am} - S_a + C_{af}, \quad (3.71)$$

where  $C_{ac}$ ,  $C_{am}$ ,  $S_a$  and  $C_{af}$  represent the annual capital cost, maintenance cost and salvage value of the dryers, the annual operational cost of the fan respectively.

$$C_{ac} = C_{ds} F_{cr}, \quad (3.72)$$

where  $C_{ds}$  is capital cost of the drying system (in HUF/USD) and  $F_{cr}$  is capital recovery factor (see Eq. (3.75)). The cost of materials of the drying system ( $C_{ds}$ ) is the total sum of the prices of all materials used to build the drying system like the cost of solar air heater, drying chamber, trays etc and auxiliary components like fans, chimney etc if needed. The annual operational cost of the fan ( $C_{af}$ ) was calculated employing Eq. (3.73):

$$C_{af} = N_{fa} P_r C_e, \quad (3.73)$$

where  $N_{fa}$  the number of hours fan operates in a year,  $P_r$  rate power of fan and  $C_e$  unit cost of electricity but if the fan is operated using photo voltaic it becomes zero.

The  $S_f$  (salvage value factor) and  $F_{cr}$  (capital recovery factor) were computed using Eq. (3.74) and Eq (3.75) respectively (Philip et al., 2022):

$$S_f = \frac{r}{(1+r)^n - 1}, \quad (3.74)$$

$$F_{cr} = \frac{r(1+r)^n}{(1+r)^n - 1}, \quad (3.75)$$

where  $r$  denotes the rate of interest and  $n$  is the life of the solar dryer in years.

The cost of drying per kilogram of product within the dryer ( $C_d$ ) was determined using Eq. (3.76) (Singh and Gaur, 2021):

$$C_d = \frac{C_{ac}}{P_{dy}}, \quad (3.76)$$

where  $P_{dy}$  is the annual quantity of product dried inside the dryer per year and it was estimated using Eq. (3.77):

$$P_{dy} = \frac{M_d D}{D_b}, \quad (3.77)$$

where,  $M_d$  is the amount of crop dried inside the drier per batch,  $D$  and  $D_b$  are the numbers of days the dryer operates in a year and drying period of dryer per batch respectively. The price per kilogram of the dried product ( $C_{dp}$ ) was equated using Eq. (3.78):

$$C_{dp} = C_d + C_{fpd}, \quad (3.78)$$

where  $C_{fpd}$  represents the cost of fresh product per kilogram of dried product, determined as follows:

$$C_{fpd} = C_{fp} \frac{M_f}{M_d} \quad (3.79)$$

Here,  $M_f$  is the quantity of fresh product loaded inside the dryer, and  $C_{fp}$  is the cost of fresh product.

The savings per kilogram of dried product ( $S_{kg}$ ) are expressed as:

$$S_{kg} = S_{pc} - C_{dp}, \quad (3.80)$$

$S_{pc}$  refers to the selling price of dried products per kilogram.

The savings gained from the dryer for each batch of crop drying ( $S_{dc}$ ) can be calculated as:

$$S_{dc} = S_{kg} M_d \quad (3.81)$$

The savings achieved from the dryer per day ( $S_{dc,d}$ ) are calculated as:

$$S_{dc,d} = \frac{S_{dc}}{D} \quad (3.82)$$

The savings generated by the dryer after  $j$  years ( $S_j$ ) is expressed as:

$$S_j = S_{dc,d} D (1 + i)^{j-1} \quad (3.83)$$

where  $i$  is the inflation rate.

The economic feasibility of the drying system was evaluated using established financial indicators, including net present value (NPV), benefit-cost ratio (BCR), and payback period ( $P_t$ ) analysis.

The net present value of the solar dryers represents the difference between the present value of all expected cash inflows and the total capital investment cost over the project's lifetime. NPV was computed using Eq. (3.84) (Mohammed et al. 2020):

$$NPV = \sum P_N (1 + r)^n - C_{ds} \quad (3.84)$$

$$P_N = S_j (1 + r)^{-n} \quad (3.85)$$

where  $P_N$  is the discounted present value ( $S_j$ ) to be invested during  $n$  years in the future. The investment with a positive NPV was selected.  $i$  is the discounting (or depreciation) rate of the dryers, and  $C_{ds}$  is the capital cost of dryers. BCR were determined using Eq. (3.86) (Aniesrani Delfiya et al., 2024):

$$BCR = \frac{\sum_{t=1}^{t-n} B_t}{\sum_{t=1}^{t-n} C_t}, \quad (3.86)$$

where  $B_t$  is benefits in year  $t$ ,  $C_t$  is costs in year  $t$ .

The time required for the dryer to recover the invested amount is referred to as the payback time. The payback time for the developed drying system was determined using Eq. (3.87) (Singh and Gaur, 2021):

$$P_t = \frac{\ln \left[ 1 - \frac{C_{ds}}{S_1} (r - i) \right]}{\ln \left( \frac{1+i}{1+r} \right)}, \quad (3.87)$$

where  $S_1$  is the saving obtained from the dryer after the first year.

## 4. RESULTS

This chapter presents the detailed results of the experiments conducted to achieve the thesis objectives. The following sections will discuss the outcomes of various experimental and main computational results related to the solar drying system.

### 4.1. CFD results of the trays and validation

This chapter discusses the findings from the simulation and experiment. It also discusses essential points that arise from the results and compares the simulated value to the experimental result.

#### 4.1.1. Temperature distribution in the trays

Fig. 4.1 presents the temperature distribution contour across the trays obtained from the simulation. The contour map reveals that the bottom tray experiences the highest temperature, with each successive tray showing a slight decrease in temperature as you move upward. This gradient in temperature indicates an uneven heat distribution, suggesting that products on the trays will dry at varying rates. Consequently, the bottom tray dried products more rapidly than those placed on higher trays, with this pattern continuing to the top tray.

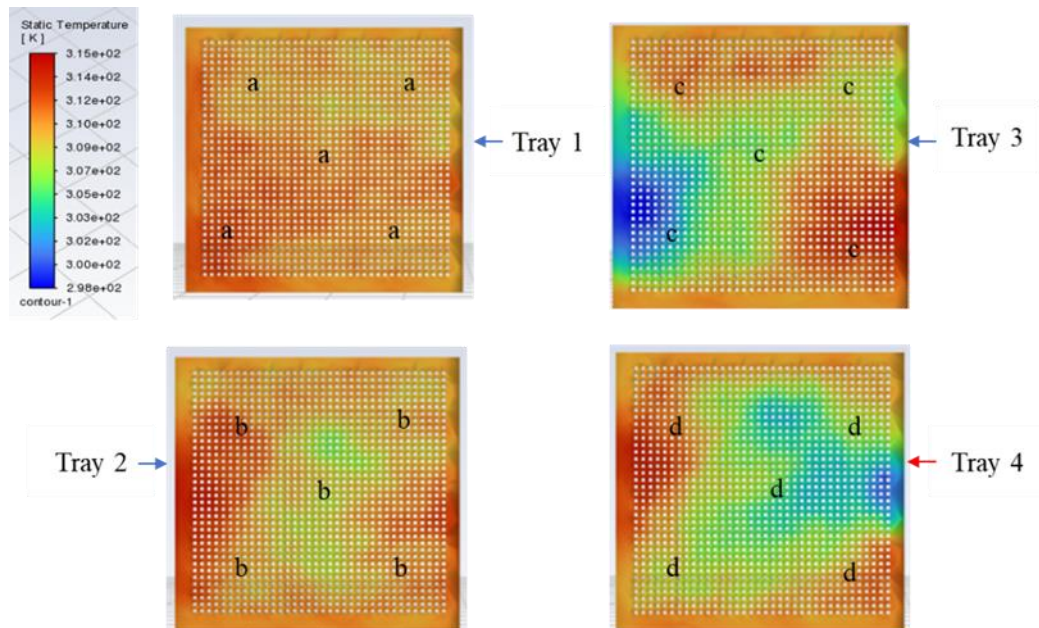


Fig. 4.1. Simulated contours static temperature of the four trays

#### 4.1.2. Validation of the simulation results

Simulated results were compared with experimental data to validate them. The average values from both the experimental and simulation data were taken for analysis. Temperature readings from the tray simulations reading of trays labelled *a*, *b*, *c*, and *d*, as shown in Fig. 4.1. A statistical comparison, summarized in Table 4.1, reveals strong agreement between the *CFD* predictions and experimental measurements, further confirming the accuracy of the *CFD* model in capturing the thermal behaviour of the system. The calculated *RMSE* of 1.77 and *PBIAS* of 2.74% highlight the model's reliability, indicating minimal error and bias.

Table 4.1. Comparison of experimental and *CFD* results for tray temperatures

Conditions	Tray1	Tray 2	Tray 3	Tray 4
Experimental results (°C)	40.95	39.06	38	37.13
Simulation results (°C)	41.85	40	36.25	35.7
Deviation	0.9	0.94	1.75	1.43
Relative error (%)	2.1	2.35	4.8	4

#### 4.2. Experimental results

To assess dryer performance, experiments were carried out under four loading conditions: unloaded, half-capacity (250 g/tray), semi-full capacity (405 g/tray), and full-capacity (500 g/tray).

Half-loaded capacity: This represents the initial test condition, where each tray was loaded with 250 g of material, resulting in a total of 1 kg per dryer.

Semi-full Loaded capacity: This intermediate loading condition used 405 g per tray, total of 1.62 kg per dryer.

Full-loaded capacity: This condition reflects the maximum operational load, with 500 g of material per tray and a total of 2 kg per dryer. The full-load test assesses the dryer's peak performance.

For the essence of the calculation, the initial and final moisture content of the apples were assumed to be 80% (wet basis) and 24%, respectively, as reported by Sharma et al. (2009). Additionally, the  $h_{fg}$  was calculated to be 2501.715 kJ/kg.

##### *Solar intensity and ambient temperature*

The solar intensity and the ambient temperature are shown in Fig. 4.2. Solar radiation typically increases during the morning, peaks around midday (12:00–13:00), and gradually decreases in the afternoon. The average solar radiation values were recorded as 830 W/m<sup>2</sup> on day 1 (with triangular baffles or case I), 810 W/m<sup>2</sup> on day 2 (with the rectangular baffles integrated or case II), and 850 W/m<sup>2</sup> on day 3 (with swirler baffles or case III). The corresponding ambient temperatures for these days were 30 °C, 27 °C, and 33 °C, respectively.

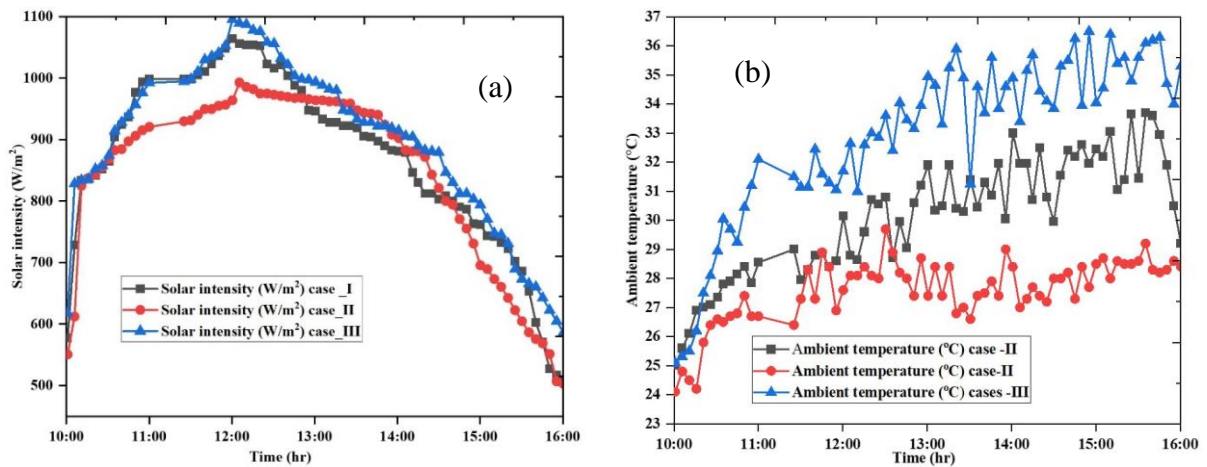


Fig. 4.2. Solar intensity (a) and ambient temperature (b) during the experiment



### 4.3. Evaluation of the drying system

#### 4.3.1. Temperature distribution under the unloading and loading conditions

Fig. 4.3 and Fig. 4.4 illustrates the temperature distribution in dryer 1 and dryer 2 during loading and unloading. Under unloading conditions, where the dryer is completely empty throughout the day, the temperature variation across the trays was minimal (see Fig. 4.3 (a) and Fig. 4.4 (c)), suggesting uniform heat distribution. This could be due to the absence of products on the trays, which allows for unrestricted airflow and a more consistent distribution of heat across the drying chamber. Additionally, with fewer obstructions, the drying system may reach a steady-state condition more quickly, leading to stabilized temperatures across all trays. In contrast, during the loading phase, significant temperature differences were observed, with the first tray exhibiting higher temperatures. This is likely due to airflow blockage or restricted circulation caused by the presence of products, which disrupts the uniform distribution of heat.

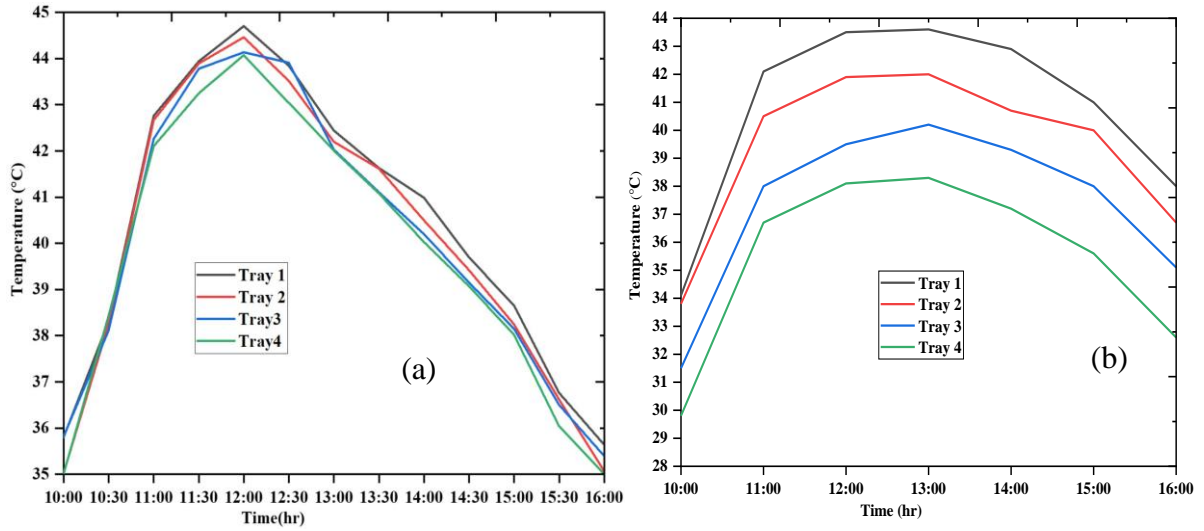


Fig. 4.3. Temperature distribution of the trays of dryer 1: unloading (a) and loading (b)

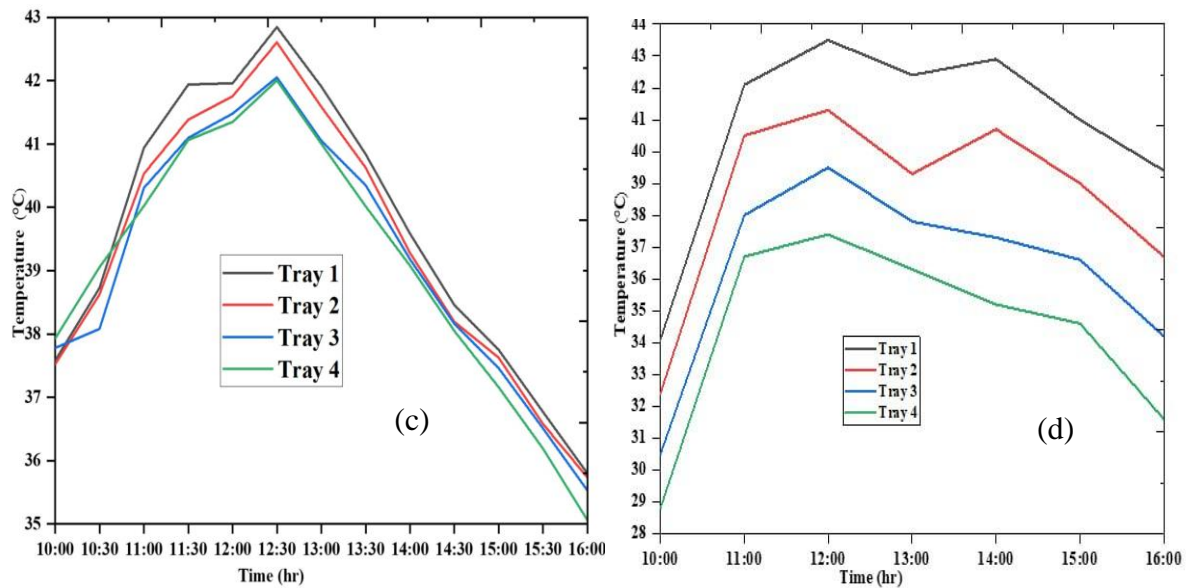


Fig. 4.4. Temperature distribution of the trays of dryer 2: unloading (c) and loading (d)

#### 4.3.2. Humidity analysis

The relative humidity (RH) at three different points in dryer's inlet (bottom), mid-section, and outlet (top) from 10:00 to 16:00 under half, semi-full and full capacity. In all three-measurement points inlet (bottom), mid-section, and outlet (top) show a consistent decline in relative humidity over time in all the three conditions (i.e., under the half, semi full loading, and full loading condition). The vertical distribution shows highest humidity at the outlet of the dryer, intermediate at the middle of the dryer, and lowest readings at the inlet of the dryer, indicating potential heat-driven moisture accumulation in upper sections or restricted airflow patterns.

The loading conditions demonstrate a direct impact on humidity characteristics. Half-load capacity maintains humidity at 35-40% (at the inlet of the dryer), 40-45% (at the middle of the dryer), and 45-50% (at the outlet) (see Fig. 4.5 (a)). Semi-full loads show a consistent 5% increase at each level (40-45%, 45-50%, 55-60%) (see Fig. 4.5 (b)), while full-load conditions reach 45-50%, 50-55%, and 60-65% (see Fig. 4.5 (c)) respectively. This establishes a clear 10-15% total humidity increase from minimum to maximum loading, with semi-full data confirming the progressive relationship.

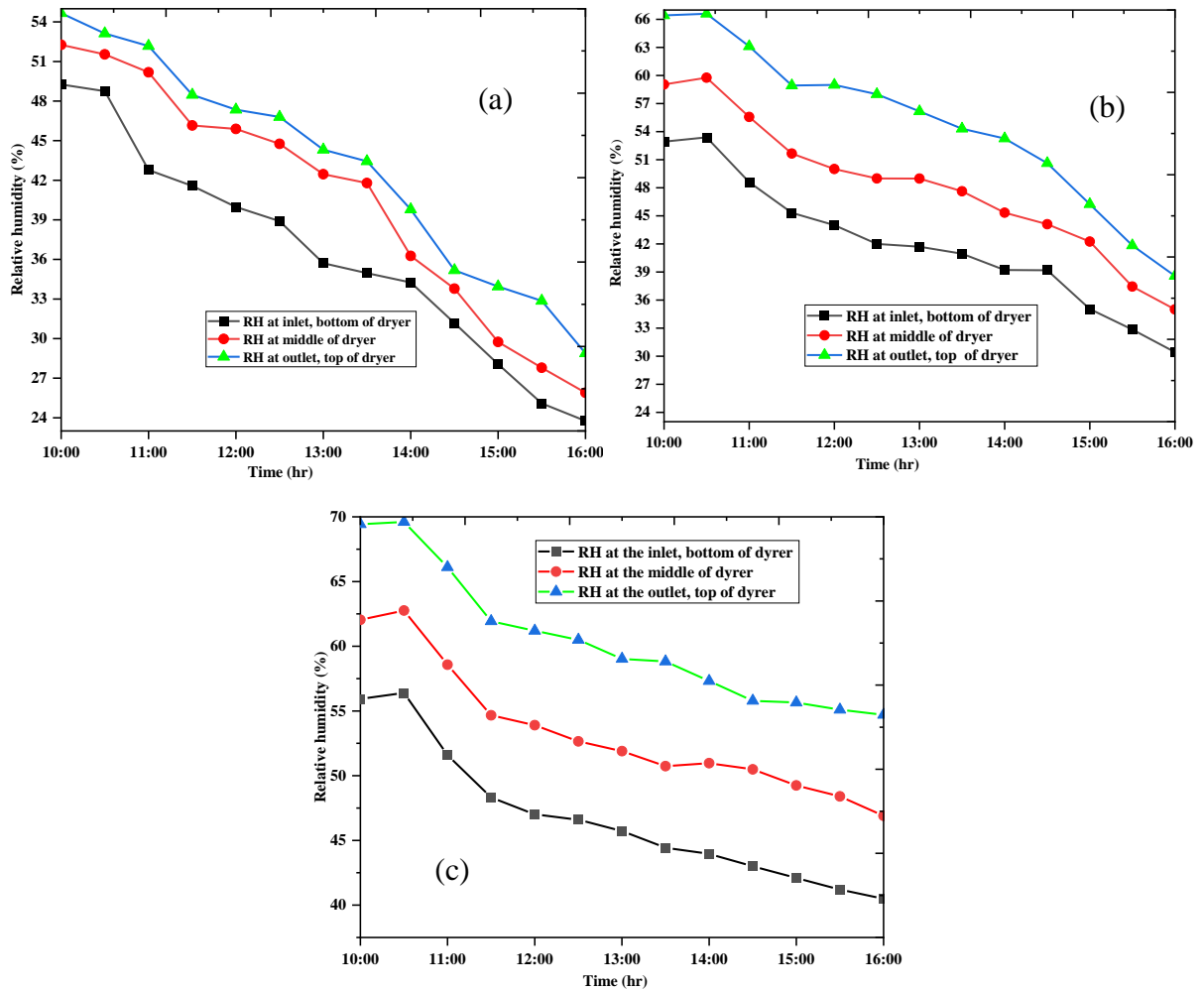


Fig. 4.5. RH in dryer 1 under the half loading capacity (a), semi full capacity (b) and full loading capacity (c)



In general, from the experimental results that moisture evaporation rates are significantly influenced by the load level. Under half-load conditions, rapid humidity reduction occurs, while semi-full loads show a more moderate decline. Full-load operations, on the other hand, maintain the most stable humidity levels. These results suggest that increased loading elevates the humidity.

#### 4.3.3. Efficiency of the solar air heaters and drying system

The efficiency of the solar air heater and corresponding dryer is shown in Fig. 4.6 (a) and Fig. 4.6 (b) respectively. The stated Figures illustrate a clear trend of increasing efficiency as solar radiation intensifies from the morning to midday, with the solar air heater achieving its peak efficiency and the dryers around noon. After this peak, the efficiency gradually declines as solar radiation decreases in the afternoon. This pattern emphasizes the crucial role of solar intensity, which serves as the primary factor influencing the solar drying system efficiency.

On day 1, the SAH achieved an average thermal efficiency of 53.70%, while on day 2, it was 51.09%, and on day 3, it reached 54.80%. Similarly, the drying chambers exhibited similar characteristics, with dryer 1 showing efficiencies of 18.79% on day 1, 18.75% on day 2, and 18.84% on day 3. Since the efficiency trends were nearly identical across all units, only data from one representative dryer and heater are presented.

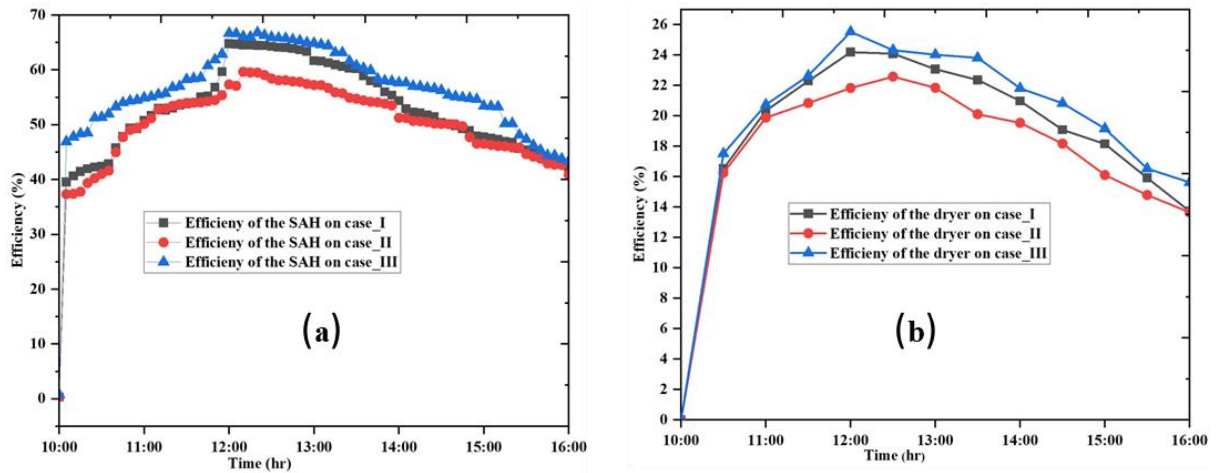


Fig. 4.6. Thermal efficiency of the solar air heater (a) and dryer (b)

The efficiency of the solar air heater ( $\eta_{sah}$ ) is expressed as a function of solar irradiance in  $W/m^2$  ( $I_r$ ), ambient temperature in  $^{\circ}C$  ( $T_{am}$ ), and the outlet temperature of the solar air heater ( $T_{sah,o}$ ) in  $^{\circ}C$  (see Eq. (4.1):

$$\eta_{sah} = \beta_0 + \beta_1 I_r + \beta_2 T_{am} + \beta_3 T_{sah,o} \quad (4.1)$$

$\beta_0 = -31.7764$ ,  $\beta_1 = 0.0567$ ,  $\beta_2 = 0.7388$ ,  $\beta_3 = 1.0123$  with  $R^2 = 0.989$  and  $p < 0.001$  for all parameters.

The average thermal efficiency of the dryer was observed to vary with its operating capacity as shown in Fig. 4.7. When the drying chamber was loaded to half capacity, its efficiency was 12.05%, increasing to 18.75% at semi-full loading capacity, and reaching 23.50% when loaded to full capacity. This trend demonstrates that the dryer operates more efficiently as its load increases. A higher load allows for better heat utilization, reducing energy losses and improving

moisture removal efficiency. The thermal efficiency of the dryer is directly linked to the amount of moisture removed, as more energy is effectively used for evaporation rather than being lost to the surroundings. However, beyond an optimal capacity, excessive loading may restrict airflow and heat distribution, potentially decreasing efficiency.

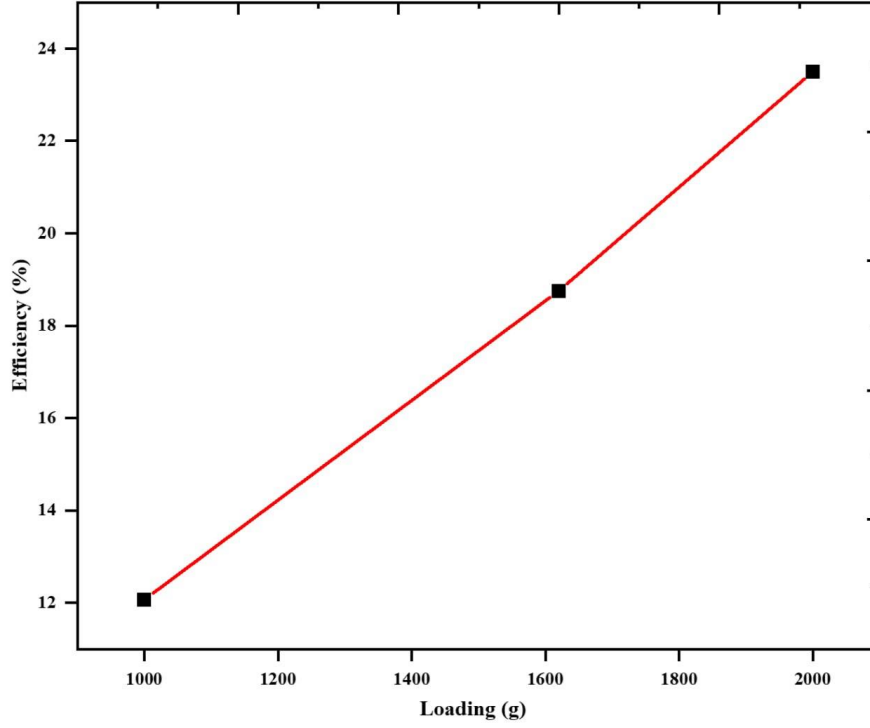


Fig. 4.7. Average efficiency of the dryer in different loadings

Thus, the efficiency of the dryer can be related by the following linear equation (i.e., Eq. (4.2)). The developed equation helps to predict the dryer's efficiency based on the loading of the dryer. This straightforward approach can be applied to enhance system design, optimize operation, and ensure maximum drying efficiency throughout the process:

$$\eta_{ac} = \lambda L_c + b, \quad (4.2)$$

where,  $\lambda$  defined as the ratio of the vertical change to the horizontal change (or slope),  $L_c$  represents the loading capacity of the dryer and  $b$  is the y-intercept (or constant). The estimated values of  $\lambda$  and  $b$  were 0.00997 and 2.33, respectively. The value of  $b$  is highly dependent on the unit of measurement. For instance, if the loading is expressed in kilograms instead of grams, the  $b$  value would be significantly different (e.g., 9.97 instead of 0.00997).

#### 4.3.4. Comparative evaluation of dryer designs

A direct comparison of various solar dryer designs reported in the literature can be challenging due to differences in factors such as geographical location, climatic conditions, and the type of product being dried. Additionally, the performance of a drying system is significantly influenced by the design and type of solar air heater employed. To minimize these discrepancies, I was focused comparison on systems utilizing single-pass, forced-convection dryers that exclude enhancements such as phase change materials, fins, or auxiliary backup systems. Initially, the study intended to compare results with dryers tested in similar climates,

but due to data limitations, the focus shifted to forced-airflow dryers of comparable design, omitting environmental influences. Fig. 4.8. presents a comparison of the average efficiencies of the dryers and solar air heaters of the study with those reported in the literature. The efficiency levels of both the solar air heater and the dryer of the current study align with those observed in previous studies, underscoring its competitive performance. The dryer used in this study demonstrated higher efficiency compared to most of the dryers designed by the authors listed in Fig. 4.8.

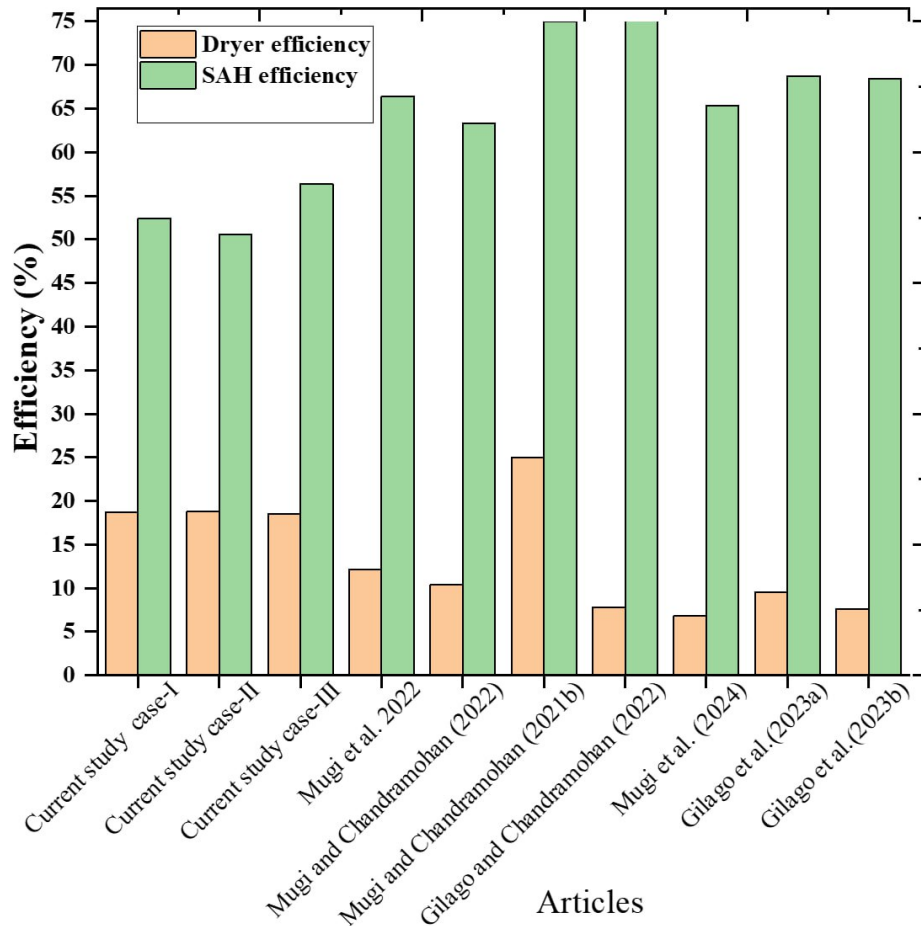


Fig. 4.8. Comparison of the SAH and dryer efficiencies of the current study within existing literature

#### 4.3.5. Specific heat energy consumption and specific moisture extraction rate

To calculate the specific moisture extraction rate (SMER) and specific heat energy consumption (SHE), were evaluated both dryers under full and half-capacity conditions (see Fig. 4.9). This comparative analysis determines the most practical and efficient loading configuration for optimal dryer performance. Over time, both *SHE* and *SMER* exhibit a general trend of increasing energy consumption and decreasing moisture extraction efficiency as the drying process continues. This is due to the diminishing moisture content in the material, which requires more energy to extract less moisture. However, dryers operating under full load are more efficient overall.

When the dryer operates under full load, *SHE* was distributed across a larger amount of material, making the process more energy-efficient. The energy required to remove moisture from each unit of mass is lower, as the dryer has more material to process, allowing for better thermal efficiency and moisture extraction (higher *SMER*). In contrast, under half load, the dryer consumes more energy per unit of mass, as the available heat is not fully utilized, resulting in lower thermal efficiency and a reduced moisture extraction rate. The smaller load makes the dryer less efficient, requiring more energy to evaporate moisture from a limited amount of material. Full load operation maximizes thermal efficiency and moisture extraction by allowing the dryer to maintain a stable temperature and utilize heat more effectively. On the other hand, under half load, the heat may not be distributed evenly, and the dryer struggles to extract moisture efficiently, leading to higher energy consumption and lower *SMER*. This difference in efficiency can be attributed to the economy of scale, where larger loads allow for better utilization of the dryer's capacity, resulting in both lower *SHE* and higher *SMER*. Conversely, operating at half load leads to underutilization of the system, causing inefficiency and higher energy consumption for each unit of moisture removed.

In general, the energy consumption and moisture extraction rate are indirectly related, as shown in Fig. 4.9. The linear regression analysis: *SHE* vs *SMER* of both dryers under full and half loading capacity is shown Appendix A5.

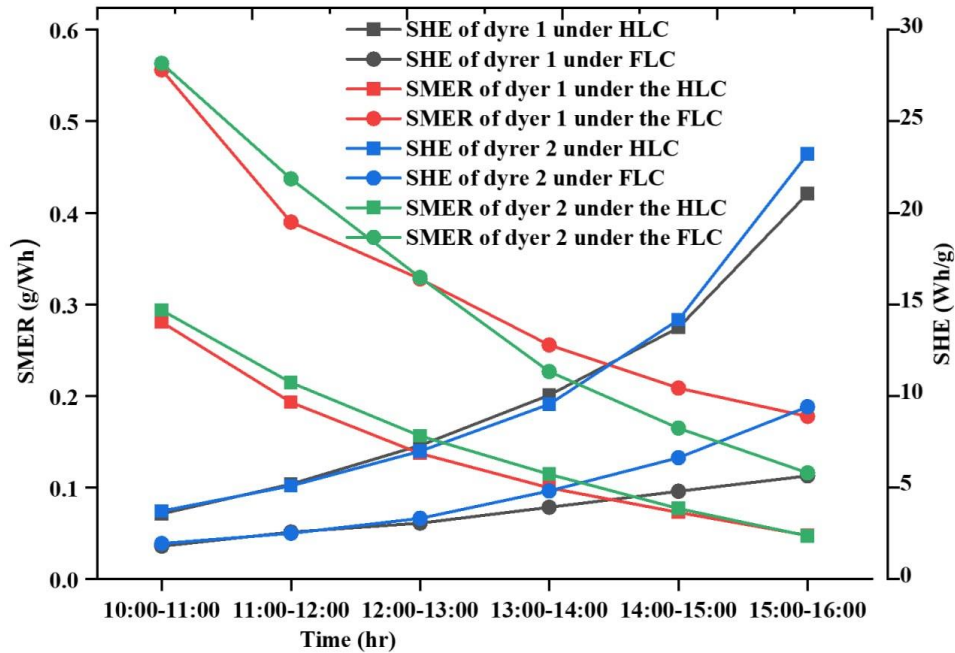


Fig. 4.9 Variation of the specific moisture extraction rate (SMER) and specific heat energy consumption (SHE) with time

#### 4.3.6. Exergy analysis of solar air heaters

To minimize redundancy, exergy analysis was conducted and compared for both day 1 and day 2. The exergy inflow for both solar air heaters over the two days are depicted in Fig. 4.10 (a). The data demonstrates typical behaviour for solar air heaters, with the highest exergy inflows occurring when solar radiation is at its peak during midday, followed by a gradual decline as radiation decreases in the afternoon. This pattern is consistent with the behaviour of solar

radiation, which peaks at midday and diminishes in the late afternoon. This observation is further supported by Mugi and Chandramohan (2021b) noted that exergy increased until noon, as solar radiation was higher during that time, and then decreased towards the evening. For day 1, the average exergy inflow of  $SAH_1$  was 378.1743 W, while  $SAH_2$  recorded 377.2133 W on day 1. On day 2,  $SAH_1$  had an average exergy inflow of 376.7432 W, whereas  $SAH_2$  showed 375.603 W. These results suggest that day 1 provided more favourable conditions for both solar air heaters (SAHs), possibly due to better solar irradiance. The values for  $SAH_1$  and  $SAH_2$  are quite close to each other throughout the day, suggesting similar performance for both solar air heaters under the same environmental conditions. Similarly, the exergy outflows for both SAHs follow the same trend as the inflows (Fig. 4.10(b)). Understanding these trends is critical for system design optimization and efficiency improvement in solar air heaters.

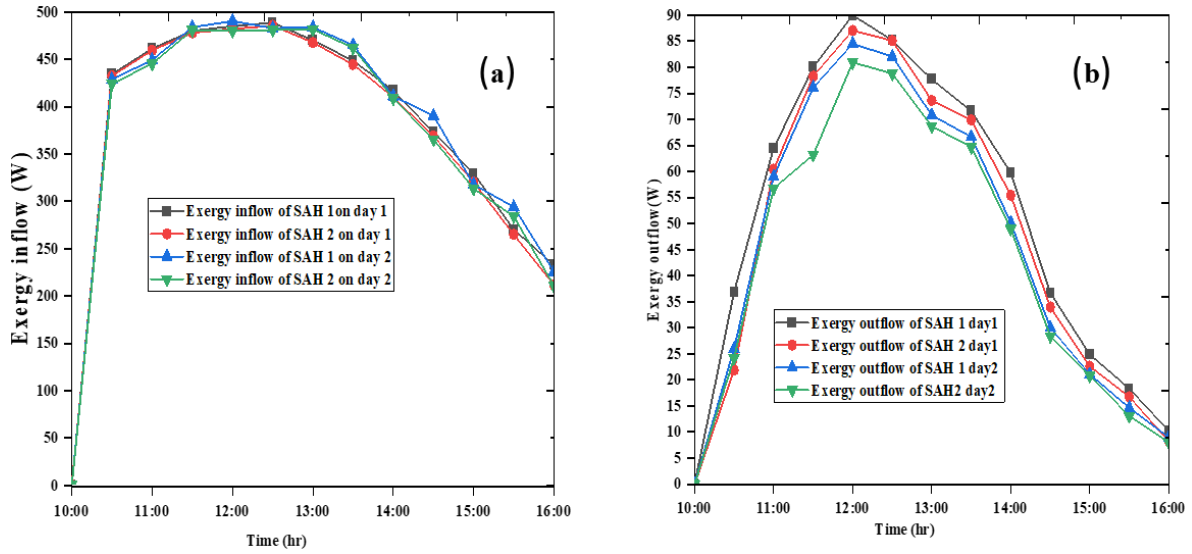


Fig. 4.10. Exergy inflow (a) and exergy outflow (b) of the solar air heater

#### 4.3.6.1. Exergy inflow and outflow of the drying chambers

Fig. 4.11 illustrates the temporal variation of exergy inflows and outflows for both dryers. A noticeable decline in both exergy inflows and outflows occurs after 12:00 p.m. for both dryers. This observation is consistent with the findings of Singh et al. (2023), which suggests that as the temperature within the drying chamber decreases after 1:00 p.m., there is a corresponding reduction in exergy. This analysis provides important insights into how energy is being utilized and lost throughout the day, offering potential areas for improving dryer performance and energy efficiency. On day 1, dryer 1 had an average exergy inflow of 17.62 W, and dryer 2 has 16.74 W. The average exergy outflows were 4.44 W for dryer 1 and 3.54 W for dryer 2, with both dryers peaking at noon before decreasing towards the end of the day.

Comparable trends in exergy inflow, outflow, and losses have also been observed in previous studies by Kumar et al. (2024) and Chowdhury et al. (2011). Their findings support the consistency of these exergy behaviour patterns across similar energy systems, further validating the results presented in this study.

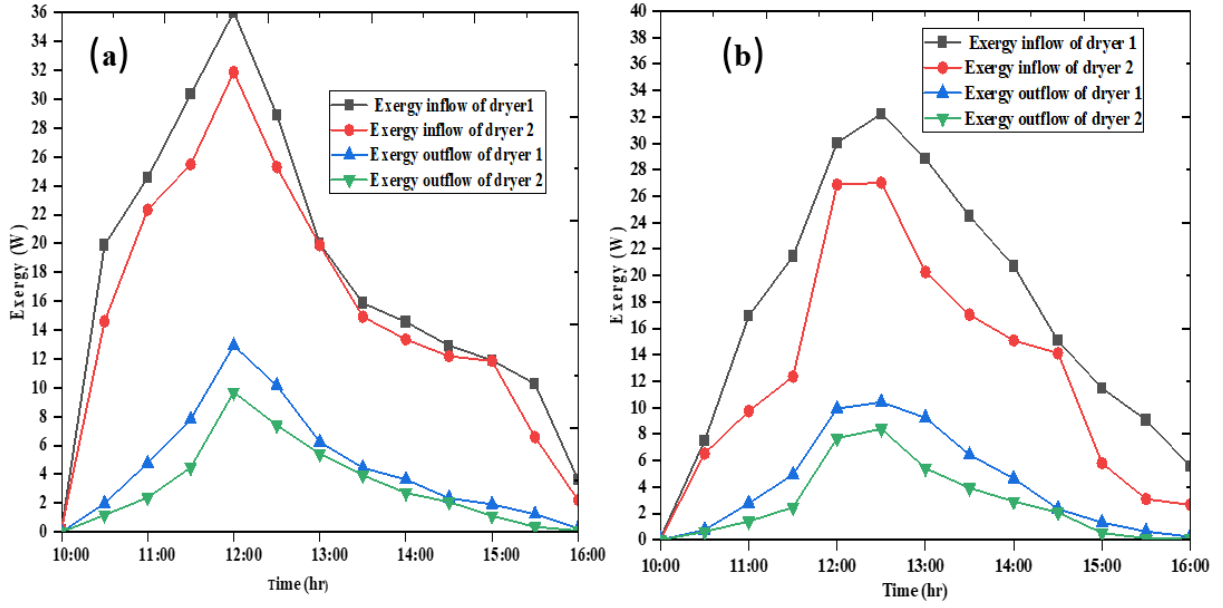


Fig. 4.11. Exergy analysis of the drying chambers: day1 (a) and day 2 (b)

#### 4.3.6.2. Exergy inflow of the trays of dryers

The exergy inflow of the trays for both days is shown in Fig. 4.12. As shown in the indicated Figures, the exergy inflow in both days and both dryers demonstrate significant variations over time. The exergy flow of tray 1 consistently exhibits the highest exergy values, indicating it is the most efficient or possesses the highest beneficial work potential among the four systems analysed. In contrast, tray 4 shows the lowest exergy inflow values, suggesting it is the least efficient in terms of useful work output. The peak exergy values for most systems occur around noon, which aligns with typical solar thermal systems performance due to maximum solar radiation and energy input at this time. Both dryers follow expected thermal trends with peak efficiency around midday and decreasing exergy delivery with tray depth.

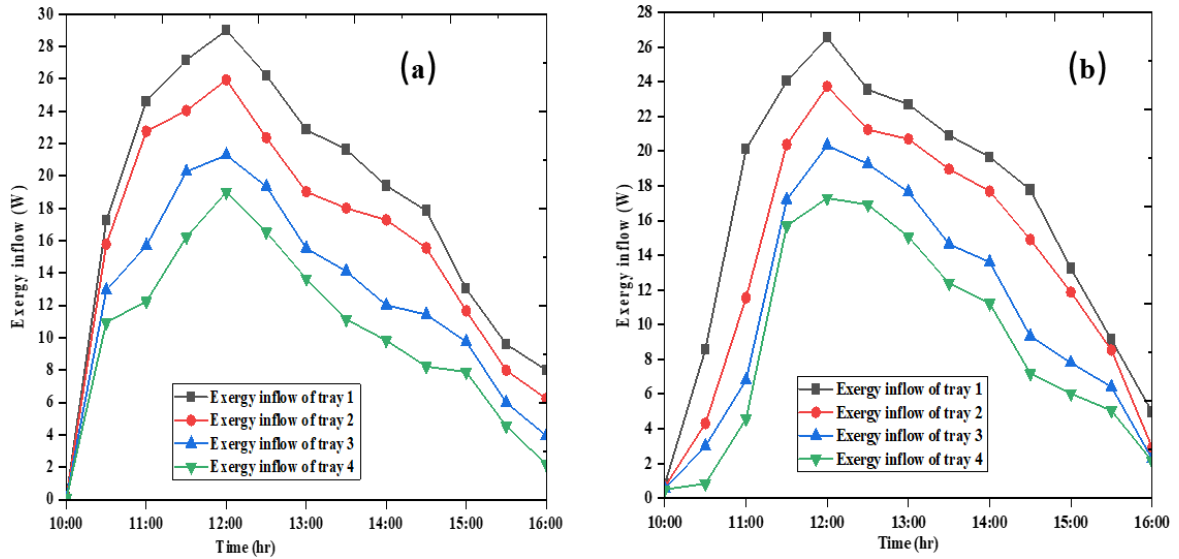


Fig. 4.12. Exergy inflow of the trays of dryer 1 (a) and dryer 2 (b) on day 1



## 4.3.6.3. Exergy outflow analysis of trays of dryers

The exergy outflow data of both dryer 1 and dryer 2 (see Fig.4.13) exhibits clear and consistent thermal behaviour throughout the drying cycle. Generally, the exergy outflow begins at very low values around 10:00 in the morning, gradually increases to a peak around midday (12:00 – 12:30), and then steadily declines until 16:00. This trend mirrors the natural diurnal pattern of solar energy availability, particularly in solar-assisted drying systems. The midday peak indicates the period of highest thermal activity, where the trays experience maximum heat and air flow, allowing for the greatest potential drying efficiency.

Across all time intervals, the lower tray (tray 1) consistently has the highest exergy outflow, while the top tray (tray 4) has the lowest. This vertical gradient highlights the typical pattern in multi-tray drying systems where the lower trays receive and retain more energy due to their proximity to the heat source and less obstruction by other trays. Conversely, as air and heat move upward through the chamber, energy is absorbed by the products loaded on the lower trays and diminished by losses, resulting in reduced outflow in lower trays. This pattern is observed in both dryers. The average exergy outflows in dryer 1 are 8.82 W, 7.68 W, 6.56 W, and 5.05 W for trays bottom tray through top tray, respectively. In comparison, dryer 2 has average outflows of 7.51 W (tray 1), 6.66 W (tray 2), 5.77 W (tray 3), and 4.89 W (tray 4). These findings are crucial for optimizing dryer performance, particularly in balancing airflow, improving energy distribution to lower trays, and maximizing drying efficiency across all layers.

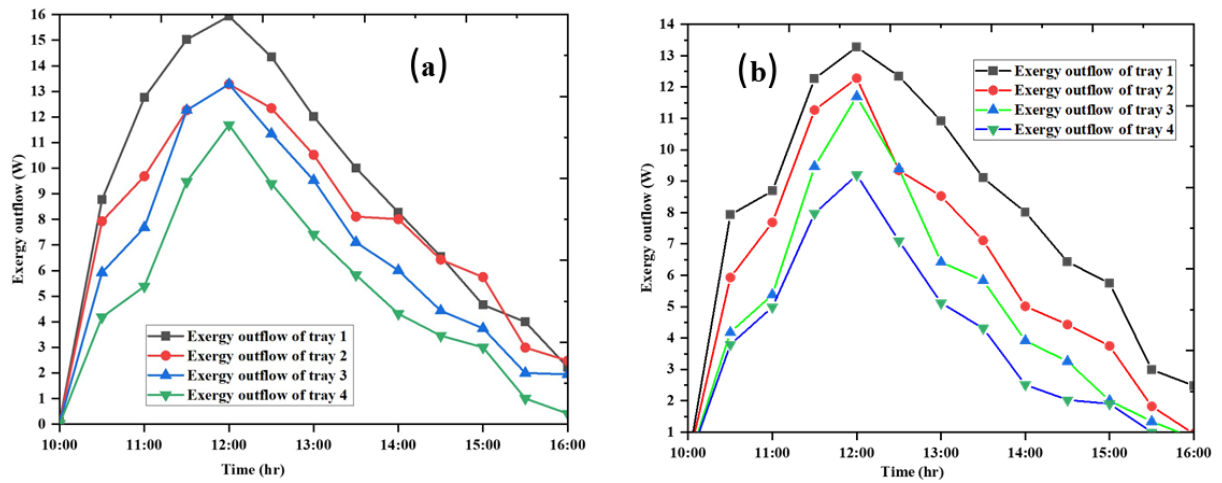


Fig. 4.13. Exergy outflow of the trays of dryer 1 (a) and dryer 2 (b)

## 4.3.6.4. Exergy efficiency of the drying system

As illustrated in Fig. 4.14(a),  $SAH_1$  and  $SAH_2$  achieved their highest exergy efficiencies around noon on both days. The exergy efficiency of the solar collector follows a parabolic curve, closely matching the solar irradiance pattern in Fig. 4.2. This alignment indicates that the  $SAH$ s and drying chambers performance depends heavily on solar energy availability efficiency peaks at maximum sunlight and drops as irradiation decreases. The parabolic trend demonstrates how solar variability affects the  $SAH$ s thermal conversion effectiveness. Thus, the  $SAH$ s exergy efficiency is inherently dependent on daily solar fluctuations, emphasizing the difficulties in achieving consistent solar energy utilization.

Similarly, in Fig. 4.12 (b), both dryers achieved their highest exergy efficiency around noon. The average exergy efficiency of  $SAH_1$  and  $SAH_2$  on day 1 were 11.85% and 10.15%, respectively, while the corresponding dryers had average exergy efficiencies of 20.37% and 19.50%. The drying chamber shows a consistent increase in exergy efficiency over time, indicating superior energy conversion for moisture removal compared to the solar collector. This improvement is driven by stabilized thermal conditions and reduced moisture content, with peak efficiency consistently occurring at 12:00 p.m. On day 2, the average exergy efficiency of dryer 1 was 17.93%, and dryer 2's was 16.73%. In general, the performance of the drying components dryers was heavily influenced by solar radiation, with efficiencies peaking around midday and declining in the morning and evening.

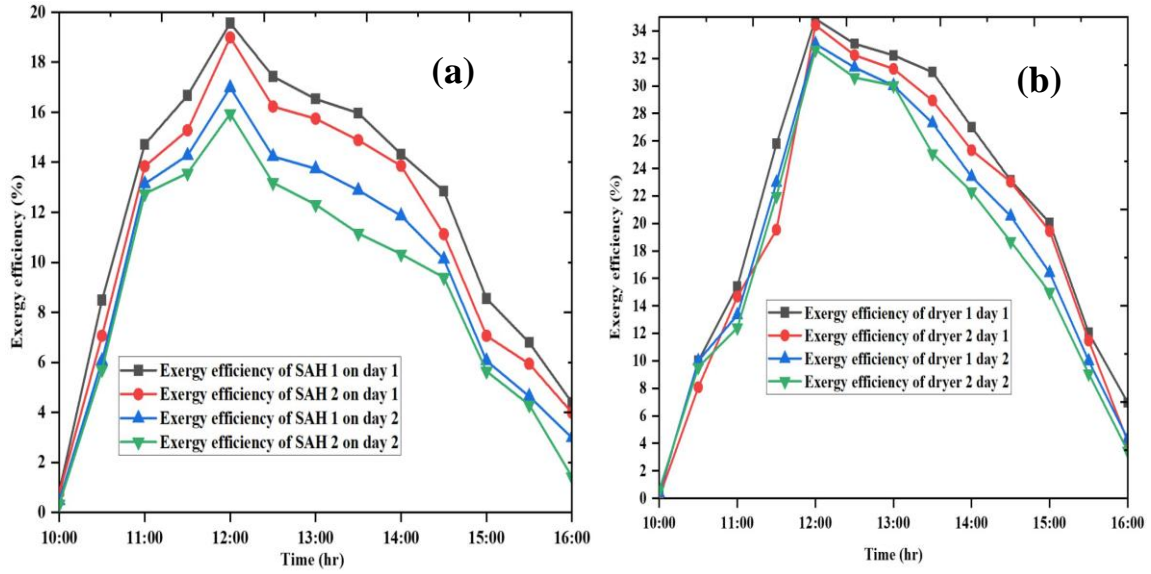


Fig. 4.14. Exergy efficiency of the solar air heaters (a) and drying chambers (b)

#### 4.4. Drying characteristics of golden apple

##### 4.4.1. Moisture content analysis

For the half-load capacity, the final moisture content of the apple in dryer was 6.3%, while in dryer 2, it was 9.22%. In the case of full-load capacity, the final  $m_c$  in dryer 1 was 10.8%, and in dryer 2, it was 11.64%, achieved within 6 hours. Thus, dryer 1 demonstrated a higher moisture extraction rate in both cases. Moreover, as the loading capacity decreases, the rate of moisture extraction increases. Therefore, the full capacity is more effective at moisture removal, with both dryers achieving lower final mass and moisture content compared to half capacity. Dryer 1 begins with a slightly higher initial moisture content of 71.07% compared to dryer 2's 70.78% during the 10:00 – 11:00 (see Fig. 4.15). Both dryers exhibit a consistent and steady decrease in moisture content over time, with dryer 1 showing a slightly higher weight loss than dryer two at most intervals. This suggests that a dryer may be marginally more efficient in removing moisture when operating under half capacity. In general, both dryers display a consistent reduction in weight over time, further confirming their effectiveness in the drying process.



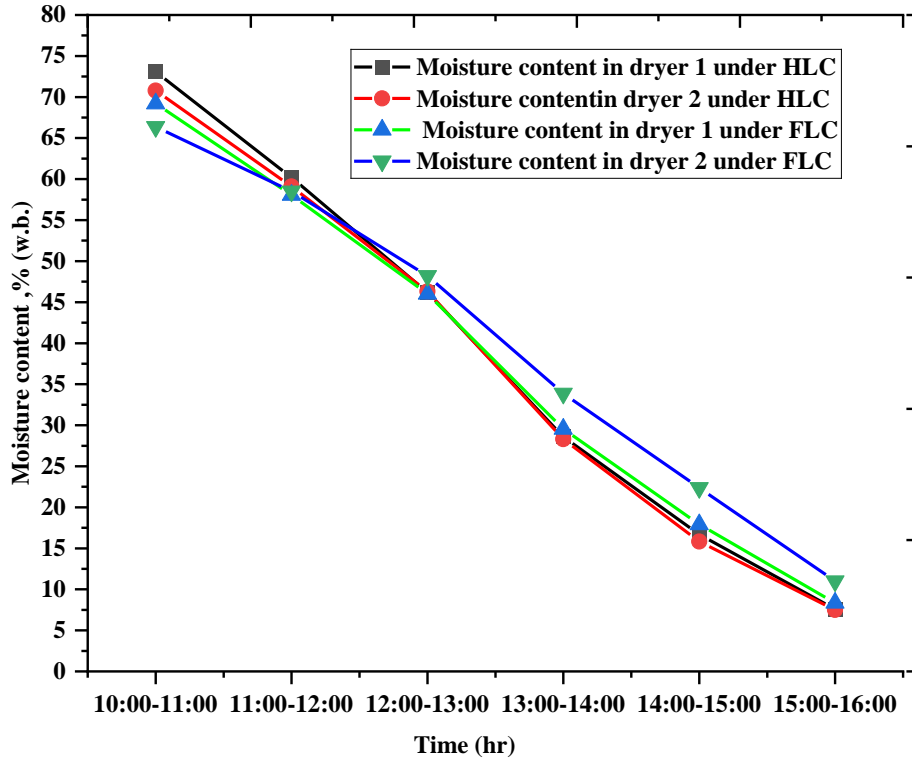


Fig. 4.15. Moisture content changes

#### 4.4.2. Moisture ratio and drying curve investigation

The moisture ratio and drying curve of the sample under both half and full-capacity conditions are depicted in Fig. 4.16 (a) and Fig. 4.16 (b), respectively. The  $MR$  decreases over time for all conditions, indicating the effectiveness of the drying process in reducing moisture content. Under half capacity, dryer one generally exhibits a slightly lower  $MR$  than dryer 2, suggesting that dryer 1 is marginally more efficient at moisture removal. Both dryers show a consistent decrease in  $MR$  over time.

Additionally, full capacity operation results in a higher  $MR$  for a more extended period compared to half capacity, likely due to the larger volume of material being dried. As illustrated in Fig. 4.16 (b), there is not a straightforward linear segment in the drying curves that would indicate a constant rate period. Instead, the curves show a gradual decline in the drying rate from the start, suggesting that the drying process is primarily in the falling rate period. In general, the drying curves for both dryer one and dryer two under half and full capacity occur under a falling rate period.

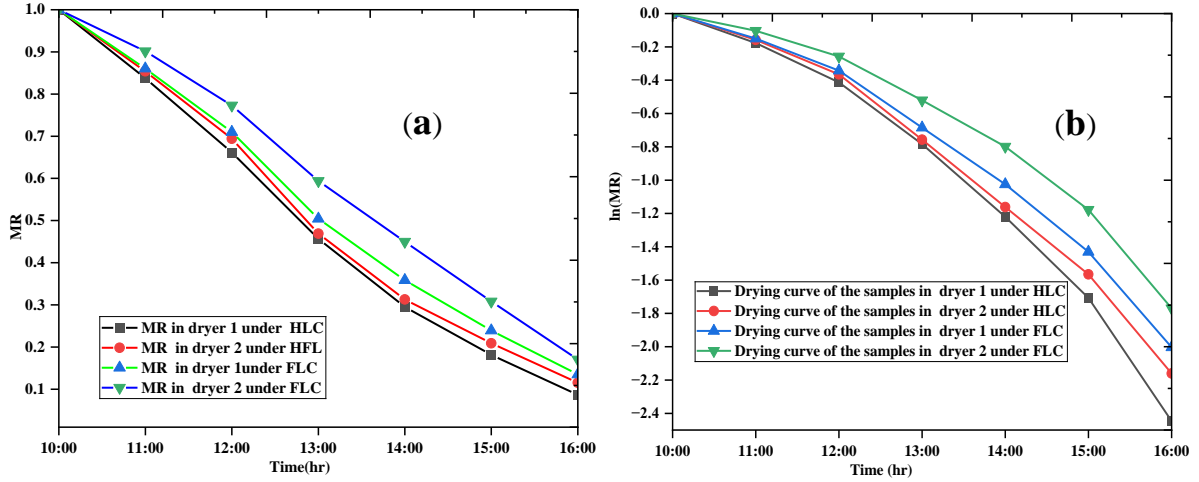


Fig. 4.16 Moisture ratio (a) and drying curve of the apple samples (b)

#### 4.4.3. Selecting the best-fitting model

As shown in Appendix A6 the Midilli and Kucuk (2003) model demonstrates strong performance, achieving an  $R^2$  value of 0.9956, an  $RMSE$  of 0.0321 and an  $\chi^2$  value of 0.1010, indicating its reliability for accurate predictions. In addition, both the two-term and logarithmic models demonstrate strong performance. The results were nearly identical across all cases for both days, with the Midilli and Kucuk (2003) model providing the best fit for thin-layer drying. The differences in statistical metrics were minimal, involving fractional decimals, and remained consistent across all drying conditions and parameters.

The results of the selected thin-layer drying models for golden apple samples are formulated as follows. The equations are valid for all loading stated in the thesis.

Midilli and Kucuk (2003):

$$MR = 2.82 \exp(-5.02 t^{1.80}) + 0.0029 t \quad (4.3)$$

Logarithmic:

$$MR = 9.2 \exp(-5.29 t) \quad (4.4)$$

Two terms:

$$MR = 4.7 \exp(-3.97 t) + 0.0010 \exp(-1.0970 t) \quad (4.5)$$

The Midilli and Kucuk (2003) model has been effectively utilized to describe the drying behaviour of apple slices in various studies, such as Noori et al. (2021), Das and Akpinar (2020), and Demirpolat (2019). The logarithmic model has been effectively used to describe the drying kinetics of apple slices, as demonstrated by Stegou-Sagia and Fragkou (2018).

#### 4.4.4. Moisture diffusivity evaluation

The average thickness of the samples was calculated as 0.00525 m, yielding a half-thickness of 0.002625 m. The natural logarithm of the  $MR$  was plotted against time. The result of the regression equation with a slope of -0.2318 (i.e., slope) and an intercept of 0.04344. The model exhibited a strong fit, with an  $R^2$  value of 0.9945 and an  $RMSE$  of 0.04073. The  $D_{eff}$  ranged from approximately  $1.997 \cdot 10^{-7} \text{ m}^2/\text{s}$  to  $2.0599 \cdot 10^{-7} \text{ m}^2/\text{s}$ . For the second drying case (dryer 2

with 2 kg), similar patterns were observed. The regression model had a slope of -0.2264 (i.e., slope) and an intercept of 0.02491, with an  $R^2$  of 0.999 and  $RMSE$  of 0.01652. The  $D_{eff}$  values ranged from  $1.947 \cdot 10^{-7} \text{ m}^2/\text{s}$  to  $1.99 \cdot 10^{-7} \text{ m}^2/\text{s}$ . In a study conducted by Das and Akpinar (2020), the activation energy and effective moisture diffusivity values of apples ranged between  $0.062 \cdot 10^{-7}$  to  $0.084 \cdot 10^{-7} \text{ m}^2/\text{s}$  and  $33.2 - 40.01 \text{ kJ/mol}$  and from  $0.031 \cdot 10^{-6}$  to  $0.049 \cdot 10^{-6} \text{ m}^2/\text{s}$ , respectively. Lingayat et al. (2020) estimated the average  $D_{eff}$  for apples as  $4.28 \cdot 10^{-9} \text{ m}^2/\text{s}$ . Thus, the results align with those found in the existing literature.

#### 4.5. Colour change analysis

As shown in Fig. 4.17, the images illustrate the apple slices at different stages: before drying (Fig. 4.17, A), after drying in outdoor lighting (Fig. 4.17, B), and after drying in indoor lighting (Fig. 4.17, C). The result shows that apple slices dried in a solar-powered chamber, they turned brown naturally as they lost moisture. Their texture changed from smooth and moist to wrinkled and dry, showing that they dried properly. The lighting made them look darker outside and more golden inside, and the overall drying quality stayed consistent.

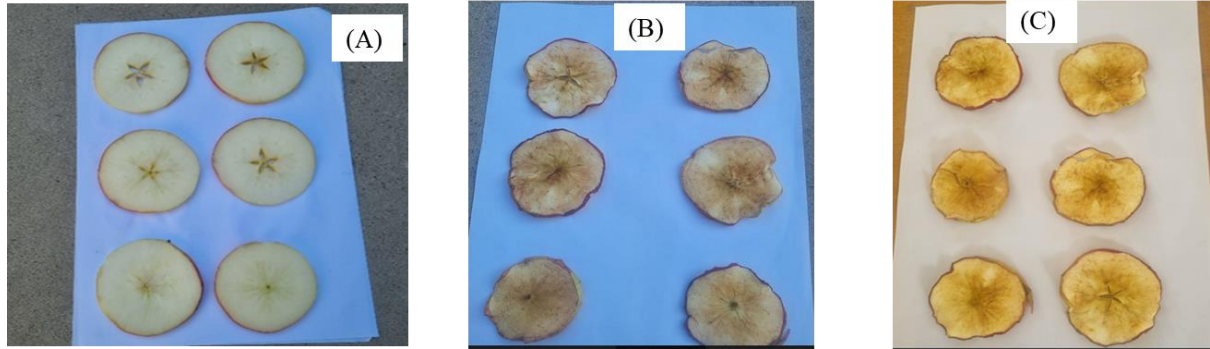


Fig. 4.17. Selected sample of apple slices before and after drying

The colour parameters of the apple slices before drying and after drying conditions are shown in Fig. 4.18. The results show that both curves exhibit a similar overall shape. However, differences in peak height and the width of the saturation peaks suggest that drying temperatures significantly influence both the intensity and consistency of colour saturation in apple slices. Drying in the drying chamber results in higher saturation (more vivid colour) and a slightly altered chroma angle (HUE) range compared to drying at ambient temperature or open sun drying.

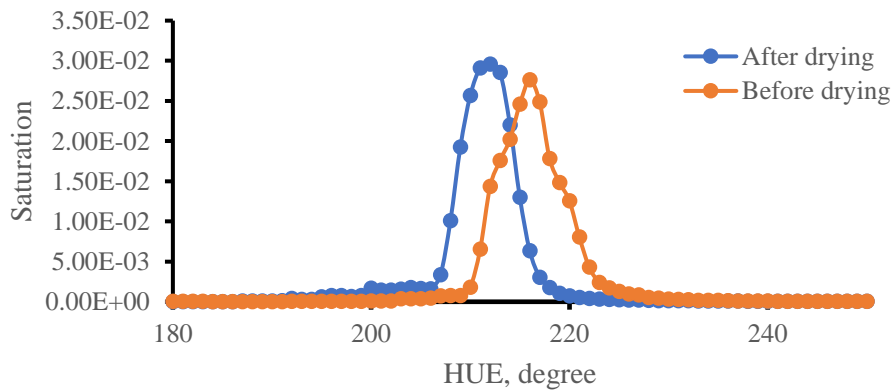


Fig. 4.18. Graphical representation of the apple slice before and after drying

#### 4.6. Enhancement of the drying uniformity

##### 4.6.1. Effect of integrating triangular baffles

The weight loss of the samples with and without triangular baffles is shown in Fig. 4.19. The dryer without baffles showed greater moisture variation between trays compared to the one with triangular baffles. The triangular baffles likely improved airflow consistency, promoting more uniform drying. During weight loss, the average  $C_v$  was 10.26% with triangular baffles and 11.16% without triangular baffles (see Fig. 4.22 (a)). A detailed analysis of enhancement tools such as drying rate, weight loss, and standard deviation is presented in Appendix A7.

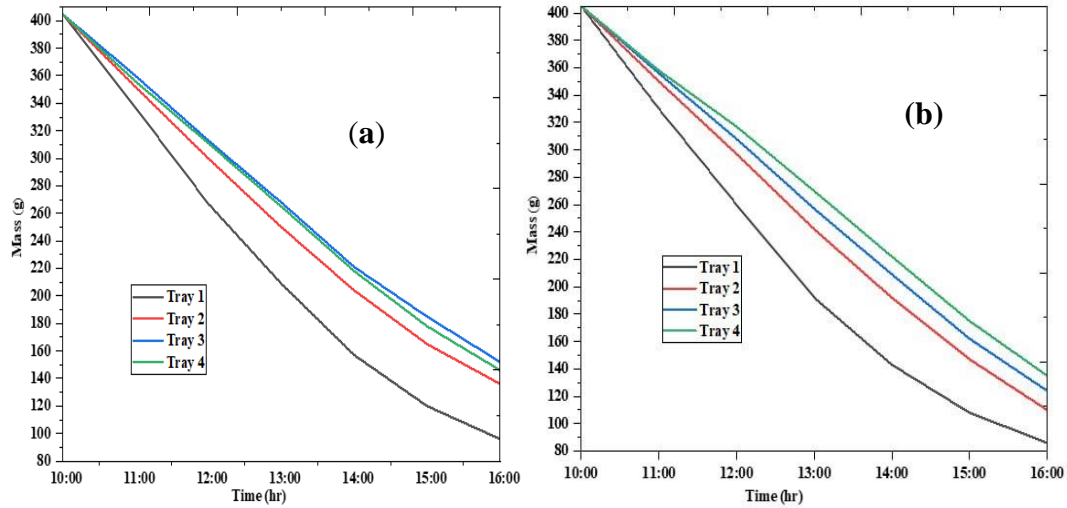


Fig. 4.19. Moisture content reduction of the dryer with triangular baffles (a) and without triangular baffles (b)

##### 4.6.2. Effect of integrating rectangular baffles

The moisture loss of the samples with and without integrating rectangular baffles is shown in Fig. 4.20. So, the analysis revealed that rectangular baffles reduced variability (average  $C_v = 10.97\%$ ) compared to unbaffled operations (12.56%), yet triangular baffles provided more significant consistency enhancement (10.26% vs 11.16%) (see Fig. 4.20b). Statistical evaluation showed rectangular baffles had weaker overall significance (average  $p = 0.032$ ). The drying chamber with rectangular baffled exhibits improved uniformity compared to unbaffled configurations.

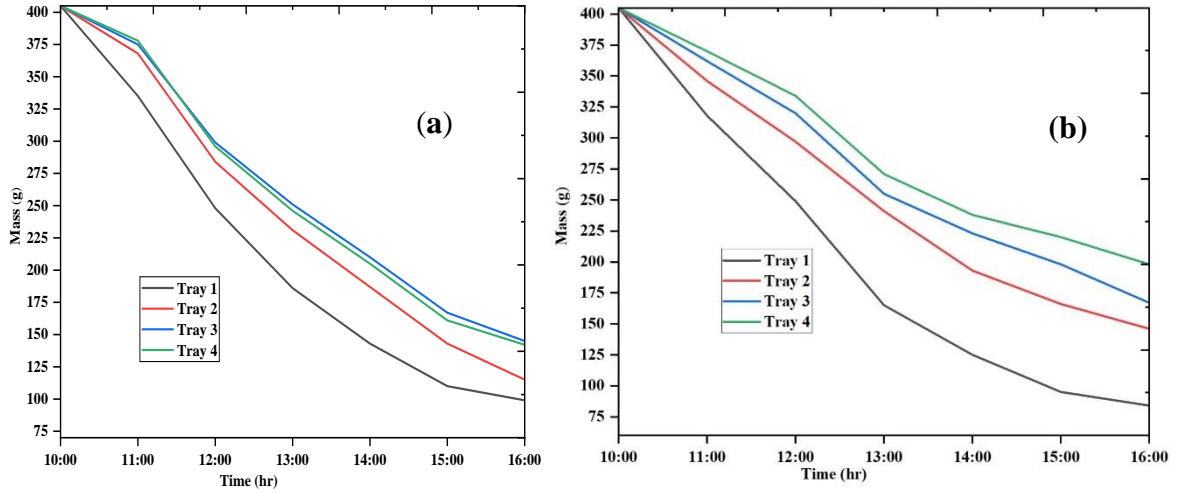


Fig. 4.20. Moisture content reduction of the dryer with rectangular baffles (a) and without rectangular baffle (b)

#### 4.6.3. Effect of adding swirler

The addition of a swirler demonstrated significant improvements across all measured parameters compared to non-swirler configurations (see Fig. 4.21). The process variability was substantially reduced, with the swirler configuration showing markedly lower coefficients of variation (average  $C_v$  of 8.86% vs 14.96% without swirler), indicating 40.8% improvement in operational consistency. Statistical analysis revealed exceptional significance throughout the swirler operation (average  $p = 0.0028$ ), in contrast, the non-swirler condition showed weaker significance (average  $p = 0.0205$ ). With a swirler, drying is more uniform, with controlled moisture removal and tighter mass differentials. It also creates a unique reverse drying pattern, where upper trays dry slower than some middle trays. Without a swirler, drying is faster in lower trays but less consistent, with more significant variability and more aggressive moisture loss early on. The swirler enhances airflow dynamics by creating controlled turbulence, improving heat distribution, reducing uneven drying, and preventing case hardening, leading to better inter-tray consistency at a steady drying rate.

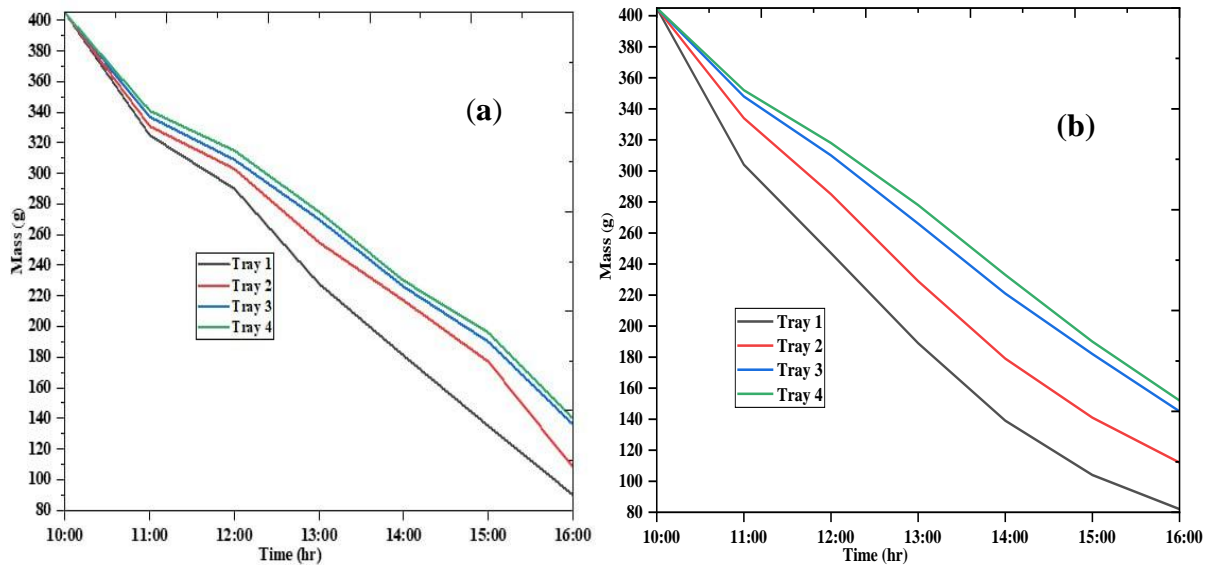


Fig. 4.21. Moisture content reduction of dryer 1 with swirler (a) and without swirler (b)

#### 4.6.4. Coefficient of variance

As depicted in Fig. 4.22, the  $C_v$  in all cases was initial uniformity (10:00), which is 0.00%, showing drying was not started every tray had equal mass. As the drying progresses, the  $C_v$  increases, but it does so gradually: The drying chambers with triangular and rectangular baffles and swirled have a lower coefficient of variance. Thus, the baffles or swirled help reduce drying variability, leading to a more uniform drying process. In contrast, without baffles or swirled, the drying process becomes more variable, with greater fluctuations in moisture content and less uniform drying overall.

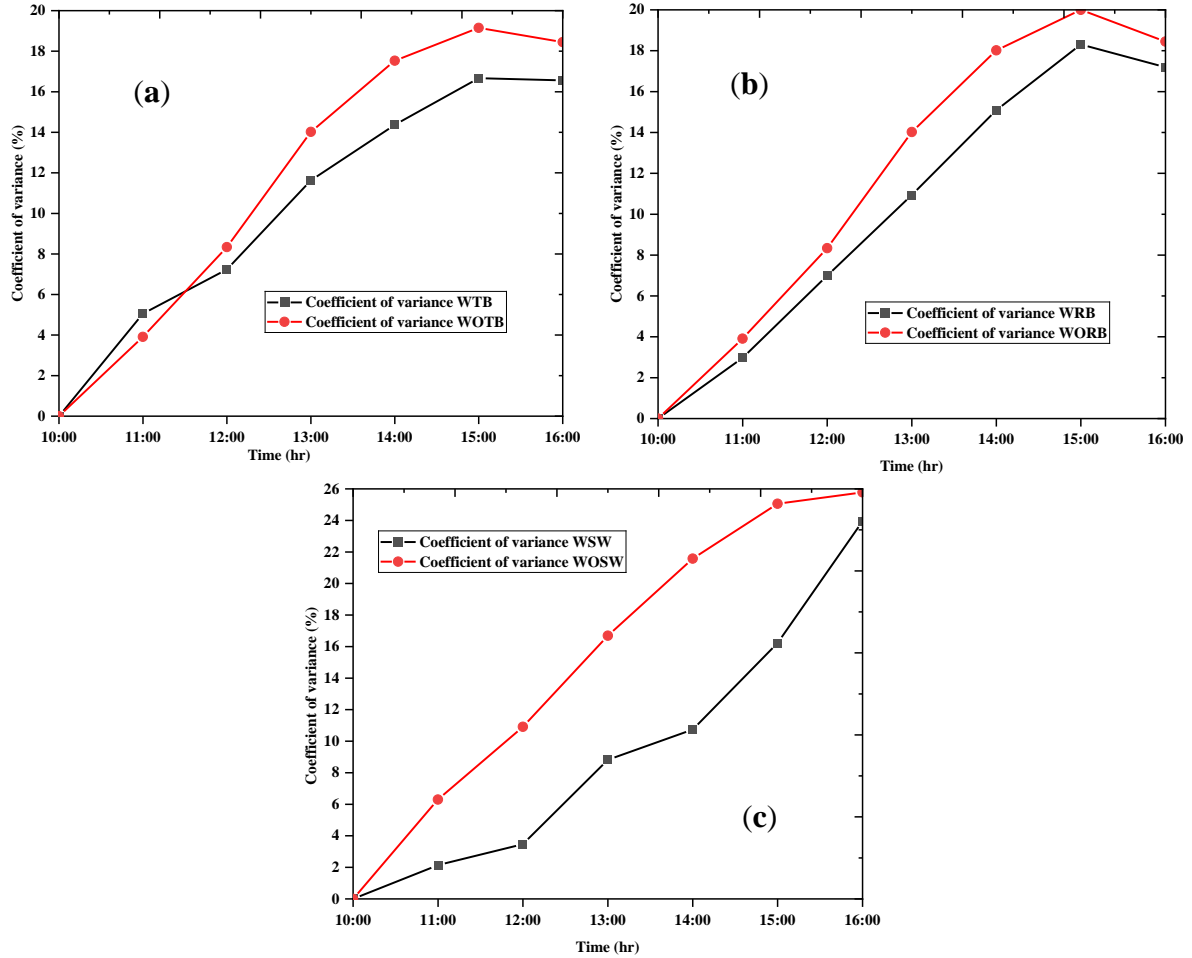


Fig. 4.22. Coefficient of the dryers with and without triangular baffles (a), with and without rectangular baffles (b) with and without swirler (c)

#### 4.7. Temperature distribution of the enhancement methods

As shown in Fig. 3.11 the RTD sensors were positioned at the centre of each tray.

##### 4.7.1. Effect of triangular baffles

The temperature distribution with triangular baffles is significantly more uniform compared to without baffles, as depicted in Fig. 4.23. In the case of triangular baffles, the temperature differences range from 1.0 to 3.3 °C, indicating a relatively uniform distribution across the trays. On the other hand, without the triangular baffles, the temperature differences are much more significant, ranging from 3.8 to 7.6 °C, which suggests a less uniform distribution. This

demonstrates that the presence of triangular baffles helps to improve heat distribution by reducing temperature gradients, resulting in a more uniform temperature profile across the trays.

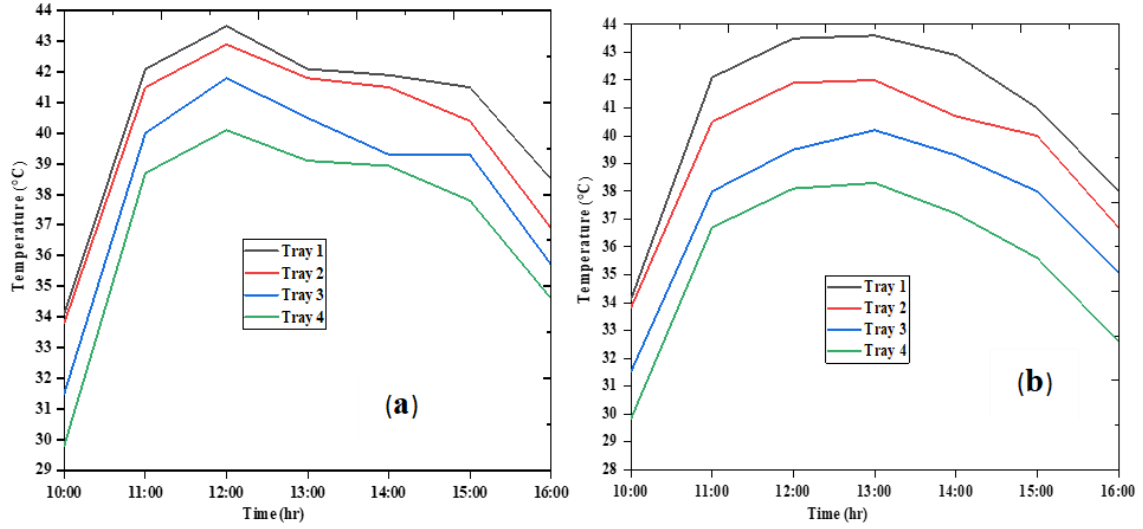


Fig. 4.23. Temperature distribution with triangular baffles (a) and without triangular baffles (b)

#### 4.7.2. Effect of rectangular baffles

The temperature distribution with rectangular baffles shows generally uniform results, as illustrated in Fig. 4.24, with temperature differences ranging from 1.2 to 6.8 °C. The most significant variation occurs at the beginning of the day, but this difference progressively decreases as the day continues. In contrast, without rectangular baffles, the temperature differences are more significant, ranging from 4.2 to 8.7 °C, indicating a less uniform distribution. Overall, the temperature distribution with rectangular baffles is more uniform compared to those without them.

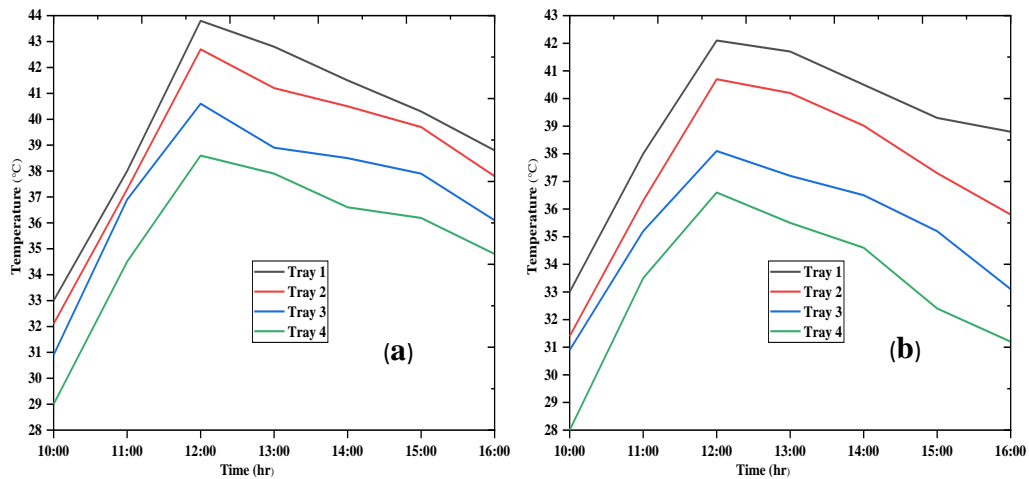


Fig. 4.24. Temperature distribution with rectangular baffles (a) and without rectangular baffles (b)



#### 4.7.3. Effect of swirler

The temperature distribution with the swirler shows a generally uniform pattern (see Fig. 4.25), with temperature differences ranging from 2.0 to 4.8 °C. In contrast, without the swirler, the temperature differences are larger, ranging from 5.0 to 7.3 °C, indicating a less uniform distribution. In general, the temperature distribution with the swirler is more uniform than without it, as the temperature differences are consistently more minor, demonstrating that the swirler enhances heat distribution, reduces temperature gradients, and promotes better thermal uniformity across the trays.

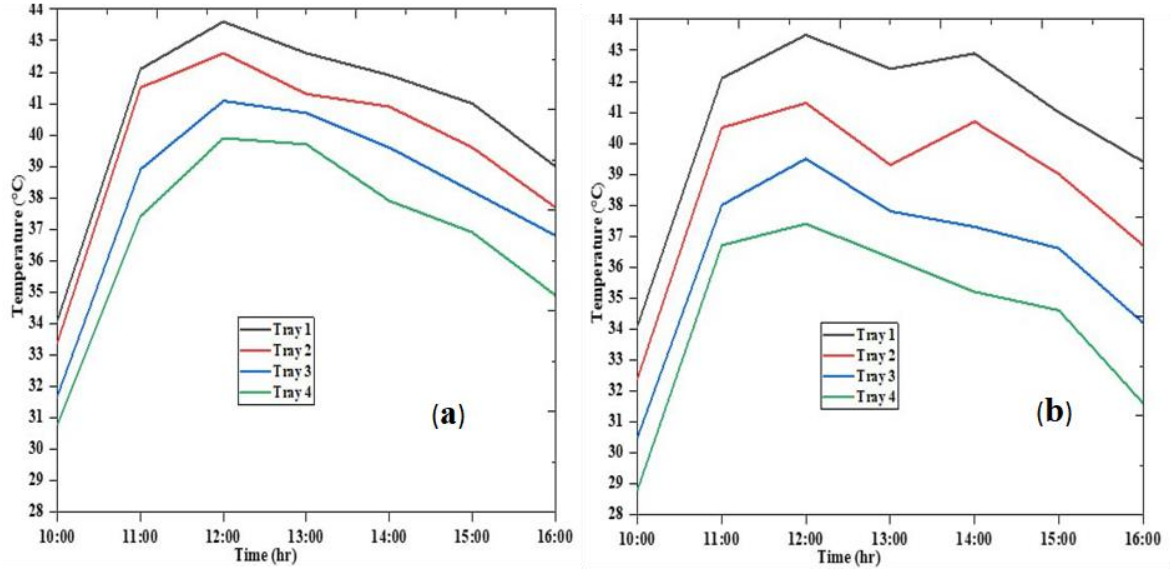


Fig.4.25. Temperature distribution with swirler (a) and without swirler (b)

#### 4.8. Effect of tray spacing

##### *Weight loss percentage and average drying rate of dryer*

The study investigated the effects of varying tray spacing (10 cm, 20 cm, and 30 cm) and tray arrangement configurations on drying performance. Different tray layouts were systematically tested, including variations in both vertical spacing and positional sequencing. Thus, based on experimental results the 10 cm gap between tray 1 and tray 2 yielded the highest performance in both mass reduction and drying rate among all tested configurations (see Appendix A8). The second-best arrangement was the 20 cm gap between tray 1 and tray 3, which showed strong but slightly lower efficiency. Conversely, the combination of tray 1 and tray 4 exhibits the lowest mass reduction and drying rate, making it the least efficient configuration. Thus, as the gap between the trays increases, both the mass reduction and drying rate tend to decrease. More significant gaps, such as the 30 cm configuration, result in lower efficiency compared to smaller gaps. In addition, as the number of trays increases, the weight loss and efficiency decrease compared to dryers with fewer trays.

To characterize the influence of tray spacing and the number of trays on the drying performance including drying rate, weight loss, and  $MR$  in the custom-designed drying chamber, multiple linear regression (MLR) models were developed. The developed linear models effectively characterize drying performance across vertical tray positions, where  $T_I$  represents the bottom



position (nearest the heat source) and ascending numbers indicate progressively higher trays. These models demonstrate robust predictive capability, with  $R^2$  values of 0.82–0.88, indicating they explain 82–88% of observed variability in drying rate, weight reduction, and moisture ratio through three key parameters: tray spacing, number of trays count and location of the tray. The following expression were developed used to express the  $DR$ , moisture loss ( $ML$ ) and  $MR$ .

$$DR = \beta_0 + \beta_1 T_s + \beta_2 T_n + \beta_3 T_l + \beta_4 (T_s T_n) \quad (4.6)$$

$$ML = \alpha_0 + \alpha_1 T_s + \alpha_2 T_n + \alpha_3 T_l + \alpha_4 (T_s T_n) \quad (4.7)$$

$$MR = \gamma_0 + \gamma_1 T_s + \gamma_2 T_n + \gamma_3 T_l + \gamma_4 (T_s T_l) \quad (4.8)$$

where  $\beta$ ,  $\alpha$ ,  $\gamma$  represent regression coefficients,  $T_s$  is tray spacing (cm),  $T_n$  represents number of trays and  $T_l$  is tray location (1 = bottom, 4 = top tray).

$$\beta_0 = 68.50, \beta_1 = -0.20, \beta_2 = -2.30, \beta_3 = -3.10, \beta_4 = 0.04 (R^2 = 0.88)$$

$$\alpha_0 = 92.40, \alpha_1 = -0.16, \alpha_2 = -2.70, \alpha_3 = -4.60, \alpha_4 = 0.03 (R^2 = 0.85)$$

$$\gamma_0 = 0.95, \gamma_1 = -0.06, \gamma_2 = -0.15, \gamma_3 = -0.18, \gamma_4 = 0.01 (R^2 = 0.82)$$

#### 4.9. Taguchi analysis

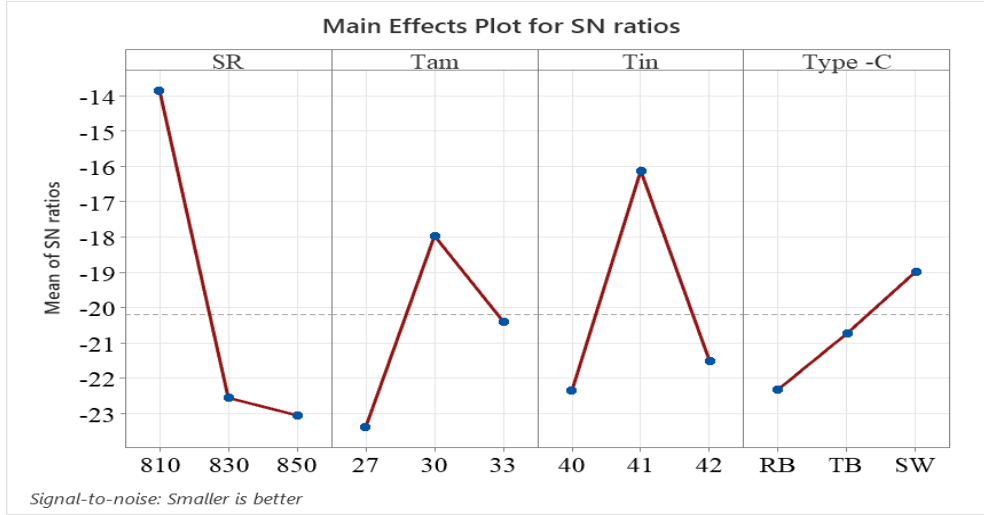
The calculated results for the coefficient of variation in temperature distribution, moisture loss reduction, and the measured pressure drop were used as response variables. Appendix A9 presents the coefficient of variation for mass reduction across the trays or the drying chamber as a whole, along with the pressure drop in dryers utilizing flow-enhancing designs such as triangular baffles, rectangular baffles, or swirl-type designs.

##### 4.9.1. Coefficient of variance as a response parameter

Fig. 4.26 presents another set of Taguchi analysis results, highlighting the impact of different factors like solar radiation ( $SR$ ), temperature enter to the drying chamber ( $T_{in}$ ), ambient temperature ( $T_{am}$ ) and type of enhancement methods (Type-C) of the drying uniformity. Among these factors,  $T_{in}$  was identified as the most influential, as shown in Table 4.2, indicating that fluctuations in inlet temperature significantly affect moisture removal rates. Precise control of  $T_{in}$  is essential to ensuring stable heat distribution and minimizing drying in consistencies. The second most influential factor was Type-C, highlighting the importance of baffles, swirls and other configurations that influence turbulence and moisture distribution, meaning an optimized configuration can reduce drying variability.  $SR$  ranked third, suggesting that while it plays a role in drying uniformity, its impact is moderate compared to  $T_{in}$  and Type-C. The least influential factor was  $T_{am}$ , indicating that ambient temperature has minimal effect on drying uniformity. While external conditions can contribute to slight variations, their effect is much smaller than that of heat input factors like  $T_{in}$  and  $SR$ . Overall, optimizing  $T_{in}$  and Type-C should be prioritized to enhance drying uniformity, while managing  $SR$  exposure can further improve stability. Controlling ambient conditions may offer minor benefits but is not as critical as adjusting the primary heat and airflow parameters. The best combination of  $SR$  level 3,  $T_{am}$  level 1,  $T_{in}$  level 1 and Type-C level 1 or the  $RB$ , is shown in Fig. 4.26.

Table 4.2. Response for signal-to-noise ratios of the  $C_v$ 

Level	SR	$T_{am}$	$T_{in}$	Type -C
1	1.2683	1.7331	0.8941	0.7403
2	2.0883	1.5459	1.2597	1.9094
3	1.2791	1.3567	2.4819	1.9860
Delta	0.8201	0.3764	1.5879	1.2458
Rank	3	4	1	2

Fig. 4.26. Main effect plot using the signal-to-noise ratio for  $C_v$ 

#### 4.9.2. Pressure as response variable

Fig. 4.27 shows the analysis of pressure drop as a response variable in drying uniformity enhancement methods.  $SR$  was the most influential factor, as shown in Table 4.3. Variations in  $SR$  significantly impact temperature gradients and airflow behaviour, leading to fluctuations in pressure resistance within the system. The second most significant factor is  $T_{in}$ . Maintaining a stable  $T_{in}$  is essential to ensure a balanced pressure profile, preventing excessive resistance build up or inefficiencies in the drying chamber. Type-C ranks third, indicating that the design of baffles, swirlers, or duct systems influences airflow resistance. Poorly designed configurations can create air stagnation zones or excessive turbulence, leading to uneven temperature distribution. So, such problems can be optimizing by using baffles or swirls can enhance airflow uniformity and reduce pressure drop variations. Finally,  $T_{am}$  have the least impact. The optimal combination is  $SR$  level 2,  $T_{am}$  level 3,  $T_{in}$  level 3 and Type -C level 3.

Table 4.3. Pressured drop response for signal to noise ratios

Level	SR	$T_{am}$	$T_{in}$	Type-C
1	-20.85	-21.46	-21.46	-21.47
2	-27.94	-27.24	-27.13	-27.16
3	-27.81	-27.90	-28.01	-27.96
Delta	7.10	6.45	6.55	6.49
Rank	1	4	2	3

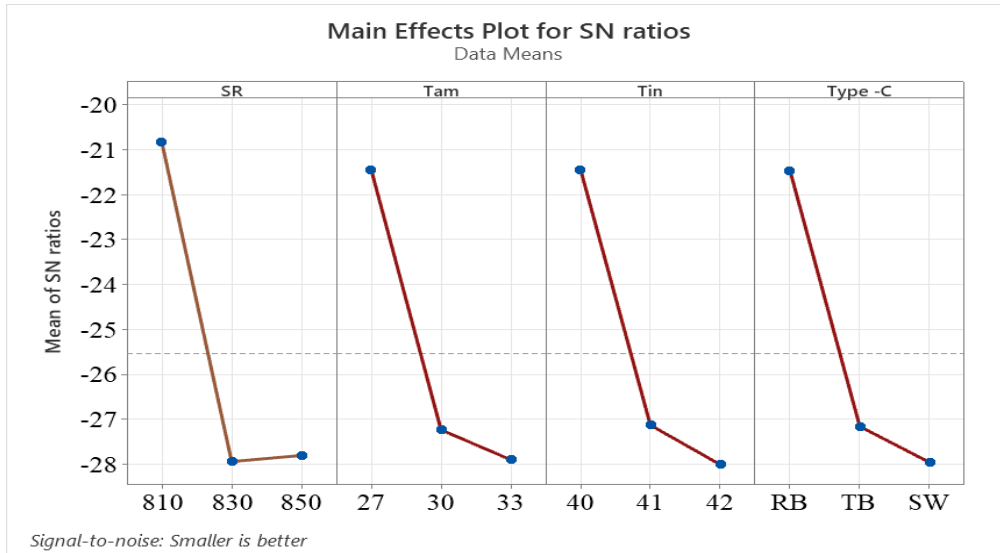


Fig. 4.27. Main effect plot using the signal-to-noise ratio for the pressure drop response

#### 4.10. Feasibility study of the drying system

In Europe, particularly in Hungary, solar radiation is available partially from mid-April to mid-September. However, the most effective drying period is from June to August. The current study assumes that the solar dryer is used annually to dry apples during these three months (June to August). Consequently, the cost analysis of the solar dryer does not include the additional cost of using it as a dry cabinet outside the compelling drying season. An economic analysis of the drying system was carried out, taking into account the state of the Hungarian economy as of 2024. In Hungary as reported in December 2024 the interest rate was 6.4% and the rate of inflation was 4.6%, in addition, as stated in many literatures the salvage value was taken 10% of the annual capital cost, and the maintenance cost is 10% of the annual capital cost ( $C_{ac}$ ) (Aniesrani Delfiya et al., 2024). Since the dryers made from polystyrene foam thermal insulation boards are assumed to last many years, how every here in the stay the life span of the dryer was assumed 10 years. The cost of electricity in Hungary is currently (i.e., December 2024) 0.091 USD per kWh or 32.84 Hungarian forint per kWh. A comprehensive cost analysis, including the fabrication of the drying system and related expenses, is provided in Appendix A10.

As shown in Table 4.4, the benefit achieved from the dryer in the first summer will be \$265.88. Overall, the analysis yielded  $NPV$  of \$2,850.93, confirming the project's profitability. Additionally, the benefit-cost ratio  $BCR$  of 4.08 well above the threshold of 1 indicates strong economic viability. With a payback period of 1.73 years (less than two years), the project demonstrates a rapid recovery of costs. These results collectively highlight the project as a highly attractive investment, offering promising financial returns.

Table 4.4. Saving obtaining from the drying system ( $S_j$ ) over the next 10 years

Year	The savings generated by the dryer after $j$ years ( $S_j$ ) (USD)
1	265.88
2	278.117
3	290.91
4	304.29
5	318.29
6	332.9320
7	348.24
8	364.26
9	381.02
10	398.54

## 5. NEW SCIENTIFIC RESULTS

This section presents the new scientific findings from this research work as follows:

### 1. *Improvement in drying uniformity*

Based on experimental results, I enhanced the flow uniformity with the drying system using the baffles and swirlers. The addition of baffles and swirlers significantly enhances the uniformity within the drying chamber. Thus, I proved that rectangular baffles increase the drying rate and uniformity, reducing temperature gradients from 4.2 – 8.7 °C to 1.2 – 6.8 °C. Triangular baffles narrowing the temperature differences averagely from 3.8 to 7.6 °C to 1.0 – 3.3 °C. Furthermore, I proved that swirlers optimize drying uniformity across trays and improve heat distribution, reducing temperature gradients from 5.0 – 7.3 to 2.0 – 4.8 °C. The uniform airflow pattern created by the baffles and swirlers prevents localized moisture build up, ensuring that the product is evenly dried and reducing the risk of uneven drying or product degradation. These findings underscore the significance of design modifications in enhancing the performance of solar dryers, making them more effective and reliable for various applications.

### 2. *Modelling of drying behaviour of apple slices*

I have proven that the Midilli and Kucuk (2003) model ( $R^2 = 0.9956$ ,  $RMSE = 0.0321$ ,  $x^2 = 0.0101$ ), the Logarithmic model ( $R^2 = 0.9903$ ,  $RMSE = 0.0348$ ,  $x^2 = 0.0112$ ), and the two-term model ( $R^2 = 0.9944$ ,  $RMSE = 0.0521$ ,  $x^2 = 0.0266$ ) provided best fit for the thin-layer drying behaviour of apple slices (Golden delicious), compared to other models listed out in the study. The apples were cut into cylindrical pieces with diameters ranging from 0.075 ( $\pm 0.01$ ) to 0.083 ( $\pm 0.01$ ) meters and thicknesses between 0.004 and 0.0065 ( $\pm 0.001$ ) meters. These selected models provided the most accurate predictions of moisture ratio and drying behaviour, offering robust tools for optimizing dehydration processes.

Midilli and Kucuk (2003):

$$MR = a \exp(-k t^n) + b t.$$

The estimated coefficients and *drying constant* for the model are:  $a = 2.82$ ,  $b = 0.0029$ ,  $k = 5.02$ ,  $n = 1.80$  with  $R^2$  of 0.9956.

Logarithmic:

$$MR = a \exp(-k t) + c.$$

The derived model coefficients and drying constants are:  $a = 9.2$ ,  $k = 5.29$ ,  $c = 0$  with  $R^2$  of 0.9903.

Two-term:

$$MR = a \exp(-k t) + b \exp(k_1).$$

The best-fit values of coefficients and drying constants for the model are:  $a = 4.7$ ,  $k = 3.97$ ,  $b = 0.0010$ ,  $k_1 = 1.0970$  with  $R^2$  of 0.9944.

### 3. Influence of tray spacing and number of trays

Based on the experiments conducted the number of trays and the spacing between them play a crucial role in determining the drying rate, weight loss, and moisture ratio of the samples. These factors significantly influence heat and mass transfer during the drying process, and optimizing tray arrangements can enhance overall drying efficiency. By adjusting these parameters, it is possible to achieve more uniform moisture removal and improve the drying performance of the system. I have developed the following formulas based on tray spacing and the number of trays used, which can be applied to calculate the drying rate (DR), moisture loss (ML), and moisture ratio (MR):

$$DR = \beta_0 + \beta_1 T_s + \beta_2 T_n + \beta_3 T_l + \beta_4 (T_s T_n),$$

$$ML = \alpha_0 + \alpha_1 T_s + \alpha_2 T_n + \alpha_3 T_l + \alpha_4 (T_s T_n),$$

$$MR = \gamma_0 + \gamma_1 T_s + \gamma_2 T_n + \gamma_3 T_l + \gamma_4 (T_s T_l).$$

The model coefficients of correlation expressed as follows:

$$\beta_0 = 68.50, \beta_1 = -0.20, \beta_2 = -2.30, \beta_3 = -3.10, \beta_4 = 0.04 (R^2 = 0.88),$$

$$\alpha_0 = 92.40, \alpha_1 = -0.16, \alpha_2 = -2.70, \alpha_3 = -4.60, \alpha_4 = 0.03 (R^2 = 0.85),$$

$$\gamma_0 = 0.95, \gamma_1 = -0.06, \gamma_2 = -0.15, \gamma_3 = -0.18, \gamma_4 = 0.01 (R^2 = 0.82).$$

### 4. Correlation solar air heater efficacy with solar irradiance, ambient temperature and outlet temperature

Based on the experimental results, I have developed a multiple linear model to estimate the relationship between the solar air heater efficiency and factors such as the amount of solar insolation received, the temperature output from the solar air heater (SAH), and the ambient temperature. The developed equation serves as a practical tool for optimizing SAH performance and can be integrated into control systems for real-time efficiency adjustments. The model was statistically validated using p-value analysis, which confirmed that all predictors (solar insolation, ambient temperature, and SAH outlet temperature) are significant contributors to efficiency, with each coefficient yielding  $p < 0.05$ . The developed relation allows for performance and operational optimization of the solar air heater:

$$\eta_{sah} = \beta_0 + \beta_1 I_r + \beta_2 T_{am} + \beta_3 T_{sah,o}$$

where  $\beta_0 = -31.7764$ ,  $\beta_1 = 0.0567$ ,  $\beta_2 = 0.7388$ ,  $\beta_3 = 1.0123$  with  $R^2 = 0.989$  and  $p < 0.001$  for all parameters.

### 5. Correlation between dryer efficiency and the loadings

Based on the experiment conducted, I developed linear equation that relates the dryer efficiency to its loading capacity in gram. This enables users to maximize drying performance while avoiding the inefficiencies of under-loading, which wastes energy, and over-loading, which impedes airflow. For end-users, particularly farmers and small-scale operators, this correlation directly translates into energy savings by minimizing drying time and fuel consumption by applying the predicted optimal loading range. Together, these findings connect research with real-world use, offering practical strategies for efficiency of the dryer operation:

$$\eta_{dc} = \lambda L_c + b$$

$$\lambda = 0.00997, b = 2.33 (R^2 = 0.99)$$

where,  $\lambda$  defined as the ratio of the vertical change to the horizontal change,  $L_c$  represents the loading capacity of the dryer and  $b$  is the  $y$ -intercept (or constant). The estimated values of  $\lambda$  and  $b$  were 0.00997 and 2.33, respectively.

## 6. CONCLUSION AND SUGGESTIONS

In conclusion, a computational and experimental analysis of solar drying chamber to model the drying kinetics and to enhance the flow uniformity of the dryer was conducted. In this research work, the solar drying chamber found in the laboratory, was used as the initial design for the current study experiment, was evaluated using computational fluid dynamics. The *CFD* simulation results helped in refining and optimizing the design to improve its flow behaviour. Based on the *CFD* analysis, several enhanced solar drying chamber designs were developed and evaluated using the same *CFD* approach. The design that yielded the best results based on *CFD* simulations were then fabricated and subjected to experimental analysis. In the fabricated design, the impact of baffles and a swirler, which were incorporated to enhance flow and heat transfer within the chamber, was thoroughly investigated. Additionally, the drying behaviour of apple slices was studied in the newly developed solar dryer. The performance of the dryer was evaluated using energy and exergy analysis and other indicators like moisture content reduction, and drying rate of the apple slices.

To assess dryer performance, experiments were conducted under four different loading conditions: unloaded, half-capacity (250 g/tray), semi-full capacity (405 g/tray), and full-capacity (500 g/tray). The temperatures of the absorbers in the solar air heaters, along with the efficiencies of both the dryer and the solar air heaters, as well as the temperature entering the drying chamber, followed the pattern of solar radiation, peaking around midday and gradually decreasing over time. This trend highlights the direct influence of solar radiation on the thermal performance of the system, with higher radiation levels contributing to increased efficiency during the peak hours of the day.

The study evaluated the impact of flow-enhancing tools, such as baffles and swirlers, on the airflow uniformity within the solar drying system. Experimental results revealed that these modifications significantly improved thermal distribution and reduced spatial moisture variability, leading to more consistent drying performance. Statistical analysis ( $p < 0.05$ ) confirmed that both baffles and swirlers contributed to measurable improvements in drying uniformity, with swirlers showing a marginally greater effect due to their ability to promote turbulent mixing. Additionally, the baffles were found to minimize dead zones, ensuring more efficient heat transfer across the drying chamber.

Future improvements could include conducting multi-season trials to evaluate performance in varying climates, testing novel geometries like perforated plates, and exploring hybrid configurations such as baffles with angled swirlers. Investigating the synergistic effects of combined enhancements across different chamber zones and assessing post-drying product quality (colour, texture) to align with industry standards are also recommended. Additionally, exploring other flow-enhancing geometries and combination effects of multiple enhancements (e.g., baffles + swirlers) could improve results. Expanding the integration of enhancements beyond the plenum area to other chamber zones may also provide further benefits. Further research should be focused on the effect of tray spacing configuration such as tray 2 and tray 3, tray 2 and tray 4, tray 3 and tray 4 and other configurations beyond those stated in the thesis.



## 7. SUMMARY

### MODELLING AND PERFORMANCE OPTIMIZATION OF SOLAR DRYING CHAMBER USED FOR AGRICULTURAL PRODUCTS

A comprehensive experimental analysis was carried out to enhance the drying uniformity and to mathematically model the drying behaviour of apple slices under the climatic conditions of Gödöllő, Hungary (47° 35' 39" N, 19° 21' 59" E). The primary focus of the study was on improving the performance of the solar drying chamber by incorporating flow enhancements such as baffles, a swirler, and optimized tray spacing. Additionally, the study explored the effects of varying the number of trays within the drying chamber. The enhancements used were rigorously tested in the Solar Energy Laboratory at the Hungarian University of Agriculture and Life Sciences (MATE).

To achieve the stated research objectives, experiments were conducted using three drying chambers. Two of these chambers were identical and used as benchmarks or references for comparison. The study examines the thermal efficiency of dryers, showing that higher loading capacities improve performance. Thermal efficiency increased from 12.05% at half-load to 23.50% at full-load, with higher loads enhancing heat utilization and moisture removal. However, overloading can reduce efficiency due to hindered airflow and heat distribution. Full-load operation was found to be more energy-efficient, with a better (SMER) and lower specific SHE compared to half-load operations. Exergy analysis revealed that peak efficiency occurred around midday when solar radiation was strongest. Lower trays in the drying chambers showed better energy retention due to their proximity to the heat source. These findings provide key insights for optimizing solar drying systems for improved energy and performance.

Among the evaluated drying models, the Midilli and Kucuk (2003) model demonstrated superior fitting performance ( $R^2 = 0.9956$ ,  $RMSE = 0.0321$ ,  $x^2 = 0.0101$ ), followed by the logarithmic model ( $R^2 = 0.9903$ ,  $RMSE = 0.0348$ ,  $x^2 = 0.0112$ ) and then the two-term model ( $R^2 = 0.9944$ ,  $RMSE = 0.0521$ ,  $x^2 = 0.0266$ ). The colour analysis showed that dryers produced quality final dried products. Drying occurred primarily in the falling rate period, with no distinct constant-rate phase.

Adding the baffles significantly improved air flow uniformity and moisture removal. Specifically, rectangular baffles reduced temperature gradients from 4.2–8.7 °C to 1.2–6.8 °C, while triangular baffles further enhanced thermal distribution, narrowing variations to 1.0–3.3 °C. The integration of swirlers also optimized heat distribution, lowering tray-to-tray temperature differences from 5.0–7.3 °C to 2.0–4.8 °C. Taguchi analysis confirmed that solar irradiance and inlet temperature are the dominant factors governing drying uniformity. Collectively, these enhancements substantively mitigate non-uniform drying, underscoring their potential to advance solar dryer design for industrial and agricultural applications. Based on the economic indicators used, the project is profitable and feasible.

## 8. ÖSSZEFOGLALÁS (SUMMARY IN HUNGARIAN)

### MEZŐGAZDASÁGI TERMÉKEKHEZ HASZNÁLT NAPKOLLEKTOROS SZÁRÍTÓSZEKRÉNY MODELLEZÉSE ÉS TELJESÍTMÉNYÉNEK OPTIMALIZÁLÁSA

Átfogó kísérleti vizsgálatokat kerültek elvégzésre az aszalás egyenletességének fokozása és az almaszeletek szárítási viselkedésének matematikai modellezésére Gödöllő város éghajlati viszonyai között. A vizsgálat elsődleges célja a napkollektoros szárítókamrák teljesítményének javítása volt olyan áramlásjavító elemek beépítésével, mint a terelőlapok, a légkeverő és az optimalizált tálcátávolság. A dolgozatban a szárítókamrán belül a tálcák szám változtatásának hatásai is vizsgálat tárgyát képezték. A kidolgozott fejlesztések a MATE Napenergia Laboratóriumában kerültek tesztelésre.

A kísérletek három szárítókamra segítségével kerültek elvégzésre, amelyek közül az összehasonlíthatóság miatt kettő azonos volt. A vizsgálati eredmények alapján kimutatható volt, hogy a nagyobb töltési kapacitások javítják a szárítás termikus hatékonyságát. A termikus hatásfok félterhelésnél 12,05%-ról 23,50%-ra nőtt teljes terhelésnél, a nagyobb terhelések javítják a hőhasznosítást és a nedvesség eltávolítását. A túlterhelés azonban csökkentheti a hatékonyságot az akadályozott légáramlás és hőelosztás miatt. Az exergiaelemzés kimutatta, hogy a legnagyobb hatásfok dél körül következett be, amikor a napsugárzás a legerősebb. A szárítókamrák alsó tálcái a hőforráshoz való közelségük miatt jobb energiamegtartást mutattak. Ezek az eredmények kulcsfontosságú információkkal szolgálnak a napenergiával működő szárítórendszerek optimalizálásához a jobb energiafelhasználás és teljesítmény érdekében.

Az értékelt szárítási modellek közül a Midilli és Kucuk (2003) modell mutatott jobb illeszkedési teljesítményt ( $R^2 = 0,9956$ ,  $RMSE = 0,0321$ ,  $x^2 = 0,0101$ ), ezt követte a logaritmikus modell ( $R^2 = 0,9903$ ,  $RMSE = 0,0348$ ,  $x^2 = 0,0112$ ), majd a kétagú modell ( $R^2 = 0,9944$ ,  $RMSE = 0,0521$ ,  $x^2 = 0,0266$ ). A színelemzés azt mutatta, hogy a szárítók minőségi szárított végtermékeket állítottak elő. A száradás elsősorban a csökkenő száradási sebességű időszakban következett be, különálló állandó sebességű szakasz nélkül.

A terelőlapok hozzáadása jelentősen javította a légáramlás egyenletességét és a nedvesség eltávolítását. A téglalap alakú terelőlapok 4,2–8,7 °C-ról 1,2–6,8 °C-ra csökkentették a hőmérséklet-gradienseket, míg a háromszög alakú terelőlapok tovább javították a hőeloszlást, 1,0–3,3 °C-ra csökkentve az eltéréseket. A légkeverők beépítése szintén optimalizálta a hőeloszlást, 5,0–7,3 °C-ról 2,0–4,8 °C-ra csökkentve a tálcák közötti hőmérsékletkülönbségeket. A Taguchi-elemzés megerősítette, hogy a napsugárzás és a bemeneti hőmérséklet voltak a szárítás egyenletességét meghatározó tényezők. Ezek a fejlesztések együttesen jelentősen csökkentik a nem egyenletes szárítást, ami kiemeli a napkollektorok ipari és mezőgazdasági alkalmazásokban történő továbbfejlesztésének lehetőségét. A felhasznált gazdasági mutatók alapján a projekt nyereséges és megvalósítható.

## 9. APPENDICES

### A1: Bibliography

1. Abbasi, M., Ghafari-Nazari, A., Reddy, S., and Fard, M. (2014): A new approach for optimizing automotive crashworthiness: concurrent usage of ANFIS and Taguchi method. *Structural and Multidisciplinary Optimization*, 49, 485–499.  
DOI: 10.1007/s00158-013-0986-6
2. Abuşka, M. (2018): Energy and exergy analysis of solar air heater having new design absorber plate with conical surface. *Applied Thermal Engineering*, 131, 115–124.  
DOI: 10.1016/j.applthermaleng.2017.11.129
3. Aissa, W., El-Sallak, M., and Elhakem, A. (2014): Performance of solar dryer chamber used for convective drying of sponge-cotton. *Thermal Science*, 18(suppl.2), 451–462.  
DOI: 10.2298/TSCI110710084A
4. Akbulut, A., and Durmuş, A. (2009): Thin layer solar drying and mathematical modelling of mulberry. *International Journal of Energy Research*, 33(7), 687–695.  
DOI: 10.1002/er.1504
5. Akpinar, E. K., and Bicer, Y. (2005): Modelling of the drying of eggplants in thin-layers. *International Journal of Food Science and Technology*, 40(3), 273–281.  
DOI: 10.1111/j.1365-2621.2004.00886.x
6. Aktaş, M., Ceylan, I. and Yilmaz, S. (2009): Determination of drying characteristics of apples in a heat pump and solar dryer. *Desalination*, 239(1–3), 266–275.  
DOI: 10.1016/j.desal.2008.03.023
7. Al-Juamily, K. E. J., Khalifa, A. J. N. and Yassen, T. A. (2007): Testing of the performance of a fruit and vegetable solar drying system in Iraq. *Desalination*, 209(1-3), 163–170. DOI: 10.1016/j.desal.2007.04.026
8. Al-Kayiem, H. H., and Gitan, A. A. (2021): Flow uniformity assessment in a multi-chamber cabinet of a hybrid solar dryer. *Solar Energy*, 224, 823–832.  
DOI: 10.1016/j.solener.2021.06.058
9. Al-Neama, M. A., Farkas I. (2018): Evaluation of temperature and relative humidity stratifications in a solar drying chamber, *Journal of Scientific and Engineering Research*, Vol 5., No 10., 2018, pp. 59-65. ISSN 2394-2630 <https://jsaer.com/download/vol-5-iss-10-2018/JSAER2018-05-10-59-65.pdf>
10. Aniesrani Delfiya, D. S., Lincy Mathai, Murali, S., Neethu, K. C., Anuja R Nair, and George Ninan. (2024): Comparison of clam drying in solar, solar-hybrid, and infrared dryer: Drying characteristics, quality aspects, and techno-economic analysis. *Solar Energy*, 274, 112554. DOI: 10.1016/j.solener.2024.112554
11. Ansys Fluent User's Guide, Release 13.0, (2010).  
<https://www.fluid.tuwien.ac.at/322057?action=AttachFile&do=get&target=flu ug.pdf>

12. Ashfaq, S., Ahmad, M., Munir, A., and Ghafoor, A. (2017): Improvement of air homogeneity in paddy dryer with central air flow channel. *International Journal of Food Engineering*, 13(10), 20150408. DOI: 10.1515/ijfe-2015-0408
13. Atalay, H., Turhan Çoban, M., and Kınca, O. (2017): Modeling of the drying process of apple slices: Application with a solar dryer and the thermal energy storage system. *Energy*, 134, 382–391. DOI: 10.1016/j.energy.2017.06.030
14. Aukah, J., Muvengi, M., Ndiritu, H., and Onyango, C. (2018): Prediction of airflow and temperature distribution in hybrid solar-biomass dryer using computational fluid dynamics. *Journal of Sustainable Research in Engineering*, 4(3), 76–89. <https://jsre.jkuat.ac.ke/index.php/jsre/article/view/73>
15. Babu, A. K., Kumaresan, G., Antony Aroul Raj, V., and Velraj, R. (2019): CFD studies on different configurations of drying chamber for thin-layer drying of leaves. *Energy Sources, Part A: Recovery, Utilization and Environmental Effects*, 42(18), 2227–2239. DOI: 10.1080/15567036.2019.1607935
16. Badaoui, O., Djebli, A., and Hanini, S. (2022): Solar drying of apple and orange waste: Evaluation of a new thermodynamic approach, and characterization analysis. *Renewable Energy*, 199, 1593–1605. DOI: 10.1016/j.renene.2022.09.098
17. Bagheri, H., Arabhosseini, A., Kianmehr, M. H., and Chegini, G. R. (2013): Mathematical modelling of thin layer solar drying of tomato slices. *Agricultural Engineering International: the CIGR Journal*, 15(1), 146–153. <https://cigrjournal.org/index.php/Ejournal/article/view/2206>
18. Bains, R. and Langrish, T. A. G. (2007): Choosing an appropriate drying model for intermittent and continuous drying of bananas. *Journal of Food Engineering*, 79(1), 330–343. DOI: 10.1016/j.jfoodeng.2006.01.068
19. Balijepalli, R., Chandramohan, V. P., and Kirankumar, K. (2017): Performance parameter evaluation, materials selection, solar radiation with energy losses, energy storage and turbine design procedure for a pilot scale solar updraft tower. *Energy Conversion and Management*, 150, 451–462. DOI: 10.1016/j.enconman.2017.08.043
20. Barbosa, E. G., Araujo, M. E. V. de, Oliveira, A. C. L. de, and Martins, M. A. (2023): Thermal energy storage systems applied to solar dryers: Classification, performance, and numerical modeling: An updated review. *Case Studies in Thermal Engineering*, 45, 102986. DOI: 10.1016/j.csite.2023.102986
21. Belessiotis, V. and Delyannis, E. (2011). Solar drying. *Solar Energy*, 85(8), 1665–1691. DOI: 10.1016/j.solener.2009.10.001
22. Benhamza, A., Boubekri, A., Atia, A., Hadibi, T., and Arıcı, M. (2021): Drying uniformity analysis of an indirect solar dryer based on computational fluid dynamics and image processing. *Sustainable Energy Technologies and Assessments*, 47, 101466. DOI: 10.1016/j.seta.2021.101466

23. Ben Mabrouk, S., Benali, E., Oueslati H. (2012) Experimental study and numerical modelling of drying characteristics of apple slices. *Food and Bioproducts Processing*, 90, 719–728. DOI: 10.1016/j.fbp.2012.02.001
24. Blanco-Cano, L., Soria-Verdugo, A., Garcia-Gutierrez, L. M., and Ruiz-Rivas, U. (2016): Modeling the thin-layer drying process of Granny Smith apples: Application in an indirect solar dryer. *Applied Thermal Engineering*, 108, 1086–1094. DOI: 10.1016/j.applthermaleng.2016.08.001
25. Borah, A., Hazarika, K., and Khayer, S. M. (2015): Drying kinetics of whole and sliced turmeric rhizomes (*Curcuma longa* L.) in a solar conduction dryer. *Information Processing in Agriculture*, 2(2), 85–92. DOI: 10.1016/j.inpa.2015.06.002
26. Celma, A. R., and Cuadros, F. (2009): Energy and exergy analyses of OMW solar drying process. *Renewable Energy*, 34(3), 660–666. DOI: 10.1016/j.renene.2008.05.019
27. Chauhan, R., Singh, T., Kumar, N., Patnaik, A., and Thakur, N. S. (2017): Experimental investigation and optimization of impinging jet solar thermal collector by Taguchi method. *Applied Thermal Engineering*, 116, 100–109. DOI: 10.1016/j.applthermaleng.2017.01.025
28. Cook, D., Julias, M., and Nauman, E. (2014): Biological variability in biomechanical engineering research: Significance and meta-analysis of current modeling practices. *Journal of Biomechanics*, 47(6), 1241–1250. DOI: 10.1016/j.jbiomech.2014.01.040
29. Chowdhury, M. M. I., Bala, B. K., and Haque, M. A. (2011): Energy and exergy analysis of the solar drying of jackfruit leather. *Biosystems Engineering*, 110(2), 222–229. DOI: 10.1016/j.biosystemseng.2011.08.011
30. Das, M., and Akpinar, E. K. (2020): Determination of thermal and drying performances of the solar air dryer with solar tracking system: Apple drying test. *Case Studies in Thermal Engineering*, 21, 100731, 1–15. DOI: 10.1016/j.csite.2020.100731
31. Davis, R., John, P. (2018): Application of Taguchi-Based Design of Experiments for Industrial Chemical Processes. In: Editor: Valter Silva, Statistical Approaches with Emphasis on Design of Experiments Applied to Chemical Processes, IntechOpen, 137. DOI: 10.5772/intechopen.69501
32. Demirpolat, A. B. (2019): Investigation of mass transfer with different models in a solar energy food-drying system. *Energies*, 12(18). DOI: 10.3390/en12183447
33. Devan, P. K., Bibin, C., Asburris Shabrin, I. Gokulnath, R., and Karthick, D. (2020). Solar drying of fruits - A comprehensive review. *Materials Today: Proceedings*, 33, 253–260. DOI: 10.1016/j.matpr.2020.04.041
34. Dincer I. (2011): Exergy as a potential tool for sustainable drying systems. *Sustainable Cities and Society*, 1(2), 91–96. DOI: 10.1016/j.scs.2011.04.001

35. Dissa, A. O., Bathiebo, J., Kam, S., Savadogo, P. W., Desmorieux, H., and Koulidiati, J., (2009): Modelling and experimental validation of thin layer indirect solar drying of mango slices. *Renewable Energy*, 34(4), 1000–1008.  
DOI: 10.1016/j.renene.2008.08.006
36. Doymaz, I., and İsmail, O. (2011): Drying characteristics of sweet cherry. *Food and Bioproducts Processing*, 89(1), 31–38. DOI: 10.1016/j.fbp.2010.03.006
37. Doymaz, I. (2013): Experimental study on drying of pear slices in a convective dryer. *International Journal of Food Science and Technology*, 48(9), 1909–1915.  
DOI: 10.1111/ijfs.12170
38. Doymaz, I., and Özdemir, Ö. (2014): Effect of air temperature, slice thickness and pre-treatment on drying and rehydration of tomato. *International Journal of Food Science and Technology*, 49(2), 558–564. DOI: 10.1111/ijfs.12337
39. Ekka, J. P., and Palanisamy, M. (2020): Determination of heat transfer coefficients and drying kinetics of red chilli dried in a forced convection mixed mode solar dryer. *Thermal Science and Engineering Progress*, 19, 100607.  
DOI: 10.1016/j.tsep.2020.100607
40. El Hage, H., Herez, A., Ramadan, M., Bazzi, H., and Khaled, M., (2018): An investigation on solar drying: A review with economic and environmental assessment. *Energy*, 157, 815–829. DOI: 10.1016/j.energy.2018.05.197
41. El-Beltagy, A., Gamea, G. R., and Essa, A. H. A. (2007): Solar drying characteristics of strawberry. *Journal of Food Engineering*, 78(2), 456–464.  
DOI: 10.1016/j.jfoodeng.2005.10.015
42. El Khadraoui, A., Bouadila, S., Kooli, S., Farhat, A., and Guizani, A. (2017): Thermal behavior of indirect solar dryer: Nocturnal usage of solar air collector with PCM. *Journal of Cleaner Production*, 148, 37–48. DOI: 10.1016/j.jclepro.2017.01.149
43. Eltief, S. A., Ruslan, M. H., and Yatim, B. (2007): Drying chamber performance of V-groove forced convective solar dryer. *Desalination*, 209(1-3), 151–155.  
DOI: 10.1016/j.desal.2007.04.024
44. Erbay, Z., and Icier, F. (2010): A review of thin layer drying of foods: theory, modeling, and experimental results. *Critical reviews in food science and nutrition*, 50(5), 441–464.  
DOI: 10.1080/10408390802437063
45. Falade, K. O., and Solademi, O. J. (2010): Modelling of air drying of fresh and blanched sweet potato slices. *International Journal of Food Science and Technology*, 45(2), 278–288. DOI: 10.1111/j.1365-2621.2009.02133.x
46. Farkas, I. (2013): Integrated use of solar energy for crop drying. *Drying Technology*, 31(8), 866–871. DOI: 10.1080/07373937.2013.790410
47. Farkas, I., Mészáros, Cs., and Bálint, Á. (2000). Mathematical and physical foundations of drying theories. *Drying Technology*, 18(3), 541–559.  
DOI: 10.1080/07373930008917725

48. Fernandes, L., and Tavares, P. B. (2024): A review on solar drying devices: Heat transfer, air movement and type of chambers. *Solar*, 4(1), 15–42.  
DOI: 10.3390/solar4010002
49. Folayan, J. A., Osuolale, F. N., and Anawe, P. A. L. (2018): Data on exergy and exergy analyses of drying process of onion in a batch dryer. *Data in Brief*, 21, 1784–1793.  
DOI: 10.1016/j.dib.2018.10.132
50. Forson, F. K., Nazha, M. A. A., Akuffo, F. O., and Rajakaruna, H. (2007): Design of mixed-mode natural convection solar crop dryers: Application of principles and rules of thumb. *Renewable Energy*, 32(14), 2306–2319.  
DOI: 10.1016/j.renene.2006.12.003
51. Hussein, J. B., Filli, K. B., and Oke, M. O. (2016): Thin layer modelling of hybrid, solar and open sun drying of tomato slices. *Research Journal of Food Science and Nutrition*, 1(1), 15–27. DOI: 10.31248/RJFSN2016.010
52. Fudholi, A., Sopian, K., Yazdi, M. H., Ruslan, M. H., Gabbasa, M., and Kazem, H. A. (2014): Performance analysis of solar drying system for red chili. *Solar Energy*, 99, 47–54. DOI: 10.1016/j.solener.2013.10.019
53. Fudholi, A., Ridwan, A., Yendra, R., Pani Desvina, A., Hartono, H., Khan Bin Majahar Ali, M., Suyono, T., and Sopian, K. (2018): Solar drying technology in Indonesia: an overview. *International Journal of Power Electronics and Drive Systems (IJPEDS)*, 9(4), 1804–1813. DOI: 10.11591/ijpeds.v9.i4.pp1804-1813
54. Gamli, F. (2014): A review based on the relationship among drying, curve fitting and mathematical models in food systems. *Advance Research in Agriculture and Veterinary Science*, 1(2), 47–53.
55. Getahun, E., Delele, M. A., Gabbiye, N., Fanta, S. W., Demissie, P., and Vanierschot, M. (2021): Importance of integrated CFD and product quality modeling of solar dryers for fruits and vegetables: A review. *Solar Energy*, 220, 88–110.  
DOI: 10.1016/j.solener.2021.03.049
56. Ghorbani, H., Wood, D. A., Choubineh, A., Tatar, A., Abarghoyi, P. G., Madani, M., and Mohamadian, N. (2020): Prediction of oil flow rate through an orifice flow meter: Artificial intelligence alternatives compared. *Petroleum*, 6(4), 404–414.  
DOI: 10.1016/j.petlm.2018.09.003
57. Gilago, M. C., & Chandramohan, V. P. (2022): Performance evaluation of natural and forced convection indirect type solar dryers during drying ivy gourd: An experimental study. *Renewable Energy*, 182, 934–945. DOI: 10.1016/j.renene.2021.11.038
58. Gilago, M. C., Mugi, V. R., and Chandramohan, V. P. (2023a): Evaluation of drying kinetics of carrot and thermal characteristics of natural and forced convection indirect solar dryer. *Results in Engineering*, 18, 101196.  
DOI: 10.1016/j.rineng.2023.101196

59. Gilago, M. C., Mugi, V. R., Chandramohan, V. P., & Suresh, S. (2023b): Evaluating the performance of an indirect solar dryer and drying parameters of pineapple: comparing natural and forced convection. *Journal of Thermal Analysis and Calorimetry*, 148, 3701–3709. DOI: 10.1007/s10973-023-11955-2
60. Gorjian, S., Hosseingholilou, B., Jathar, L. D., Samadi, H., Samanta, S., Sagade, A. A., Kant, K., and Sathyamurthy, R. (2021): Recent advancements in technical design and thermal performance enhancement of solar greenhouse dryers. *Sustainability*, 13(13), 7025. DOI: 10.3390/su13137025
61. Hao, W., Zhang, H., Liu, S., and Lai, Y. (2021): Design and prediction method of dual working medium solar energy drying system. *Applied thermal Engineering*, 195, 117153. DOI: 10.1016/j.applthermaleng.2021.117153
62. Heydari, A., and Mesgarpour, M. (2018): Experimental analysis and numerical modeling of solar air heater with helical flow path. *Solar Energy*, 162, 278–288. DOI: 10.1016/j.solener.2018.01.030
63. Hossain, S., Islam, R., Ahmed, T., Sani, A., Hossain Sarker, S., Akhtaruzzaman, and Alam, S. M. S. (2025): Design, fabrication, and performance evaluation of an indirect solar-powered vegetable dryer. *Solar Energy Advances*, 5, 100096. DOI: 10.1016/j.seja.2025.100096
64. Husham Abdulmalek, S., Khalaji Assadi, M., Al-Kayiem, H. H., and Gitan, A. A. (2018): A comparative analysis on the uniformity enhancement methods of solar thermal drying. *Energy*, 148, 1103–1115. DOI: 10.1016/j.energy.2018.01.060
65. Inyang, U. E., Oboh, I. O., and Etuk, B. R. (2018): Kinetic models for drying techniques–food materials. *Advances in Chemical Engineering and Science*, 8(2), 27–48. DOI: 10.4236/aces.2018.82003
66. Iranmanesh, M., Samimi Akhijahani, H., and Barghi Jahromi, M. S. (2020): CFD modeling and evaluation the performance of a solar cabinet dryer equipped with evacuated tube solar collector and thermal storage system. *Renewable Energy*, 145, 1192–1213. DOI: 10.1016/j.renene.2019.06.038
67. Jahromi, M. S. B., Iranmanesh, M., and Akhijahani, H. S. (2022): Thermo-economic analysis of solar drying of Jerusalem artichoke (*Helianthus tuberosus* L.) integrated with evacuated tube solar collector and phase change material. *Journal of Energy Storage*, 52(PA), 104688. DOI: 10.1016/j.est.2022.104688
68. Jain, D., and Tewari, P. (2015): Performance of indirect through pass natural convective solar crop dryer with phase change thermal energy storage. *Renewable Energy*, 80, 244–250. DOI: 10.1016/j.renene.2015.02.012
69. Jamil, B., and Akhtar, N. (2017): Comparative analysis of diffuse solar radiation models based on sky-clearness index and sunshine period for humid-subtropical climatic region of India: A case study. *Renewable and Sustainable Energy Reviews*, 78, 329–355. DOI: 10.1016/j.rser.2017.04.073



70. Joshi, M., Kumar, N., and Baredar, P. (2019): Optimization of solar dryer using Taguchi method. *International Journal of Recent Technology and Engineering*, 8(3), 3320–3326.  
DOI: 10.35940/ijrte.C5684.098319
71. Kaleta, A. and Górnicki, K. (2010): Some remarks on evaluation of drying models of red beet particles. *Energy Conversion and Management*, 51(12), 2967–2978.  
DOI: 10.1016/j.enconman.2010.06.040
72. Kaleta, A., Górnicki, K., Winiczenko, R., and Chojnacka, A. (2013): Evaluation of drying models of apple (var. Ligol) dried in a fluidized bed dryer. *Energy Conversion and Management*, 67, 179–185. DOI: 10.1016/j.enconman.2012.11.011
73. Kamaruddin, S., Khan, Z. A., and Foong, S. H. (2010): Application of Taguchi method in the optimization of injection moulding parameters for manufacturing products from plastic blend. *International Journal of Engineering and Technology*, 2(6), 574–580.  
DOI: 10.7763/IJET.2010.V2.184
74. Kolesnikov, G., and Gavrilov, T. (2020): Modeling the drying of capillary-porous materials in a thin layer: Application to the estimation of moisture content in thin-walled building blocks. *Applied Sciences*, 10(19), 6953. DOI: 10.3390/app10196953
75. Kucuk, H., Midilli, A., Kilic, A., and Dincer, I. (2014): A review on thin-layer drying-curve equations. *Drying Technology*, 32(7), 757–773.  
DOI: 10.1080/07373937.2013.873047
76. Kumar, M., Shimpy, Sahdev, R. K., Sansaniwal, S. K., Bhutani, V. and Manchanda, H. (2023): Experimental forced convection greenhouse and indirect cabinet drying of date fruits: a comparative study. *Journal of Thermal Analysis and Calorimetry*, 148, 5437–5454. DOI: 10.1007/s10973-023-12057-9
77. Kumar, A., Kumar, R., and Kumar, D. (2024): Assessment of an indirect solar dryer for small-scale resin production: Energy, exergy, economic (3E), and sustainability analysis. *Sustainable Energy Technologies and Assessments*, 103950.  
DOI: 10.1016/j.seta.2024.103950
78. Kurtbas, İ., and Durmuş, A. (2004): Efficiency and exergy analysis of a new solar air heater. *Renewable Energy*, 29(9), 1489–1501.  
DOI: 10.1016/j.renene.2004.01.006
79. Lee, D. K., In, J., and Lee, S. (2015): Standard deviation and standard error of the mean. *Korean Journal of Anesthesiology*, 68(3), 220–223.  
DOI: 10.4097/kjae.2015.68.3.220
80. Li, M., Liu, M., Xu, C., Wang, J., and Yan, J. (2023a): Thermodynamic and sensitivity analyses on drying subprocesses of various evaporative dryers: A comparative study. *Energy*, 284, 128571. DOI: 10.1016/j.energy.2023.128571
81. Li, C., Ren, G., Zhang, L., Duan, X., Wang, Z., Ren, X., Chu, Q., and He, T. (2023b): Effects of different drying methods on the drying characteristics and drying quality of *Cistanche deserticola*. *LWT*, 184, 115000. DOI: 10.1016/j.lwt.2023.115000

82. Lingayat, A., Chandramohan, V. P., Raju, V. R. K., and Kumar, A. (2020): Development of indirect type solar dryer and experiments for estimation of drying parameters of apple and watermelon: Indirect type solar dryer for drying apple and watermelon. *Thermal Science and Engineering Progress*, 16, 100477.  
DOI: 10.1016/j.tsep.2020.100477
83. Liu, Z. (2018): What is the future of solar energy? Economic and policy barriers. *Energy Sources, Part B: Economics, Planning, and Policy*, 13(3), 169-172.  
DOI: 10.1080/15567249.2017.1416704
84. Maia, C. B., Ferreira, A. G., Cabezas-Gómez, L., de Oliveira Castro Silva, J., and de Morais Hanriot, S. (2017): Thermodynamic analysis of the drying process of bananas in a small-scale solar updraft tower in Brazil. *Renewable Energy*, 114, 1005–1012.  
DOI: 10.1016/j.renene.2017.07.102
85. Madadi Avargani, V., Abdlla Maarof, H., and Zendehboudi, S. (2023): Multiphysics CFD modeling to assess performance of a perforated multi-plate indirect solar dryer with a V-corrugated absorber surface. *Applied Thermal Engineering*, 227, 120387.  
DOI: 10.1016/j.applthermaleng.2023.120387
86. Matheswaran, M. M., Arjunan, T. V., and Somasundaram, D. (2018): Analytical investigation of solar air heater with jet impingement using energy and exergy analysis. *Solar Energy*, 161, 25–37. DOI: 10.1016/j.solener.2017.12.036
87. Menges, H. O., and Ertekin, C. (2006): Thin layer drying model for treated and untreated Stanley plums. *Energy Conversion and Management*, 47(15–16), 2337–2348.  
DOI: 10.1016/j.enconman.2005.11.016
88. Meisami-asl, E., and Rafiee, S. (2009): Mathematical modeling of kinetics of thin-layer drying of apple (var. Golab)". *Agricultural Engineering International: the CIGR Ejournal*, XI, 1185. <https://cigrjournal.org/index.php/Ejournal/article/view/1185>
89. Midilli, A., and Kucuk, H. (2003): Energy and exergy analyses of solar drying process of pistachio. *Energy*, 28(6), 539–556. DOI: 10.1016/S0360-5442(02)00158-5
90. Mishra, L., Sinha, A., and Gupta, R. (2021): Energy, exergy, economic and environmental (4E) analysis of greenhouse dryer in no-load condition. *Sustainable Energy Technologies and Assessments*, 45, 101186. DOI: 10.1016/j.seta.2021.101186
91. Mohammed, S., Fatumah, N., and Shadia, N. (2020): Drying performance and economic analysis of novel hybrid passive-mode and active-mode solar dryers for drying fruits in East Africa. *Journal of Stored Products Research*, 88, 101634.  
DOI: 10.1016/j.jspr.2020.101634
92. Morosuk, T., and Tsatsaronis, G. (2013): Strengths and limitations of advanced exergetic analyses. *Proceedings of the ASME 2013 International Mechanical Engineering Congress and Exposition*, 6B. DOI: 10.1115/IMECE2013-64320

93. Mugi, V. R., and Chandramohan, V. P. (2021a): Energy and exergy analysis of forced and natural convection indirect solar dryers: Estimation of exergy inflow, outflow, losses, exergy efficiencies and sustainability indicators from drying experiments. *Journal of Cleaner Production*, 282. DOI: 10.1016/j.jclepro.2020.124421
94. Mugi, V. R., and Chandramohan, V. P. (2021b): Energy, exergy and economic analysis of an indirect type solar dryer using green chilli: A comparative assessment of forced and natural convection. *Thermal Science and Engineering Progress*, 24, 100950. DOI: 10.1016/j.tsep.2021.100950
95. Mugi, V. R., Gilago, M. C., and Chandramohan, V. P. (2022): Energy and exergy investigation of indirect solar dryer under natural and forced convection while drying muskmelon slices. *Energy Nexus*, 8, 100153. DOI: 10.1016/j.nexus.2022.100153
96. Mugi, V. R., Gilago, M. C., Chandramohan, V. P., and Valasingam, S. B. (2024): Experimental evaluation of performance, drying and thermal parameters of guava slabs dried in a forced convection indirect solar dryer without and with thermal energy storage. *Renewable Energy*, 223, 120005. DOI: 10.1016/j.renene.2024.120005
97. Musembi, M. N., Kiptoo, K. S., and Yuichi, N. (2016): Design and analysis of solar dryer for mid-latitude region. *Energy Procedia*, 100, 98–110. DOI: 10.1016/j.egypro.2016.10.145
98. Nakasone, Y., Yoshimoto, S., and Stolarski, T. A. (2006): Engineering Analysis with ANSYS Software. Elsevier Butterworth-Heinemann: Amsterdam  
DOI: 10.1016/B978-0-7506-6875-0.X5030-3
99. Nainggolan, R., Perangin-angin, R., Simarmata, E., and Tarigan, A. F. (2019): Improved the performance of the K-Means cluster using the sum of squared error (SSE) optimized by using the elbow method. *Journal of Physics: Conference Series*, 1361, 012015. DOI: 10.1088/1742-6596/1361/1/012015
100. Ndukwu, M. C., Onyenwigwe, D., Abam, F. I., Eke, A. B., and Dirioha, C. (2020): Development of a low-cost wind-powered active solar dryer integrated with glycerol as thermal storage. *Renewable Energy*, 154, 553–568. DOI: 10.1016/j.renene.2020.03.016
101. Nguyen, L. L. P., Baranyai, L., Nagy, D., Mahajan, P. V., Zsom-Muha, V., Zsom, T. (2021). Color analysis of horticultural produces using HUE spectra fingerprinting. *MethodsX*, 8, 101594. DOI: 10.1016/j.mex.2021.101594
102. Noori, A. W., Royen, M. J., and Haydary, J. (2021): Thin-layer mathematical modeling of apple slices drying, under open sun and cabinet solar dryer. *International Journal of Innovative Research and Scientific Studies*, 4(2), 43–52. DOI: 10.53894/ijirss.v4i2.55

103. Norton, T., Grant, J., Fallon, R., and Sun, D. W. (2010). Improving the representation of thermal boundary conditions of livestock during CFD modelling of the indoor environment. *Computers and Electronics in Agriculture*, 73(1), 17-36.  
DOI: 10.1016/j.compag.2010.04.002
104. Nowzari, R., Mirzaei, N., and Parham, K. (2020): Selecting the optimal configuration for a solar air heater using the Grey-Taguchi method. *Processes*, 8(3), 317.  
DOI: 10.3390/pr8030317
105. Obaideen, K., Nooman AlMallahi, M., Alami, A. H., Ramadan, M., Abdelkareem, M. A., Shehata, N., and Olabi, A. G. (2021): On the contribution of solar energy to sustainable developments goals: Case study on Mohammed bin Rashid Al Maktoum Solar Park. *International Journal of Thermofluids*, 12, 100123.  
DOI: 10.1016/j.ijft.2021.100123
106. Panagiotis A. Michailidis and Magdalini K. Krokida. (2015): Drying of foods. In: Theodoros Varzakas and Constantina Tzia (Ed.), Food engineering handbook, Food process engineering (pp. 375–431). Taylor and Francis Group, LLC.  
[https://api.pageplace.de/preview/DT0400.9781466582279\\_A38969524/preview-9781466582279\\_A38969524.pdf](https://api.pageplace.de/preview/DT0400.9781466582279_A38969524/preview-9781466582279_A38969524.pdf)
107. Panda, S. N., Saikia, R., Sagar, Narayana swamy, G., Panotra, N., Yadav, K., Singh, B. V., Rathi, S., Singh, R., and Pandey, S. K. (2024): Solar energy's role in achieving sustainable development goals in agriculture. *International Journal of Environment and Climate Change*, 14(5), 10–31. DOI: 10.9734/ijecc/2024/v14i54167
108. Paneru, B., Paneru, B., Alexander, V., Nova, S., Bhattarai, N., Poudyal, R., Narayan Poudyal, K., Dangi, M. B., and Boland, J. J. (2024): Solar energy for operating solar cookers as a clean cooking technology in South Asia: A review. *Solar Energy*, 283, 113004. DOI: 10.1016/j.solener.2024.113004
109. Panwar, N. L., Kaushik, S. C., and Kothari, S. (2012): A review on energy and exergy analysis of solar drying systems. *Renewable and Sustainable Energy Reviews*, 16(5), 2812–2819. DOI: 10.1016/j.rser.2012.02.053
110. Philip, N., Duraipandi, S., and Sreekumar, A. (2022): Techno-economic analysis of greenhouse solar dryer for drying agricultural produce. *Renewable Energy*, 199, 613–627.  
DOI: 10.1016/j.renene.2022.08.148
111. Prakash, R., and Kamatchi, R. (2024): Natural convective solar dryer powered by stepped fin plate integrated trough array solar air heater for agricultural produce preservations. *Solar Energy*, 271, 112415. <https://doi.org/10.1016/j.solener.2024.112415>
112. Rabha, D. K., and Muthukumar, P. (2017): Performance studies on a forced convection solar dryer integrated with a paraffin wax–based latent heat storage system. *Solar Energy*, 149, 214–226. DOI: 10.1016/j.solener.2017.04.012
113. Rafiee, Sh., Keyhani, A., Sharifi, M., Jafari, A., Mobli, H., and Tabatabaeeefar, A. (2009): Thin layer drying properties of soybean (Viliamz Cultivar). *Journal of Agricultural Science and Technology (JAST)*, 11(3), 289–300. <https://sid.ir/paper/546539/en>

114. Rajesh, S., Sekar, S., Sekar, S. D., and Madhankumar, S. (2024): Drying kinetics, energy, statistical, economic, and proximate analysis of a greenhouse dryer using different glazing materials for *Coccinia grandis* drying. *Solar Energy*, 284, 113047.  
DOI: 10.1016/j.solener.2024.113047
115. Rani, P., and Tripathy, P. P. (2021): Drying characteristics, energetic and exergetic investigation during mixed-mode solar drying of pineapple slices at varied air mass flow rates. *Renewable Energy*, 167, 508–519. DOI: 10.1016/j.renene.2020.11.107
116. Rashid, K. M. J. (2023): Optimize the Taguchi method, the signal-to-noise ratio, and the sensitivity. *International Journal of Statistic and Applied Mathematics*, 8(6), 64-70.  
DOI: 10.22271/math.2023.v8.i6a.1406
117. Reza Rouzegar, M., Hossein Abbaspour-Fard, M., and Hedayatizadeh, M. (2023): Design, thermal simulation and experimental study of a hybrid solar dryer with heat storage capability. *Solar Energy*, 258, 232–243.  
DOI: 10.1016/j.solener.2023.05.003
118. Rezaei, M., Sefid, M., Almutairi, K., Mostafaeipour, A., Ao, H. X., Hosseini Dehshiri, S. J., Hosseini Dehshiri, S. S., Chowdhury, S., and Techato, K. (2022): Investigating performance of a new design of forced convection solar dryer. *Sustainable Energy Technologies and Assessments*, 50, 101863. DOI: 10.1016/j.seta.2021.101863
119. Richter, C., Lincot, D., and Gueymard, C. A. (2013): *Solar Energy*. Springer New York.  
DOI: 10.1007/978-1-4614-5806-7
120. Rosli, M. A. M., Hiew, S. J., Mohd Azhar, N. I., Saputra, M., and Ali, S. (2021): A Simulation study of drying chamber for marine product. *International Journal of Integrated Engineering*, 13(6), 62–69. DOI: 10.30880/ijie.2021.13.06.005
121. Sabareesh, V., Milan, K. J., Muraleedharan, C and Rohinikumar, B. (2021): Improved solar drying performance by ultrasonic desiccant dehumidification in indirect forced convection solar drying of ginger with phase change material. *Renewable Energy*, 169, 1280–1293. DOI: 10.1016/j.renene.2021.01.085
122. Sahu, M. K., Mishra, S., and Kumar, A. (2023): Optimization of geometric and flow parameters of solar air heater roughened with artificial roughness by Taguchi method. *Archives of Thermodynamics*, 44(3), 3–33. DOI: 10.24425/ather.2023.147535
123. Sami, S., Rahimi, A., Etesami, N. (2011) Dynamic Modeling and a parametric study of an indirect solar cabinet. *Drying Technology*, 29(7), 825–835.  
DOI: 10.1080/07373937.2010.545159
124. Sammy Sadaka, and Digvir, S. Jayas. (2022): Cereal grain drying systems. In: Editor: Kurt A. Rosentrater, *Storage of Cereal Grains and Their Products*, (Fifth edition, pp. 293–329). Woodhead Publishing. DOI: 10.1016/B978-0-12-812758-2.00008-8
125. Sanghi, A., Ambrose, R. P. K., and Maier, D. (2017): CFD simulation of corn drying in a natural convection solar dryer. *Drying Technology*, 36(7), 859–870.  
DOI: 10.1080/07373937.2017.1359622

126. Sethi, C. K., Acharya, S. K., Ghanem, S. R., Behera, A., and Patnaik, P. P. (2021): Exergy, energy and economic analysis of a V-groove assist rotating tray type solar cabinet dryer for drying potato chips. *Journal of Stored Products Research*, 93, 101861.  
DOI: 10.1016/j.jspr.2021.101861
127. Sharma, A, Chen, C.R and Vu Lan, N. (2009): Solar-energy drying systems: A review. *Renewable and Sustainable Energy Reviews*, 3(6–7), 1185–1210.  
DOI: 10.1016/j.rser.2008.08.015
128. Simo-Tagne, M., Bonoma, B., Bennamoun, L., Monkam, L., Léonard, A., Zoulalian, A., and Rogaume, Y. (2019): Modeling of coupled heat and mass transfer during drying of ebony wood using indirect natural convection solar dryer. *Drying Technology*, 37(14), 1863–1878. DOI: 10.1080/07373937.2018.1544144
129. Simo-Tagne, M., and Ndi-Azese, M. (2021): Thermal, economic, and environmental analysis of a novel solar dryer for firewood in various temperate and tropical climates. *Solar Energy*, 226, 348–364. DOI: 10.1016/j.solener.2021.08.060
130. Simo-Tagne, M., Tagne Tagne, A., Ndukwu, M. C., Bennamoun, L., Obounou Akong, M. B., El Marouani, M., and Rogaume, Y. (2021): Numerical study of the drying of cassava roots chips using an indirect solar dryer in natural convection. *AgriEngineering*, 3(1), 138–157. DOI: 10.3390/agriengineering3010009
131. Singh Chauhan, P., Kumar, A., and Tekasakul, P. (2015): Applications of software in solar drying systems: A review. *Renewable and Sustainable Energy Reviews*, 51, 1326–1337. DOI: 10.1016/j.rser.2015.07.025
132. Singh, J. (2015): Review paper of study on solar dryer. *Journal of Mechanical and Engineering*, 1(1), <https://matjournals.co.in/index.php/JOMME/article/view/5796>
133. Singh, P., and Gaur, M. K. (2021): Environmental and economic analysis of novel hybrid active greenhouse solar dryer with evacuated tube solar collector. *Sustainable Energy Technologies and Assessments*, 47, 101428. DOI: 10.1016/j.seta.2021.101428
134. Singh, D., Mishra, S., and Shankar, R. (2023): Energy and exergo-environmental (3E) analysis of wheat seeds drying using indirect solar dryer. *Environmental Science and Pollution Research*, 30, 120010–120029. DOI: 10.1007/s11356-023-30503-x
135. Siqueira, V. C., Resende, O. and Chaves, T. H. (2013): Mathematical modelling of the drying of jatropha fruit: an empirical comparison. *Revista Ciencia Agronomica*, 44 (2), 278–285. DOI: 10.1590/S1806-66902013000200009
136. Sobukola, O. P., Daio, O. U., Sanni, L. O., Odunewu, A. V. and Fafiolu, B. O. (2007): Thin layer drying process of some leafy vegetables under open sun. *Food Science and Technology International*, 13(1), 35–40. DOI: 10.1177/1082013207075953

137. Sonthikun, S., Chairat, P., Fardsin, K., Kirirat, P., Kumar, A., and Tekasakul, P. (2016): Computational fluid dynamic analysis of innovative design of solar-biomass hybrid dryer: An experimental validation. *Renewable Energy*, 92, 185–191.  
DOI: 10.1016/j.renene.2016.01.095
138. Srinivasan, G., and Muthukumar, P. (2021): A review on solar greenhouse dryer: Design, thermal modelling, energy, economic and environmental aspects. *Solar Energy*, 229, 3–21. DOI: 10.1016/j.solener.2021.04.058
139. Srinivasan, G., Rabha, D. K and Muthukumar, P. (2021): A review on solar dryers integrated with thermal energy storage units for drying agricultural and food products. *Solar Energy*, 229, 22–38. DOI: 10.1016/j.solener.2021.07.075
140. Srivastava, A., Sharma, A., and Kumar, A. (2025): Performance evaluation of indirect solar drying system for potato slices: Comparative analysis with open-sun drying method. *Solar Energy*, 285, 113114. DOI: 10.1016/j.solener.2024.113114
141. Stegou-Sagia, A. and Fragkou, D. V. (2018): Thin layer drying modeling of apples and apricots in a solar-assisted drying system. *Journal of Thermal Engineering*, 4(1), 1680–1691. DOI: 10.18186/journal-of-thermal-engineering.364909
142. Tarigan, E. (2018): Mathematical modelling and simulation of a solar agricultural dryer with back-up biomass burner and thermal storage. *Case Studies in Thermal Engineering*, 12, 149–165. DOI: 10.1016/j.csite.2018.04.012
143. Toğrul, İ. T., Pehlivan, D. (2004): Modelling of thin layer drying kinetics of some fruits under open-air sun drying process. *Journal of Food Engineering*, 65(3), 413–425.  
DOI: 10.1016/j.jfoodeng.2004.02.001
144. Tsatsaronis, G. (2007): Definitions and nomenclature in exergy analysis and exergoeconomics. *Energy*, 32(4), 249–253. DOI: 10.1016/j.energy.2006.07.002
145. Ullah, F., Min, K., Khattak, M. K., Wahab, S., Wahab, N., Ameen, M., Memon, M. S., Wang, X., Soomro, S. A., Yousaf, K., Li, N., and Yang, J. (2018): Effects of different drying methods on some physical and chemical properties of loquat (*Eriobotrya japonica*) fruits. *International Journal of Fruit Science*, 18(4), 345–354.  
DOI: 10.1080/15538362.2018.1435330
146. Ullah, I., Hanif, M., Basit, A., Khattak, M. K., Shah, S. T., Ullah, A., Mohamed, H. I. (2022). Performance of two terms exponential model on the drying kinetics of solar-dried tomatoes (*Lycopersicum esculentum* L.) treated with and without chemical preservatives. *Egyptian Journal of Chemistry*, 65(3), 455–464. DOI: 10.21608/ejchem.2021.93566.4414
147. Verma, A., and Goswami, P. (2024): Integration of solar energy in agriculture leads to green energy and golden crop production. *Educational Administration: Theory and Practice*, 30(7), 261–266. DOI: 10.53555/kuey.v30i7.6626

148. Vijayan, S., Arjunan, T. V., and Kumar, A. (2016): Mathematical modelling and performance analysis of thin layer drying of bitter gourd in sensible storage based indirect solar dryer. *Innovative Food Science and Emerging Technologies*, 36, 59–67.  
DOI: 10.1016/j.ifset.2016.05.014
149. Wang, D. C., Fon, D. S., Fang, W., and Sokhansanj, S. (2004): Development of a visual method to test the range of applicability of thin layer drying equations using MATLAB tools. *Drying Technology*, 22(8), 1921–1948. DOI: 10.1081/DRT-200032878
150. Yadav, S., Lingayat, A. B., Chandramohan, V. P., and Raju, V. R. K. (2018): Numerical analysis on thermal energy storage device to improve the drying time of indirect type solar dryer. *Heat and Mass Transfer*, 54, 3631–3646. DOI: 10.1007/s00231-018-2390-7  
DOI: 10.1007/s00231-018-2390-7
151. Yahya, M., Fahmi, H., Fudholi, A., and Sopian, K. (2018): Performance and economic analyses on solar-assisted heat pump fluidised bed dryer integrated with biomass furnace for rice drying. *Solar Energy*, 174, 1058–1067.  
DOI: 10.1016/j.solener.2018.10.002
152. Yildiz, O., Ertekin, C. and Uzun, H. I. (2001): Mathematical modelling of thin layer solar drying of sultana grapes. *Energy*, 26(5), 457–465. DOI: 10.1016/S0360-5442(01)00018-4  
DOI: 10.1016/S0360-5442(01)00018-4
153. Yassen, T. A., Al-Jethelah, M. S. M., and Dheyab, H. S. (2021): Experimental study of innovative indirect solar dryers. *International Journal of Heat and Technology*, 39(4), 1313–1320. DOI: 10.18280/ijht.390430
154. Zheng, C. W. and Pan, J. (2014): Assessment of the global ocean wind energy resource. *Renewable and Sustainable Energy Reviews*, 33, 382–391.  
DOI: 10.1016/j.rser.2014.01.065
155. Zoukit, A. Ferouali, H., Salhi, I., Doubabi, S., and Abdenouri, N. (2019): Simulation, design and experimental performance evaluation of an innovative hybrid solar-gas dryer. *Energy*, 189, 116279. DOI: 10.1016/j.energy.2019.116279



## A2: Publications related to the dissertation

### Refereed papers in foreign languages:

1. **Halefom, K.**, Buzas, J., Farkas, I. (2021): Modelling and simulation of air flow on the surface of solar air heater using computational fluid dynamics, *R&D in Mechanical Engineering Letters*, Vol. 21, pp. 78–84.
2. **Kidane, H.**, Buzas, J., Farkas, I. (2023): Airflow optimization of solar drying unit using computational fluid dynamics approach, *Mechanical Engineering Letters*, Vol. 24, pp. 52–74.
3. **Kidane, H.**, Buzas, J., Farkas, I. (2023): Computational analysis of horizontally and inclined finned solar air collector, *Jurnal Tekno Insentif*, Vol. 17, pp. 150–159.  
DOI: 10.36787/jti.v17i2.1172
4. **Kidane, H.**, Farkas, I., Buzás, J. (2024): Assessing the carrying capacity of solar dryers applied for agricultural products: a systematic review, *Discover Energy*, Vol. 4, 6.  
DOI: 10.1007/s43937-024-00031-x
5. **Kidane, H.**, Farkas, I., Buzás, J. (2025): Mathematical modelling of golden apple drying and performance evaluation of solar drying systems using energy and exergy approach, *Scientific Reports*, Vol. 15(1), 7805. DOI: 10.1038/s41598-025-92133-2  
DOI: 10.1038/s41598-025-92133-2 (Scopus: Q1 IF: 3.8)
6. **Kidane, H.**, Farkas, I., Buzás, J. (2025): Characterizing agricultural product drying in solar systems using thin-layer drying models: comprehensive review, *Discover Food*, Vol. 5(1), 84. DOI: 10.1007/s44187-025-00362-1 (Scopus: Q1, IF: 4.1)
7. **Kidane, H.**, Farkas, I., Buzás, J. (2025): Performance Evaluation of Solar Drying Chambers and Drying Kinetics of Apple Slices, *Energy Reports*, Vol. 13, pp. 4528–4540. DOI: 10.1016/j.egyr.2025.04.016 (Scopus: Q1, IF: 4.7)
8. **Kidane, H.**, Farkas, I., Buzás, J. (2025): Role of computational fluid dynamics in solar air heating: a comprehensive overview of applications, benefits and future directions, *Journal of Thermal Analysis and Calorimetry*. DOI: 10.1007/s10973-025-14261-1  
DOI: 10.1007/s10973-025-14261-1 (Scopus: Q2, IF: 3.0)
9. **Kidane, H.**, Farkas, I., Buzás, J. (2025): Modeling Airflow Dynamics in Solar Drying Chambers: A Comprehensive Review of CFD Applications, *Discover Applied Sciences*. DOI: 10.1007/s42452-025-06894-6 (Scopus: Q2)
10. **Kidane, H.**, Farkas, I., Buzás, J. (2025): Design, Fabrication and Performance Evaluation of Solar Drying Chamber Used for Apple Slices, *Acta Technologica Agriculturae*, Vol. xx(xx), pp. xxx. DOI: xxxxx/xxxxxx (Scopus: Q3, IF: 1.3) (Accepted)
11. **Kidane, H.**, Farkas, I., Buzás, J. (2025): Enhancing the drying uniformity in solar drying systems: computational and experimental study, *International Journal of Thermofluids*, Vol. xx(xx), pp. xxx. DOI: xxxxx/xxxxxx (Scopus: D1) (in Progress)
12. **Kidane, H.**, Farkas, I., Buzás, J. (2025): Optimizing solar drying chamber performance: Taguchi analysis of uniformity enhancement methods, *International Journal of Energy Research*, DOI: 10.1155/er/5061778 (Scopus: Q2, IF: 4.3).

*Refereed papers in Hungarian language*

13. Buzás, J., **Halefom, K.**, Farkas, I. (2022): Napenergiás szárítók áramlástan vizsgálat, Mezőgazdasági Technika, Vol. 18, pp. 2–5.

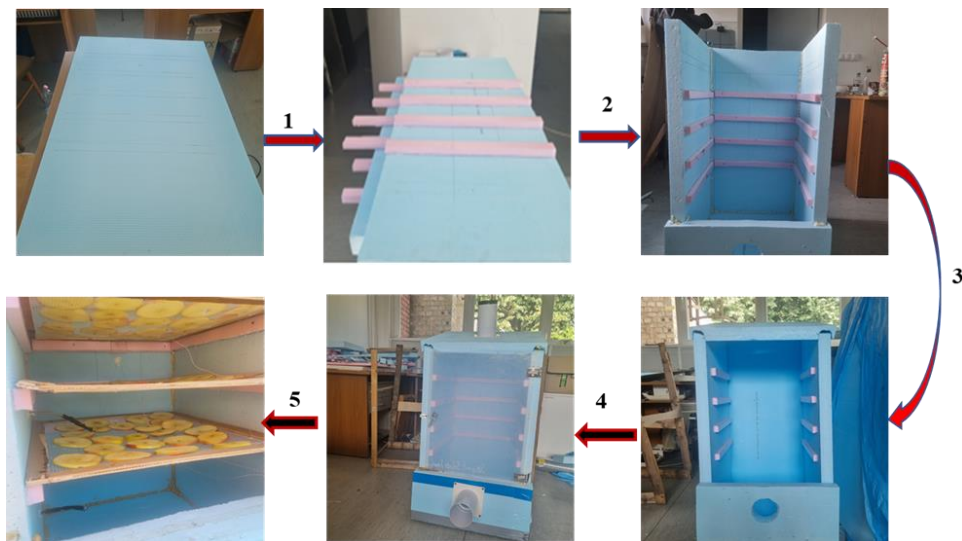
*International conference abstracts*

14. **Halefom, K.**, Buzas, J., Farkas, I. (2021): Estimation and forecasting of solar resources by artificial neural network, Book of Abstracts, 27th Workshop on Energy and Environment, December 21–21, 2021, pp. 21–21.
15. **Halefom, K.**, Buzas, J., Farkas, I. (2022): Numerical modelling and prediction of flow behaviour inside drying chamber, Book of Abstracts, 21st International Workshop for Young Scientists (BioPhys Spring 2022), Nitra, Slovakia, May 30–31, 2022, pp. 40–41. ISBN 978-83-89969-74-3.
16. **Halefom, K.**, Buzas, J., Farkas, I. (2022): Application of thermal storage systems for indirect solar dryers, Book of Abstracts, 28th Workshop on Energy and Environment, Gödöllő, Hungary, December 9–10, 2021, pp. 39–40. ISBN 978-963-623-016-6.
17. **Halefom, K.**, Buzas, J., Farkas, I. (2023): Main bottlenecks and optimizing methods of existing solar cooking methods and technologies, Book of Abstracts, 29th Workshop on Energy and Environment, 2023, pp. 43–44. ISBN 978-963-623-079-1.
18. **Kidane, H.**, Buzas, J., Farkas, I. (2023): The role of soft computing approach for analyzing solar drying systems, Book of Abstracts, BioPhys Spring 2023, Gödöllő, Hungary, June 15–16, 2023, pp. 30–36. ISBN 978-963-623-054-8.
19. **Kidane, H.**, Farkas, I., Buzas, J. (2024): Enhancing solar air heater efficiency through computational fluid dynamics analysis, Book of Abstracts, BioPhys Spring 2024, pp. 61–63.
20. **Halefom, K.**, Buzas, J., Farkas, I. (2024): Modeling the drying kinetics of golden apple in solar systems using thin layer equations, Book of Abstracts, 30th Workshop on Energy and Environment, 2024.
21. **Kidane, H.**, Farkas, I., Buzas, J. (2025): Solar drying system performance: an exergy-based evaluation, Book of Abstracts, 25th International Workshop for Young Scientists, Prague, Czech Republic, May 29–30, 2025.

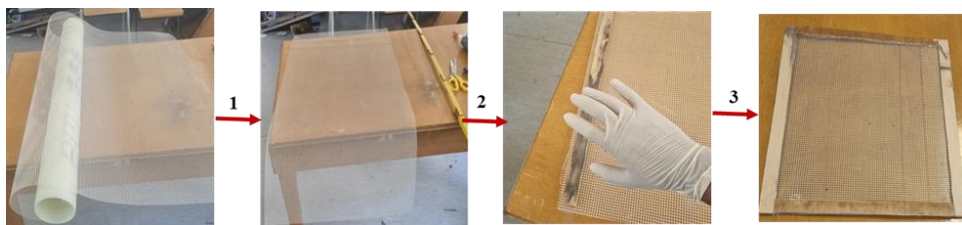
### A3: Manufacturing process process of basic drying systems



### Manufacturing process of the solar air heater











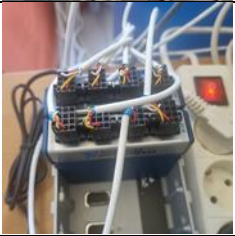
### Manufacturing process of the drying chamber



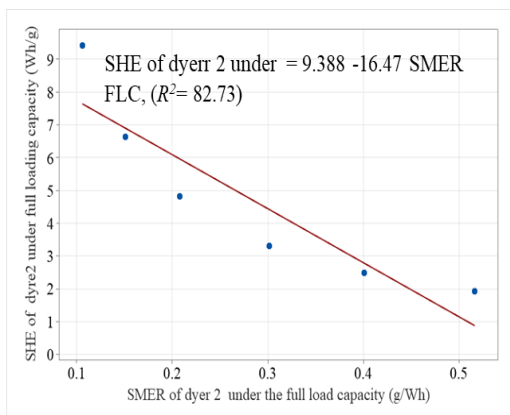
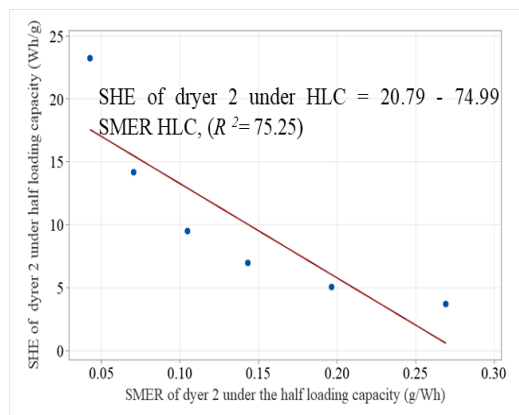
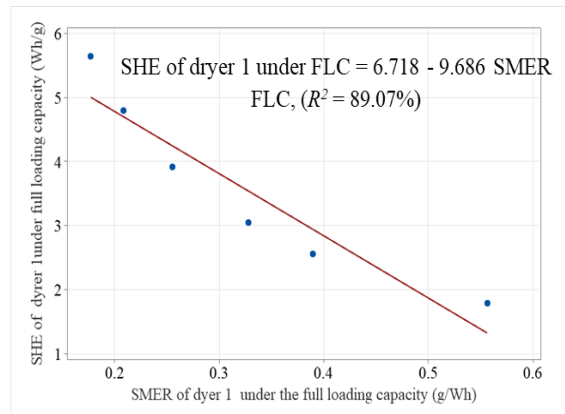
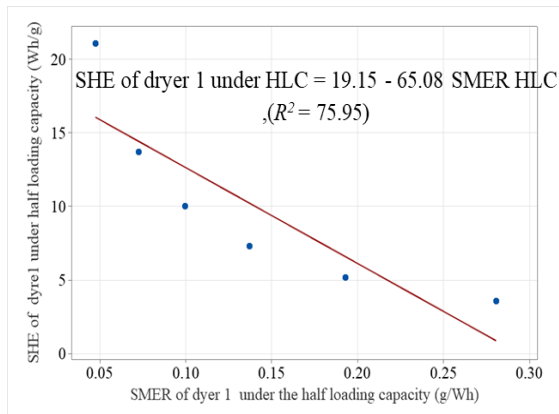
### Manufacturing process of the trays

#### A4: Accuracy and technical specifications of measurement devices

No	Instrument	Model	Range	Accuracy	Picture of the sensor
1	Resistance temperature detector (RTD) sensor	PT-100	-75 °C – 250 °C	±0.1 °C at 0 °C	
2	Digital weighing machine	Lutron GM-500	0 – 500 g	±0.02%	
3	Temperature thermocouples	T-type	-250 – 250 °C	±0.5 °C	
4	Temperature recorder	BTM-4208SD	-200 °C – 400 °C	±0.5 °C	
5	Differential pressure sensor	SENSIRION SDP-816	-500 – 500 Pa	±3%	
6	Relative humidity sensor	Honeywell HIH-4000-004	0 – 100%	±3.5%	
7	Pyranometer	Kipp and Zonen CM11	0 – 1400 W/m <sup>2</sup>	<0.6%	

8	Data logger (temperature, radiation)	Advantech ADAM- 4015+	-100 – 400 °C	±0.1%	
9	Data logger (pressure, humidity)	NI cDAQ- 9188 chassis with NI 9219 modules	0 – 5 V	±0.2%	

## A5: Regression analysis: SHE and SMER of the dryers



**A6: Statistical results of thin layer drying models for apple slice**

<b>Model name</b>	<b>Constants</b>	<b>R<sup>2</sup></b>	<b>RMSE</b>	<b>x<sup>2</sup></b>
Newton	k = 1.1	0.8956	0.321	0.0101
Wang and Singh	a = 0, b = 0	-	0.2115	0.4554
Page	n = 0	-	0.8383	6.8885
Modified page	k = 1, n = 1	0.951	0.7145	0.0121
<b>Logarithmic</b>	<b>a = 9.2, k = 5.29, c = 0</b>	<b>0.9903</b>	<b>0.0348</b>	<b>0.0112</b>
<b>Two-term</b>	<b>a = 4.7, k = 3.97, b = 0.0010, k<sub>1</sub> = 1.0970</b>	<b>0.9944</b>	<b>0.0521</b>	<b>0.0266</b>
Two-term exponential	a = 2.7, k = 0.11	0.9200	0.910	0.0812
Weibull distribution	a = 0.6, b = 0, k = 0.41, n = 0.23	0	0.1194	0.1399
Handerson and Pabis	a = 0.6, k = 0	-	0.1194	0.1399
<b>Midilli and Kucuk</b>	<b>a = 2.82, b = 0.0029, k = 5.02, n = 1.80</b>	<b>0.9956</b>	<b>0.0321</b>	<b>0.0101</b>

**A7: Drying rate and standard deviation of the enhancement tools**

<b>With triangular baffles</b>					
Time	Mean (g)	Moisture loss (g)	Drying rate (g/hr)	Std dev	p-value
10:00	405.00	0.00	0.00	0	-
11:00	349.00	56.00	56.00	17.87	0.025
12:00	304.25	100.75	50.38	22.02	0.010
13:00	258.50	146.50	48.83	30.07	0.011
14:00	214.25	190.75	47.69	30.79	0.009
15:00	173.50	231.50	46.30	28.93	0.010
16:00	136.00	269.00	44.83	22.52	0.011
Avg	262.9286	142.0714	42.00429	21.740857	0.012667

<b>Without triangular baffles</b>					
Time	Mean (g)	Moisture loss (g)	Drying rate (g/hr)	Std dev	p-value
10:00	405.00	0.00	0.00	0	-
11:00	350.50	54.50	54.50	13.72	0.110
12:00	297.50	107.50	53.75	24.82	0.010
13:00	242.25	162.75	54.25	33.96	0.005
14:00	193.50	211.50	52.88	33.92	0.004
15:00	150.00	255.00	51.00	28.72	0.004
16:00	115.75	289.25	48.21	21.36	0.005
Avg	250.6429	154.3571	44.94143	22.35714	0.023

<b>Integrated with swirler</b>					
Time	Mean (g)	Moisture loss (g)	Drying rate (g/hr)	Std dev	p-value
10:00	405.00	0.00	0.00	0.00	-
11:00	333.50	71.50	71.50	7.12	0.010
12:00	304.25	100.75	50.38	9.96	0.003
13:00	257.00	148.00	49.33	20.31	0.001
14:00	213.50	191.50	47.88	22.16	0.001
15:00	177.00	228.00	45.60	27.38	0.001
16:00	123.50	281.50	46.92	28.28	0.001
Avg	259.1071	145.8929	44.51571	16.45857	0.002833

<b>Without swirler</b>					
Time	Mean (g)	Moisture loss (g)	Drying rate (g/hr)	Std dev	p-value
10:00	405.00	0.00	0.00	0.00	-
11:00	334.50	70.50	70.50	20.38	0.088
12:00	290.00	115.00	57.50	30.48	0.009
13:00	240.50	164.50	54.83	38.31	0.007
14:00	193.00	212.00	53.00	40.50	0.006
15:00	154.25	250.75	50.15	38.31	0.006
16:00	122.75	282.25	47.04	32.37	0.007
Avg	248.5714	156.4286	47.57429	28.62143	0.0205



**A8: Result of different tray spacing configurations**

Tray spacing	Tray	Average weight reduction (%)	Average drying rate (g/hr)
10 cm	Tray 1	81.75	54.50
	Tray 2	78.25	52.83
20 cm	Tray 1	81.25	53.17
	Tray 3	76.15	51.50
30 cm	Tray 1	80.50	53.67
	Tray 4	75.50	50.67
30 cm	Tray 2	80.50	53.67
	Tray 5	76.75	51.17
20 cm	Tray 1	80.25	53.50
	Tray 3	74.00	49.33
	Tray 5	67.50	45.00
10 cm	Tray 1	78.00	52.00
	Tray 2	72.00	48.00
	Tray 3	68.50	45.67
	Tray 4	65.75	43.83

**A9: Results of Taguchi analysis**

EX no	Parameters/levels				C <sub>v</sub> of the mass as response variables			Pressure drops as response variables		
	SR	T <sub>am</sub>	T <sub>in</sub>	Type-C	RB	TB	SW	DPRB	DPTB	DPSW
1	810	33	40	TB	0.00	0.00	0.00	2.80	2.66	2.63
2	810	27	41	SW	4.77	3.92	2.13	3.12	24.20	23.24
3	810	30	42	RB	7.58	7.47	3.27	28.23	23.79	24.20
4	830	33	41	RB	12.41	11.73	7.90	27.18	23.31	23.79
5	830	27	42	TB	13.94	14.46	10.38	28.67	23.59	23.31
6	830	30	40	SW	18.68	16.80	15.47	27.36	23.03	23.59
7	850	33	42	SW	19.38	17.44	22.90	27.86	22.74	23.03
8	850	27	40	RB	0.00	0.00	0.00	28.40	22.59	22.74
9	850	30	41	TB	0.00	0.00	0.00	26.86	23.29	22.59

**A10: Fabrication cost of the drying system**

S/n	Name of the material	Total cost in HUF	Quantity
1	Aluminium flexible pipe Ø 100 mm x 3 m	6129.00	1
2	Corner edge protection anodized aluminium 30 x 30 mm x 2 m	8181.00	2
3	Assembly glue Montage Fix 280 ml	3754.00	2
4	Wall picture hook, FLOREAT-3 + nail 32 mm	2798.00	2
5	Picture frame tab, copper 32, 26 mm x 14 mm	749.00	1
6	Wall picture hook, FLOREAT-0 17 mm + nail	1499.00	1
7	Slats planed on 4 sides 19 mm x 74 mm x 2000 mm	4396.00	2
8	OBI lacquer spray heat-resistant matte black 400 ml	2799.00	1
9	Chipboard screw with countersunk head	839.00	1 package
10	RAVATHERM XPS 250 PB extruded polystyrene foam thermal insulation board, 1250 mm x 600 mm x 20 mm, 1.5 m <sup>2</sup>	1516.00	2
11	Chipboard screw with countersunk head, 0.135 kg	1282.00	
12	Chipboard screw with countersunk head, 0.115 kg	1092.00	
13	MAPEI Mapepur Roof Foam M 750 ml Adhesive foam for quick gluing of construction clays manual foam	4290.00	1
14	Copying blade JW10C wood	2540.00	1
15	Ravatherm XPS 250 PB extruded polystyrene foam thermal insulation board, 1250 mm x 600 mm x 50 mm, 6 m <sup>2</sup>	8000.00	3
16	ST Line S145 glass fabric mesh, 6 m <sup>2</sup>	1908.00	
17	Vents TT 100 duct fan RS-1-300 with speed controller	31 707.00	1
18	Switch and regulator	6000.00	
19	Plastic PVC check valve with mounting frame Ø 100 mm	4 802.00	2
20	Cover glass 50 cm x 150 cm x 4 mm	20000.00	2
21	Copper plate measuring 121 cm length, 46 cm width, and 1.2 mm thickness prices	14000.00	1
22	Electrical consumption	780.2784	3 months for 8 hours
23	Cost of the apple	1600.00	2 kg
24	Cost of dried apple	2000.00	0.5 kg
25	Labour cost	60000.00	3 days
Total		156152.27	

## 10. ACKNOWLEDGEMENT

First, I thank GOD, the Most Merciful, for giving me the strength and guidance to complete this thesis.

I am sincerely grateful to the Stipendium Hungaricum Scholarship Program and the Mechanical Engineering Doctoral School at MATE University, Hungary, for their financial support.

My deepest appreciation goes to my esteemed supervisors, Prof. István Farkas and Dr. János Buzás, for their invaluable guidance, unwavering encouragement, and steadfast support throughout this journey. Their insightful suggestions, constructive feedback, and intellectual mentorship were crucial in shaping this research. Working under their supervision has been an immensely enriching experience, and without their dedication, this thesis would not have reached fruition.

I owe everything to my parents for their endless love, sacrifices, and prayers. May GOD bless and protect them always.

I extend my sincere gratitude to express my deep appreciation to Machi Maytham Hasan Mahdi for his invaluable assistance and support throughout the experimental work his contribution was help full to this research. Additionally, I am profoundly thankful to my coordinators, Ms. Zsuzsanna Tassy, Mrs. Judit Czingli Tallárom, Mrs. Edit Dolányi Sima, and Mrs. Katalin Fekete Sivatagi, for their unwavering guidance and support.

I would like to express my deepest gratitude also to Hawassa University and its dedicated staff for their unwavering support. Special thanks go to Dr. Ir. Fasika Bete and Firehwot Tesfamariyam for their invaluable guidance and encouragement on my PhD journey.

Finally, I appreciate the ministry of higher education of Ethiopia and Hawassa university for their support.

Gödöllő, May 2025

Halefom Kidane Abrha